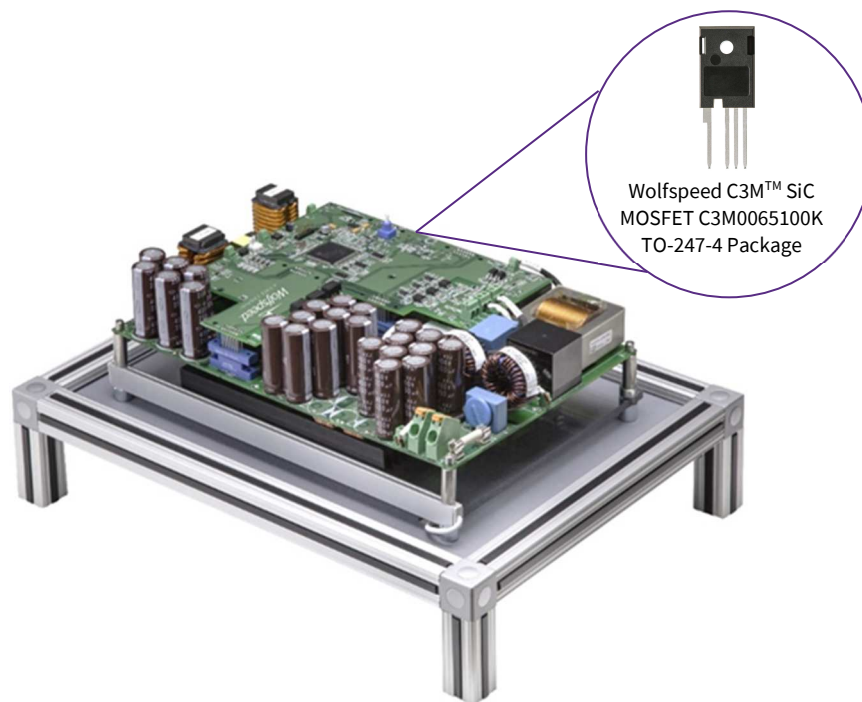


CRD-06600FF10N 6.6kW Bi-Directional EV On-Board Charger Application Note



CRD-06600FF10N 6.6kW Bi-Directional EV On-Board Charger Application Note

Contents

| | |
|---|----|
| 1. Introduction..... | 8 |
| 2. Design Specifications | 9 |
| 3. Physical Dimensions and Pinouts..... | 10 |
| 4. System Overview | 11 |
| 4.1 Power Board | 13 |
| 4.1.1 AC-DC Power Stage | 13 |
| 4.1.2 DC-DC Power Stage | 24 |
| 4.1.3 Control Structure of the Converter..... | 39 |
| 4.1.4 Gate Drive Circuitry | 43 |
| 4.1.5 Design and Layout Considerations for High Frequency Switching | 47 |
| 4.2 Controller Board..... | 50 |
| 4.2.1 Power Supply Requirements | 50 |
| 4.2.2 Analog Feedbacks | 53 |
| 4.2.3 Controller Pin Assignments..... | 56 |
| 5. Performance Data | 58 |
| 6. Appendix..... | 62 |
| 7. References | 79 |
| 8. Revision History..... | 79 |
| 9. Important Notes | 79 |

This document is prepared as a user guide to install and operate Wolfspeed® evaluation hardware. All parts of this user guide are provided in English, and the cautions are provided in English, Mandarin, and Japanese. If the end user of this board is not fluent in any of these languages, it is your responsibility to ensure that they understand the terms and conditions described in this document, including without limitation the hazards of and safe operating conditions for this board.

本文件中的所有内容均以英文书写，“注意”部分的内容以英文、中文和日语书写。作为本板子的终端用户，即使您不熟悉上述任何一种语言，您也应当确保正确理解本文件中的条款与条件，包括且不限于本板子的危险隐患以及安全操作条款。

当書類のすべての内容は英語で書きます。「注意点」の内容は英語、中国語、また日本語で書きます。当ボードの端末使用者は上記の言語が一つでもわからないなら、当端末使用者は当書類の条約と条件が理解できるのを確保すべきです。そして、当ボードの危険や安全に使用する条件を含み、また限りません。

Note: This Wolfspeed-designed evaluation hardware for Wolfspeed® components is a fragile, high voltage, high-temperature power electronics system that is meant to be used as an evaluation tool in a lab setting and to be handled and operated by highly qualified technicians or engineers. When this hardware is not in use, it should be stored in an area that has a storage temperature ranging from -40° Celsius to 105° Celsius. If this hardware is transported, special care should be taken during transportation to avoid damaging the board or its fragile components and the board should be transported carefully in an electrostatic discharge (ESD) bag, or with ESD or shorting protection that is the same as, or similar to, the protection that is or would be used by Wolfspeed when shipping this hardware, to avoid any damage to electronic components. Please contact Wolfspeed at forum.wolfspeed.com if you have any questions about the protection of this hardware during transportation. The hardware does not contain any hazardous substances, is not designed to meet any industrial, technical, or safety standards or classifications, and is not a production-qualified assembly.

本样机（易碎、高压、高温电力电子系统）由科锐为评估其功率半导体产品而设计，用以作为在实验室环境下由专业的技术人员或工程师处理和使用的评估工具。本样机不使用时，应存储在-40°C~105°C温度范围的区域内；如需运输样机，运输过程中应该特别小心，避免损坏电路板等易碎组件。如果您对此硬件在运输之中的保护有任何疑问，请联系forum.wolfspeed.com。样机应放置在防静电包装袋内谨慎运输，避免损坏电子组件。本样机不含任何有害物质，但其设计不符合任何工业、技术或安全标准或分类，也不是可用于生产的组件。

このクリーのコンポーネント用評価ハードウェアは壊れやすい高電圧の高温パワーエレクトロニクスシステムであり、ラボ環境での評価ツールとして使用され、優秀な技術者やエンジニアによって処理され、操作されることを意図している。ハードウェアが使用されていない場合、保管温度が-40°Cから105°Cの範囲に保管してください。このハードウェアを輸送する場合は、輸送中にボードまたはその壊れやすいコンポーネントに損傷を与えないよう特別な注意を払う必要がある。また電子部品の損傷を避けるためにボードを静電気放電(ESD)袋に静置して慎重に輸送すべき。ハードウェアの輸送中の保護について質問があれば

<https://forum.wolfspeed.com/> に連絡してください。ハードウェアには危険物質が含まれていないが、工業的、技術的、安全性の基準または分類に適合するように設計されておらず、生産適格組立品でもない。



CAUTION

PLEASE CAREFULLY REVIEW THE FOLLOWING PAGE, AS IT CONTAINS IMPORTANT INFORMATION REGARDING THE HAZARDS AND SAFE OPERATING REQUIREMENTS RELATED TO THE HANDLING AND USE OF THIS BOARD.

警告

请认真阅读以下内容，因为其中包含了处理和使用本板子有关的危险和安全操作要求方面的重要信息。

警告

ボードの使用、危険の対応、そして安全に操作する要求などの大切な情報を含むので、以下の内容をよく読んでください。

**CAUTION**

DO NOT TOUCH THE BOARD WHEN IT IS ENERGIZED AND ALLOW THE BULK CAPACITORS TO COMPLETELY DISCHARGE PRIOR TO HANDLING THE BOARD. THERE CAN BE VERY HIGH VOLTAGES PRESENT ON THIS EVALUATION BOARD WHEN CONNECTED TO AN ELECTRICAL SOURCE, AND SOME COMPONENTS ON THIS BOARD CAN REACH TEMPERATURES ABOVE 50 ° CELSIUS. FURTHER, THESE CONDITIONS WILL CONTINUE FOR A SHORT TIME AFTER THE ELECTRICAL SOURCE IS DISCONNECTED UNTIL THE BULK CAPACITORS ARE FULLY DISCHARGED.

Please ensure that appropriate safety procedures are followed when operating this board, as any of the following can occur if you handle or use this board without following proper safety precautions:

- Death
- Serious injury
- Electrocuting
- Electrical shock
- Electrical burns
- Severe heat burns

You must read this document in its entirety before operating this board. It is not necessary for you to touch the board while it is energized. All test and measurement probes or attachments must be attached before the board is energized. You must never leave this board unattended or handle it when energized, and you must always ensure that all bulk capacitors have completely discharged prior to handling the board. Do not change the devices to be tested until the board is disconnected from the electrical source and the bulk capacitors have fully discharged.

警告

请勿在通电情况下接触板子，在处理板子前应使大容量电容器完全释放电力。接通电源后，该评估板上可能存在非常高的电压，板子上一些组件的温度可能超过50 摄氏度。此外，移除电源后，上述情况可能会短暂持续，直至大容量电容器完全释放电量。

操作板子时应确保遵守正确的安全规程，否则可能会出现下列危险：

- 死亡
- 严重伤害
- 触电
- 电击
- 电灼伤
- 严重的热烧伤

请在操作本板子前完整阅读本文件。通电时不必接触板子。在为板子通电前必须连接所有测试与测量探针或附件。通电时，禁止使板子处于无人看护状态，或操作板子。必须确保在操作板子前，大容量电容器释放了所有电量。只有在切断板子电源，且大容量电容器完全放电后，才可更换待测试器件

警告

通電している時、ボードに接触するのは禁止です。ボードを処分する前に、大容量のコンデンサーで電力を完全に釈放すべきです。通電してから、ボードにひどく高い電圧が存在している可能性があります。ボードのモジュールの温度は50度以上になるかもしれません。また、電源を切った後、上記の状況がしばらく持続する可能性がありますので、大容量のコンデンサーで電力を完全に釈放するまで待ってください。

ボードを操作するとき、正確な安全ルールを守るのを確保すべきです。さもないと、以下の危険がある可能性があります：

- 死亡
- 重症
- 感電
- 電撃
- 電気の火傷
- 厳しい火傷

当ボードを操作する前に、完全に当書類をよく読んでください。通電している時にボードに接触する必要がありません。通電する前に必ずすべての試験用のプローブあるいはアクセサリーをつないでください。通電している時に無人監視やボードを操作するのは禁止です。ボードを操作する前に、大容量のコンデンサーで電力を完全に釈放するのを必ず確保してください。ボードの電源を切った後、また大容量のコンデンサーで電力を完全に釈放した後、試験設備を取り換えることができます。

1. Introduction

The electric vehicle (EV) market is a rapidly growing segment for transportation as the world is moving towards cleaner fuel alternatives. The battery of the EV needs to be charged while parked at home or office. While this requires only AC/DC conversion with isolation and front-end PFC (Power Factor Correction) stage, the trend in the EV market is towards the bi-directionality of the converter i.e. feeding power into the utility grid from battery side. The main reason of the bi-directionality requirement is because the EV battery is imagined as a distributed energy storage system and may play a great part in stabilizing the grid. It may feed power into the grid when demand is at peak and vehicle is stationary and draws power from the grid when demand is low.

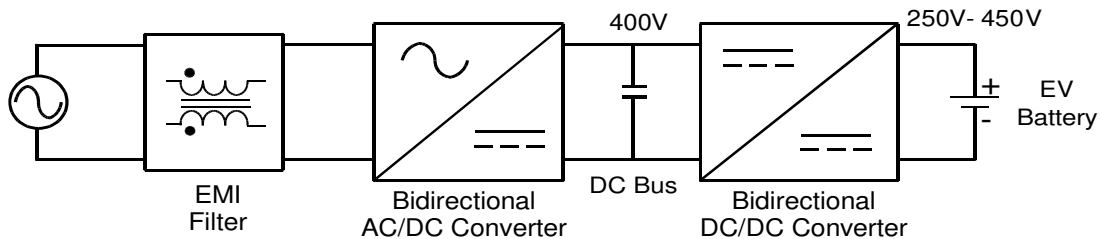


Figure 1: EV battery charging system

Figure 1 shows the most popular topology using conventional silicon (Si) devices where intermediate DC link voltage is fixed at 400 VDC. It is well known that the resonance converters are the most efficient converters due to their ability to work at the resonance frequency. The disadvantage of fixing the DC link at 400 VDC is that the converter works at a frequency far more from the resonance frequency to accommodate the widely varying EV battery voltage, thus reducing the efficiency considerably.



Figure 2: Wolfspeed's CRD-06600FF10N, 6.6 kW bi-directional EV on-board charger

In this user guide, Wolfspeed introduces a CRD-06600FF10N, 6.6 kW Bi-directional EV On-board Charger (as shown in Figure 2) based on Wolfspeed's C3M™ 1000 V, 65 mΩ silicon carbide (SiC) MOSFET (P/N: C3M0065100K) which comes in a TO-247-4 package with a Kelvin source availability. The main features of Wolfspeed's C3M SiC MOSFETs include low switching losses, fast intrinsic body diode and high frequency operation which reduce the overall weight and size of the system and are intended to maintain high efficiency of the whole system.

Wolfspeed’s CRD-06600FF10N, 6.6 kW Bi-directional EV On-board Charger comprises of two power stages: 1) Bi-directional PFC stage and 2) Isolated Bi-directional DC/DC stage (as shown in Figure 3). The Bi-directional PFC stage is based on the Totem-Pole PFC Topology while the Isolated Bi-directional DC/DC stage is based on a CLLC topology with a variable DC link voltage (as shown in Figure 3). At full load, the DC link voltage varies according to the variations in battery voltage and the CLLC topology operates at resonance or close to the resonance frequency, which is intended to optimize the efficiency of the bi-directional CLLC converter (as shown in Figure 3) and maintain overall efficiency that is better than a fixed DC link LLC converter.

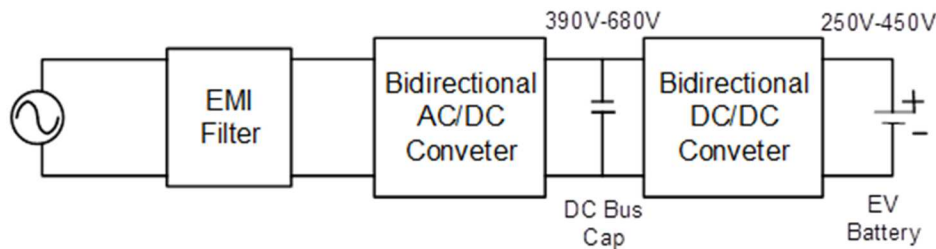


Figure 3: Bi-directional EV battery charging system with variable DC link voltage

2. Design Specifications

The design specifications of both charging and inverter modes of Wolfspeed’s CRD-06600FF10N, 6.6 kW Bi-directional EV On-board Charger are listed in Table 1.

Table 1: Design Specifications of Wolfspeed’s CRD-06600FF10N, 6.6 kW Bi-Directional EV On-Board Charger

| Charging Mode | | |
|------------------------------|-----------------------|--|
| Parameters | Values | Notes |
| Input voltage range | 90 VAC-265 VAC | Nominal Voltage = 230 VAC, Power will be limited when input voltage is below 208 VAC |
| THD and PF | THD <5% and PF > 0.99 | At Rated Power |
| Output voltage range | 250 VDC-450 VDC | Output current will be limited to 20 A when the battery voltage is below 320 VDC; constant Power between 320 VDC-430 VDC; constant voltage above 430 VDC |
| Input rated power | 6.6 kW | |
| Isolation voltage | > 2.5 kV | |
| Switching frequency of PFC | 67 kHz | |
| Switching frequency of DC/DC | 200 kHz | |
| Peak efficiency | > 96% | |
| Max ambient temperature | 65 °C | Force air cooling |
| Inverter Mode | | |
| Parameters | Values | Notes |
| Input voltage range | 250 VDC-450 VDC | When the battery voltage is below 320 VDC, it will stop delivering power |

| | | |
|-------------------------------------|----------------------------------|---|
| THD and PF | THD <5% and PF > 0.99 | At Rated Power |
| Output voltage range | Grid Voltage: 120 VAC or 230 VAC | Standalone Mode: 230 VAC, 60 Hz |
| Input rated power | 3.3 kW | |
| Isolation voltage | > 2.5 kV | |
| Switching frequency of DC/AC | 67 kHz | |
| Switching frequency of DC/DC | 200 kHz | |
| Peak efficiency | > 96% | |
| Max ambient temperature | 65 °C | Forced air cooling for the base plate or the completed PCBA |

3. Physical Dimensions and Pinouts

The Physical dimensions and the pinouts of Wolfspeed’s CRD-06600FF10N, 6.6 kW Bi-directional EV On-board Charger has been shown in Figure 4(a) and Figure 4(b).

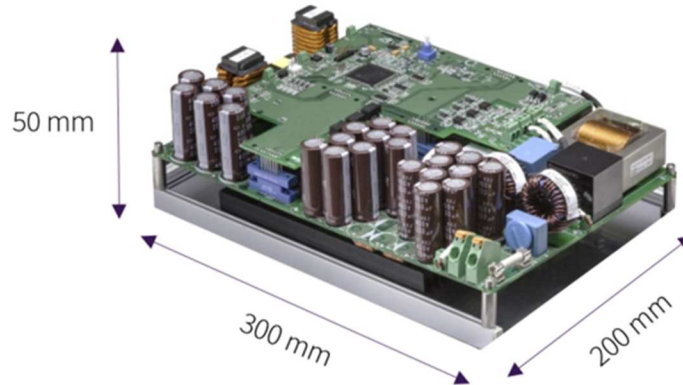


Figure 4 (a): Physical dimensions of Wolfspeed’s CRD-06600FF10N, 6.6 kW bi-directional EV on-board charger

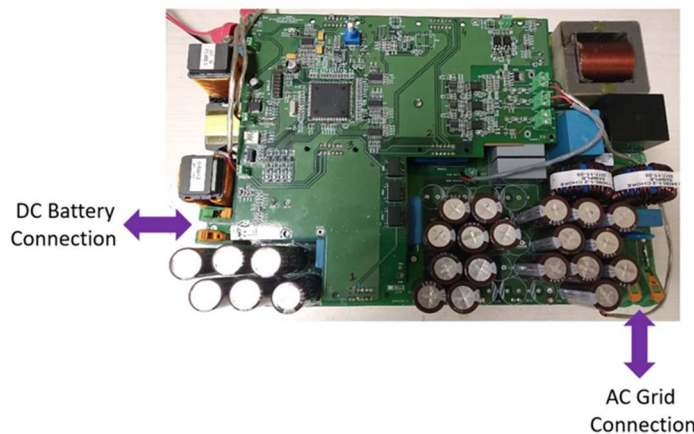


Figure 4 (b): High power connections of Wolfspeed’s CRD-06600FF10N, 6.6 kW bi-directional EV on-board charger

4. System Overview



CAUTION

IT IS NOT NECESSARY FOR YOU TO TOUCH THE BOARD WHILE IT IS ENERGIZED. WHEN DEVICES ARE BEING ATTACHED FOR TESTING, THE BOARD MUST BE DISCONNECTED FROM THE ELECTRICAL SOURCE AND ALL BULK CAPACITORS MUST BE FULLY DISCHARGED.

SOME COMPONENTS ON THE BOARD REACH TEMPERATURES ABOVE 50° CELSIUS. THESE CONDITIONS WILL CONTINUE AFTER THE ELECTRICAL SOURCE IS DISCONNECTED UNTIL THE BULK CAPACITORS ARE FULLY DISCHARGED. DO NOT TOUCH THE BOARD WHEN IT IS ENERGIZED AND ALLOW THE BULK CAPACITORS TO COMPLETELY DISCHARGE PRIOR TO HANDLING THE BOARD.

PLEASE ENSURE THAT APPROPRIATE SAFETY PROCEDURES ARE FOLLOWED WHEN OPERATING THIS BOARD AS SERIOUS INJURY, INCLUDING DEATH BY ELECTROCUTION OR SERIOUS INJURY BY ELECTRICAL SHOCK OR ELECTRICAL BURNS, CAN OCCUR IF YOU DO NOT FOLLOW PROPER SAFETY PRECAUTIONS.

警告

通电时不必接触板子。连接器件进行测试时，必须切断板子电源，且大容量电容器必须释放完所有电量。

板子上一些组件的温度可能超过50 摄氏度。移除电源后，上述情况可能会短暂持续，直至大容量电容器完全释放电量。通电时禁止触摸板子，应在大容量电容器完全释放电量后，再操作板子。请确保在操作板子时已经遵守了正确的安全规程，否则可能会造成严重伤害，包括触电死亡、电击伤害、或电灼伤。

警告

通电している時にボードに接触する必要がありません。設備をつないで試験する時、必ずボードの電源を切ってください。また、大容量のコンデンサーで電力を完全に釈放してください。

ボードのモジュールの温度は50 度以上になるかもしれません。電源を切った後、上記の状況がしばらく持続する可能性がありますので、大容量のコンデンサーで電力を完全に釈放するまで待ってください。通电している時にボードに接触するのは禁止です。大容量のコンデンサーで電力をまだ完全に釈放していない時、ボードを操作しないでください。

ボードを操作している時、正確な安全ルールを守っているのを確保してください。さもなければ、感電、電撃、厳しい火傷などの死傷が出る可能性があります。

Note: A larger copy of any diagram in this Section 4 may be obtained at <https://www.wolfspeed.com/products/power/reference-designs/> or upon request by contacting Wolfspeed at forum.wolfspeed.com

The block diagram of Wolfspeed’s CRD-06600FF10N, 6.6 kW Bi-directional EV On-board charger is shown in Figure 5. The system designed in the lab does not have a battery charging algorithm built in and customer may code their own battery charging algorithm in the DSP.

The AC-DC converter stage is configured as a totem pole PFC circuit in charging mode. The circuit has two half bridge circuits; one switching at high frequency of 67 kHz and the other at the frequency of grid voltage, typically 50 Hz. Both legs of the PFC circuit consist of two of Wolfspeed’s 1000 V, 65 mΩ SiC MOSFETs (C3M0065100K) in a parallel arrangement. The DC-DC bi-directional CLLC converter is comprised of 2 identical H-bridges separated by isolation transformer.

A resonance frequency of 200 kHz was selected for operation. All switches have isolated gate drivers with a separate isolated power supply. Ceramic de-coupling capacitors in proximity with small film capacitors have been used for the decoupling of the stray inductances.

Larger film capacitors have been used a little farther away from the devices for high frequency ripple current. A bank of electrolytic capacitors has been connected in series with DC link due to the availability of 680 VDC link voltage.

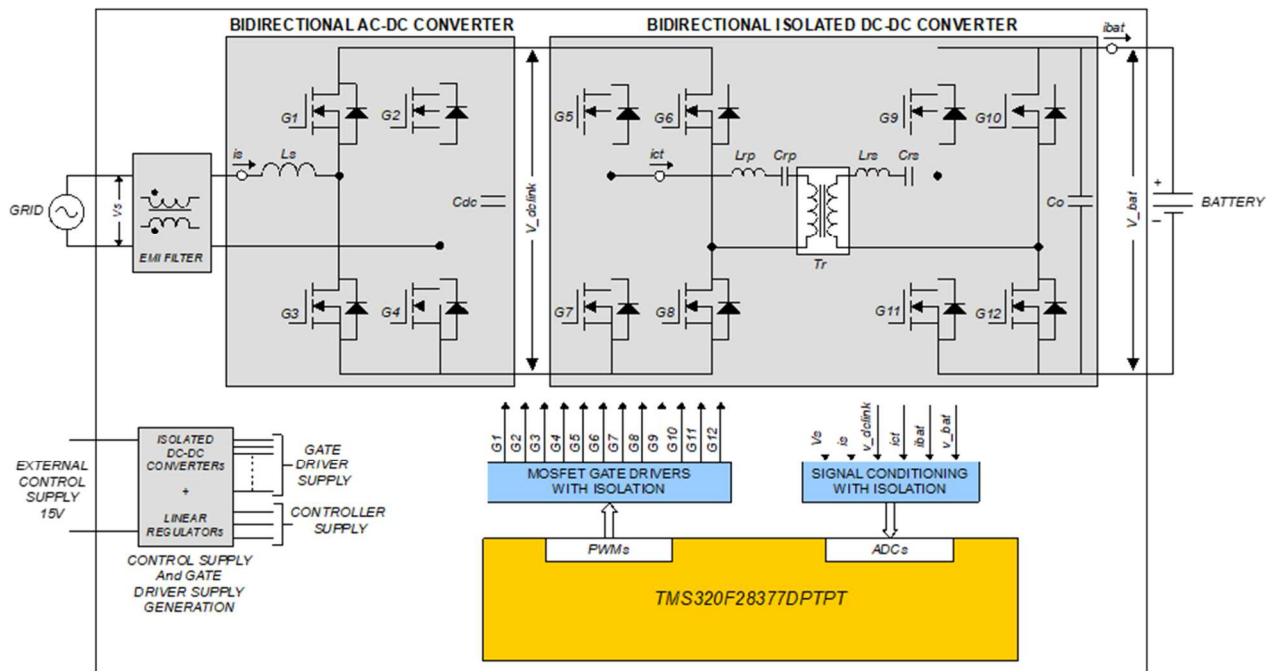


Figure 4: System level block diagram

The controller card is a Texas Instruments® (TI) DSP controller (P/N: TMS320F28377). Controller card is galvanically isolated from the power stage through isolated gate drivers, analog isolation amplifiers and the opto-isolators. For controller supply and driver supply, external isolated power supplies of 7 V and 15 V are connected to the control card.

4.1 Power Board

Note: A larger copy of any diagram in this Section 4.1 may be obtained at <https://www.wolfspeed.com/products/power/reference-designs/> or upon request by contacting Wolfspeed at forum.wolfspeed.com.

The power board of Wolfspeed’s CRD-06600FF10N, 6.6 kW Bi-directional EV On-board Charger houses the input EMI filter and the power stages of both AC-DC and DC-DC converters. The controller board is placed in such a way that the PWM signals of each power stage remain as close as possible to the respective gate driver. The gate drive circuitry has also been placed close to the respective SiC MOSFETs. To do the test measurements, the DC and AC voltages and currents are routed to the controller through separate connectors. The external power supply of the gate drivers is also routed through the controller board.

4.1.1 AC-DC Power Stage

The AC-DC converter is a H-bridge circuit with bidirectional power transfer capability. In charging mode, the converter is configured as totem pole PFC boost converter, as shown in Figure 6 and operates as a sinewave inverter with hybrid modulation (or modified unipolar modulation) in inverter mode. One leg of the converter is switched at low frequency (at grid frequency or the reference sinewave frequency) while the other leg is operated at high frequency. The EMI filter is designed to minimize the conducted emission noise to the grid and keep it to the lower level.

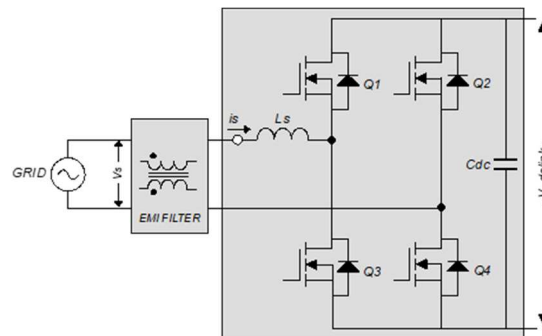


Figure 5: AC-DC converter power stage

In the charging mode, the AC-DC converter stage should regulate the DC bus voltage as well as maintain a good THD in the grid current. Without any switching, the body diodes of MOSFETs will create a full bridge uncontrolled rectifier circuit and current drawn from grid will be pulsating in nature. With a proper switching sequence and two loop control mechanism, the DC bus is regulated to the required DC voltage while maintaining the inductor current close to sinusoidal shape and in phase with the grid voltage.

The gate pulses of MOSFETs Q2 and Q4 are complementary and change their state based on the zero crossing of the grid voltage. For the positive half of the grid voltage, Q4 gate signal set as high while Q2 gate signal set as low. MOSFET Q3 is switched at high frequency with varying pulse widths based on the current loop compensator and the output of the control logic. For the negative half of the grid voltage, MOSFETs Q4 and Q2 switch their states while MOSFETs Q3 and Q1 switch their functionalities. The resultant configuration is a boost converter circuit for each half of the AC cycle (as shown in Figure 7). The schematic on the left side of the Figure 7 depicts the switching states for the positive half cycle and the schematic on the right side of the Figure 7

depicts the switching states for the negative half cycle. The blue line indicates the switching state when the current in boost inductor increases, and the load is supported by the output capacitors. The red line indicates the switching state when input voltage along with the inductor energy feed the load and the capacitor at higher voltage.

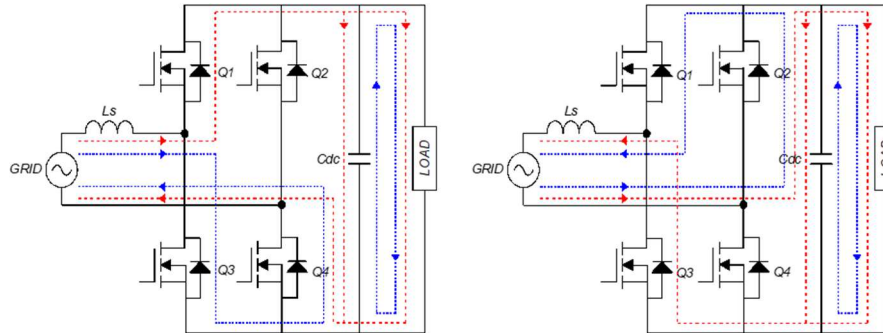


Figure 6: Totem-pole PFC current path for positive half cycle (left) and negative half cycle (right)

In the inverter mode, the circuit is configured to work as a grid tie inverter and feed the grid from the available battery energy. The switching scheme remains the same as in the totem pole PFC topology while the grid current is controlled to be in phase with the voltage.

Table 2: Specifications of the AC-DC Stage

| Parameters | Values | Notes |
|---------------------------------|-----------------------|--|
| Grid Voltage Range | 90 VAC-265 VAC | Power will be limited when input voltage is below 200 VAC |
| THD and PF | THD <5% and PF > 0.99 | At Rated Power (Both Modes) |
| DC Bus Voltage Range (1) | 390 VDC – 680 VDC | AC-DC Mode |
| DC Bus Voltage Range (2) | 480 VDC – 680 VDC | DC-AC Mode |
| Output Power (1) | 6.6 kW | AC-DC Mode: $V_{Grid} = 200 \text{ VAC to } 265 \text{ VAC}$ |
| Output Power (2) | 3.3 kW | DC-AC Mode |
| Switching Frequency | 67 kHz | |
| Converter Efficiency | > 98% | |

Inductor Design:

Referring to the specifications in Table 1, the maximum power to be handled is in charging mode. So, the inductor is designed for totem-pole PFC converter with continuous conduction mode. The input voltage is sinusoidally varying in a boost PFC converter and the ripple current in the inductor will not be constant for a known power value. The inductor current ripple (Δi_L) is given by:

$$\Delta i_L = \frac{v_{in}(V_o - v_{in})}{F_s L V_o}$$

For a maximum inductor ripple current of 15 A (approximately 35%), at 200 VAC input (283 V peak) and at maximum DC output (670 V), the required inductance value (L) would be:

$$L = \frac{v_{in}(V_o - v_{in})}{F_s V_o \Delta i_{L(\max)}} = \frac{283 \times (680 - 283)}{67000 \times 670 \times 15} = 166.8 \mu H$$

The maximum ripple current $\Delta i_{L(\max)}$ in the inductor (L) when the input voltage $v_{in} = \frac{V_o}{2}$:

$$\Delta i_{L(\max)} = \frac{V_o}{4F_s L}$$

The maximum inductor current ripple ($\Delta i_{L(\max)}$) will be 15.2A when output (V_o) is set at 680 VDC and instantaneous input voltage ($V_{in(ims)}$) is 340 V.

In the Inverter mode, the input (v_{in}) to the converter is a fixed DC bus voltage and the output (V_o) is a sinusoidal AC voltage. The converter should be in continuous conduction mode to keep the switching harmonics in grid current at the minimum level. The required value of inductance (L) in the Inverter mode with a 3A ripple current (Δi_L) (approximately 32% ripple) is:

$$L = \frac{(V_{dc} - V_{opk})V_{opk}}{V_{dc} F_s \Delta i_{L(\max)}} = \frac{(390 - 325) \times 325}{390 \times 67000 \times 3} = 303 \mu H$$

Table 3: Inductor Requirements

| Charging Mode | | |
|-----------------------|-------------|-------------------------------------|
| Parameters | Values | Notes |
| Inductance | 165 μH | At maximum Input AC Current of 33 A |
| RMS Current | 33 A | For 6.6 kW Power at 200 V |
| Peak Current | 54 A | |
| Ripple Current | 15 A | At 67 kHz |

| Inverter Mode | | |
|-----------------------|-------------|-------------------------------------|
| Parameters | Values | Notes |
| Inductance | 300 μH | At maximum Input AC Current of 33 A |
| RMS Current | 14 A | For 3.3 kW Power at 230 V |
| Peak Current | 15.5 A | |
| Ripple Current | 3 A | At 67 kHz |

$$I_{inmax_{rms}} = 34.375A$$

$$I_{inmax_{pk}} = 48.6A$$

$$I_{ripple_{pkpk}} = 0.4 * I_{inmax_{pk}} = 19.4425$$

$$I_{boost_{pk}} = I_{inmax_{pk}} + \frac{I_{ripple_{pkpk}}}{2} = 58.312$$

$$D_{min} = 1 - \frac{(\sqrt{2} * V_{inmin_{rms}})}{V_{opfc}} = 0.411$$

When the boost inductor has 24.613A DC bias current, the inductance will be:

$$L_{boost_{bias}} = \frac{(\sqrt{2} * V_{inmin_{rms}} * D_{min})}{(F_{s_{pfc}} * I_{ripple_{pkpk}})} = 132.82 \mu H$$

$$\text{Area Product required} = AeAw_{required} = \frac{L_{boost_{bias}} * I_{boost_{pk}}^2}{Kw_{boost} * B_{max_{boost}} * J_{max_{boost}}}$$

$$B_{max_{boost}} = 0.5T$$

$$J_{max_{boost}} = 750 \frac{\text{amp}}{\text{cm}^2}$$

$$AeAw_{required} = 1.72 * 10^{-7} \text{ m}^4$$

An available core with part number: APH46P60 from AMOS has been selected. The details of Part APH46P60 have been shown in Figure 8.

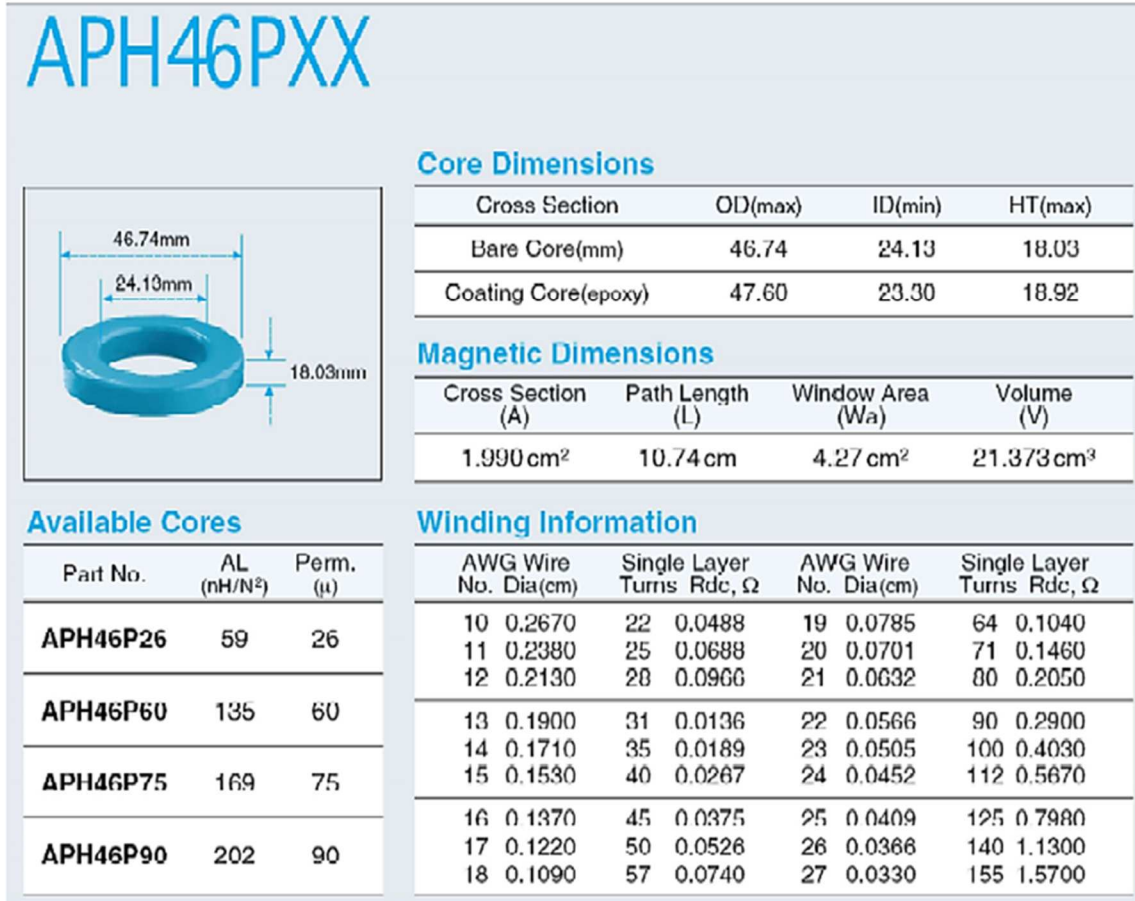


Figure 7: Core details of APH46P60

Considering 2 cores stacked the AeAW of selected inductor (L):

$$L = 2 * 1.99 * 4.27 * 10^{-8} = 1.699 * 10^{-7} \text{ m}^4$$

Inductance factor value of 2 cores stacked $AL_N = 2 * 0.135 \text{ uH} = 0.27 \text{ uH}$

$$N_{boost} = 2 * \sqrt{\left(\frac{L_{boost_{bias}}}{AL_N}\right)} = 44.35$$

$$L_{boost_{nobias}} = 531.285 \text{ uH}$$

$$H_{boost_{max}} = N_{boost} * \frac{(I_{in_{max_{pk}}} + \frac{L_{boost_{bias}} * I_{ripple_{pk2pk}}}{2 * L_{boost_{nobias}}})}{le}$$

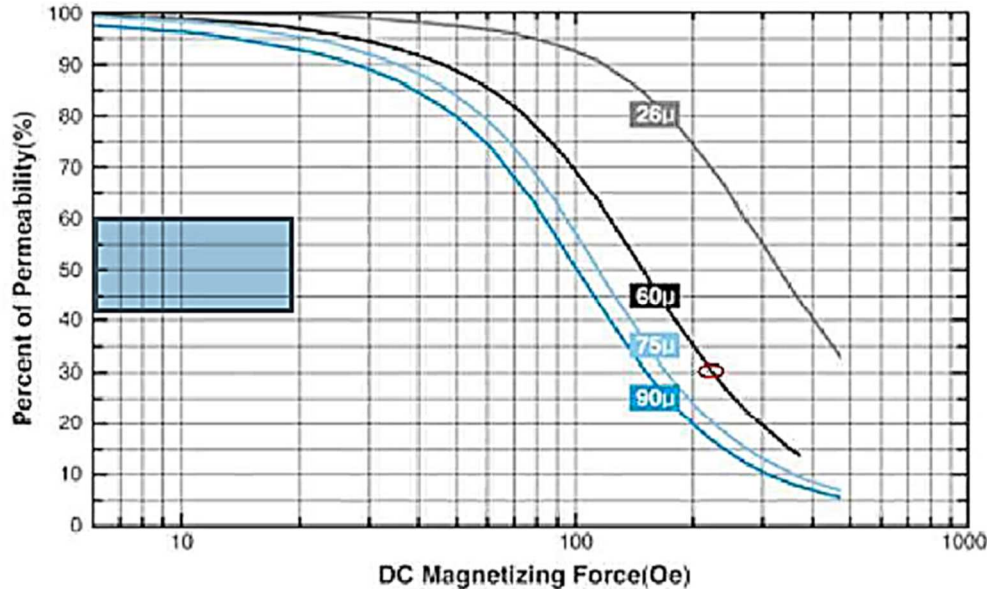


Figure 8: Percent of Permeability vs DC magnetizing force of APH46P60

$$H_{boost_{max}} = 264.822$$

The permeability with DC bias curve shows about 30% initial permeability at:

$$H_{boost_{max}} = 264.822 \text{ oersted for } 60\mu \text{ material.}$$

The inductance with $H_{boost_{max}} = 264.822$ dc bias

$$L_{boost_{bias}} = 0.3 * L_{boost_{nobias}} = 159.385 \mu\text{H.}$$

For winding $2 * 1.4$ mm wire is used and total DC resistance = $14 \text{ m}\Omega$

DC Bus Capacitor Selection:

DC Bus capacitor selection depends on the capacitor's capability of withstanding the entire output voltage range, minimizing the switching ripple as well as low frequency ripple and holding sufficient energy to support the load in an event of power outage for at least one cycle. This results in three criteria for capacitor selection.

$$C_o > \frac{P_o}{2\pi F_{grid} V_o \Delta V_o} \approx 1.5\text{mF} \text{ for } 20 \text{ V line frequency ripple}$$

$$C_o > \frac{2P_o t_{hold}}{V_{omax}^2 - V_{omin}^2}$$

$$\approx 890 \mu\text{F} \text{ to hold } 6.6 \text{ kW power for } 20 \text{ ms}$$

In inverter mode, the same criteria should be applied to DC bus capacitor selection. Since the power to be pumped to the grid is 3.3 kW , capacitors designed for charging mode are sufficient for the inverter mode.

The maximum of the three values (i.e. 1.5 mF) is the required capacitance which satisfies the switching ripple requirement. Wolfspeed has allowed slightly higher ripple here and selected a value of 1.1 mF instead of 1.5 mF .

Hold up criteria does not apply here. The RMS current that the capacitor needs to handle is:

$$I_{Co,rms} = \sqrt{\frac{8\sqrt{2} P_o^2}{3\pi V_{acmin} V_o} - \frac{P_o^2}{V_o^2}}$$

The ripple current rating corresponds to the line frequency component in the capacitor current and it can be evaluated at the minimum AC voltage for which rated power is to be supported.

$$I_{Co,rms} = \sqrt{\frac{8\sqrt{2} \times 6600^2}{3\pi \times 200 \times 680} - \frac{6600^2}{680^2}} = 17A$$

To cater the requirements of large operating voltage range and high ripple current along with the need for longer operating life, a capacitor bank made of electrolytic capacitors is used. The details of the capacitor bank are listed in Table 4. Several low value snubber capacitors close to the devices and couple of low value film capacitors have been used as well in an effort to minimize switching noise in the DC bus.

Table 4: DC Bus Capacitor Bank Specifications

| Parameters | Values | Notes |
|---|---------------------------|---|
| Capacitor used | EKXJ401ELL251MM50S | From Chemi-Con |
| Capacitor rating | 250 μF, 400 VDC | |
| Series parallel combination | 2 in series 9 in parallel | Series connection for voltage and parallel connection for ripple current rating |
| Capacitor bank rating | 1.125 mF 800 VDC | |
| Capacitor bank ESR | 0.044 Ω | At 105°C and 120 Hz ripple |
| Capacitor bank ripple current rating | 17.71 A | At 105°C and 120 Hz ripple |
| Capacitor bank life | | At 105°C with ripple |
| Operating temperature range | -40°C to +105°C | |

When the converters are not operational, the DC bus is charged to the peak of the grid voltage of 375 V. The individual capacitors are rated at 400 V and the capacitor bank can withstand the maximum grid voltage without the need of a voltage balancing circuit.

Soft Charging of DC Bus Capacitors:

When the grid is connected to the charger, the body diodes of PFC stage MOSFETs act as a single phase full bridge rectifier with a large capacitor filter at the DC Bus. The uncharged capacitors, equivalent to a short-circuited path, draw high current from the grid till they become fully charged to the peak grid voltage. This hard charging of DC Bus capacitors can damage the body diodes of the PFC stage MOSFETs.

The peak current that the body diode of MOSFET can withstand is a high pulsed current for few microseconds duration. To avoid current through the body diode for a long duration of time, a diode bridge of sufficiently large rating is connected in parallel. A small resistor to limit the inrush current is sufficient but it should have

large pulsed power handling capability. Two 220Ω resistors have been placed in series with the input lines of the AC-DC stage. The maximum current limited by the resistors is:

$$I_{inpk} = \frac{V_{acinmax}\sqrt{2}}{R_{ch}} = \frac{265\sqrt{2}}{\frac{220}{2}} = 3.43 A$$

The instantaneous power dissipation in charging resistor is around 1.29 kW which is according to the repetitive pulsed power dissipation rating of the rated capacitor.

MOSFET and Diode Requirements:

Referring to the specifications in Table 2, the MOSFETs and the diodes must be rated according to the maximum power handling capability of the charger mode. Apart from voltage and current ratings, losses in the semiconductor devices need to be considered for the device selection as well.

The low frequency switching leg contributes to the conduction losses only. Though the body diodes are sufficient for PFC action, their voltage drop is large and the switching of corresponding MOSFETs minimizes the conduction losses. On the high frequency leg, one MOSFET contributes to the conduction and switching losses. The conduction of body diode of other MOSFET is bypassed through synchronous switching causing zero switching loss in MOSFET and zero conduction loss in body diode. The maximum voltage and current that the MOSFET should withstand is:

$$V_{SWpk} = V_{omax} = 680 V$$

$$I_{SWpk} = I_{Lmax} + \frac{\Delta I_L}{2} = \frac{6600}{200}\sqrt{2} + \frac{15}{2} = 54.17 A$$

The currents in all the four MOSFETs are different, as MOSFETs Q2 and Q4 carry non-pulsating currents (bypassing current in their body diodes) for only one half of the AC cycle (as shown in Figure 10). There is an average current which is equal to the instantaneous grid current and an input voltage dependent ripple current, both are combined in the Q2 current waveform for one half of the AC cycle.

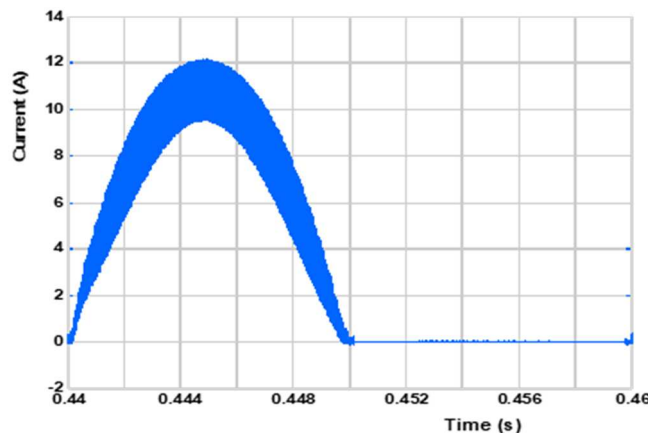


Figure 9: Current through MOSFET Q2 (or Q4)

The RMS value of MOSFET current in one switching cycle is:

$$i_{Q2rms}(\theta) = \sqrt{\left(i_{Q2avg}(\theta)\right)^2 + \frac{(\Delta i_L(\theta))^2}{12}}$$

For continuous conduction mode of operation, the RMS quantity due to the ripple current is:

$$i_{Q2rms}(\theta) \approx \sqrt{\left(i_{Q2avg}(\theta)\right)^2} = \sqrt{\left(\frac{\sqrt{2} P_{in}}{V_{inrms}} \sin(\theta)\right)^2}$$

The RMS value of MOSFET current over one cycle of line voltage is:

$$I_{Q2rms} = \sqrt{\frac{1}{2\pi} \int_0^\pi \left(i_{Q2rms}(\theta)\right)^2 d\theta} = \frac{P_{in}}{\sqrt{2} V_{inrms}}$$

The full load is to be supported for grid voltage up to 200 V. The maximum RMS current stress on MOSFETs Q2 and Q4 is:

$$I_{Q2rms} = I_{Q4rms} = \frac{6600}{\sqrt{2} \times 200} = 23.34 \text{ A}$$

The MOSFETs on the high frequency leg are operating like boost converter with synchronous rectification. The current waveform through MOSFET (Q3) is illustrated in Figure 11, neglecting the inductor ripple current slope for continuous conduction mode.

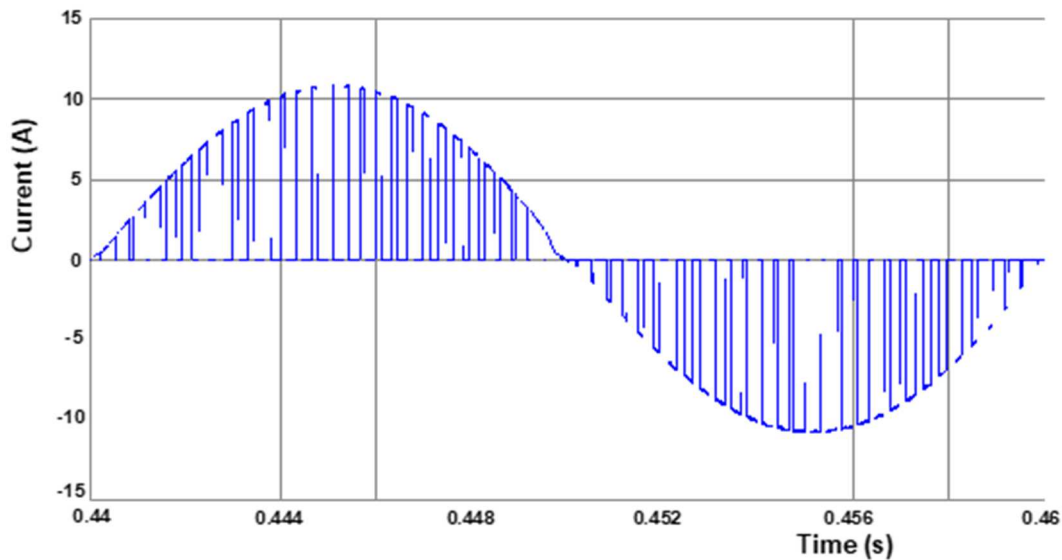


Figure 10: Current through MOSFET Q3

For the positive half cycle of AC voltage, MOSFET current flows from drain to source and for the negative half cycle, the body diode current is by passed through the MOSFET. The RMS current of MOSFET Q3 for each half cycle is:

$$i_{Q3rms+}(\theta) = \frac{\sqrt{2} P_{in}}{V_{inrms}} \sin(\theta) \sqrt{1 - \frac{\sqrt{2} V_{inrms} \sin(\theta)}{V_o}} \text{ for } 0 \leq \theta \leq \pi$$

$$i_{Q3rms-}(\theta) = \frac{\sqrt{2} P_{in}}{V_{inrms}} |\sin(\theta)| \sqrt{\frac{\sqrt{2} V_{inrms} (-\sin(\theta))}{V_o}} \text{ for } \pi < \theta \leq 2\pi$$

The RMS current of MOSFET Q3 for one full cycle of grid voltage is:

$$I_{Q3rms} = \sqrt{\frac{1}{2\pi} \left(\int_0^\pi (i_{Q3rms+}(\theta))^2 d\theta + \int_\pi^{2\pi} (i_{Q3rms-}(\theta))^2 d\theta \right)}$$

$$I_{Q3rms} = I_{Q1rms} = \frac{P_{in}}{\sqrt{2} V_{inrms}} = \frac{6600}{\sqrt{2} \times 200} = 23.34 \text{ A}$$

Power Loss Estimation:

The power loss in the AC-DC stage occurs in all four MOSFETs, the boost inductor and the input EMI filters. There are small losses in the trace resistances. The worst-case loss numbers can be obtained at rated power (6.6 kW) for the minimum input voltage (200 VRMS) and the maximum output voltage (680 VDC).

1. **Conduction Losses in the Boost Inductor:** The maximum possible conduction loss in the main inductor of the AC-DC stage is (using the dc resistance value from datasheet):

$$P_{inductor} = \left(\frac{P_{in}}{V_{inrms}} \right)^2 0.0113 = \left(\frac{6600}{200} \right)^2 0.0145 = 15.8 \text{ W}$$

$$P_{core} = 19 \text{ W at } 680 \text{ VDC link}$$

2. **Conduction Losses in MOSFETs:** Two MOSFETs are in parallel position for each switch of the AC-DC converter and the synchronous rectification is enabled in order to minimize losses in the body diodes. The RMS currents of both high and low frequency switching MOSFETs are the same. The $R_{ds(on)}$ of SiC MOSFETs depend on the gate voltage and the junction temperature as shown in Figure 12. The variation of $R_{ds(on)}$ with the operating current is not large and can be assumed constant.

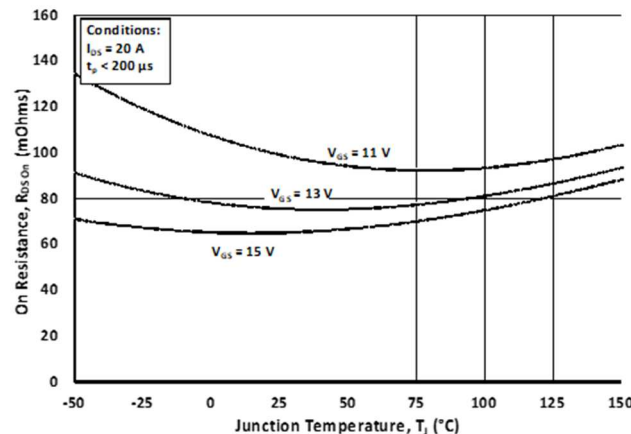


Figure 11: C3M0065100K $R_{ds(on)}$ vs temperature for various gate voltage

From Figure 12, the $R_{ds(on)}$ of MOSFET is approximately 75 mΩ for the gate voltage of 15 V at the junction temperature of 150°C. The conduction losses in each MOSFET pair is:

$$P_{CD-mosfet} = 2 \left(\frac{I_{Q1rms}}{2} \right)^2 0.075 = \left(\frac{23.34}{2} \right)^2 0.075 = 20.42 \text{ W}$$

3. **Switching Losses in MOSFETs:** The switching losses in the MOSFETs Q2 and Q4 are very low as they are switching at the grid voltage frequency. In addition to that, the reverse recovery losses of these two MOSFETs are also very low. The switching losses come into play for MOSFETs Q1 and Q3 as they are switching at 67 kHz. When one of these MOSFETs starts switching as a synchronous rectifier, the body diode turned ON first followed by the MOSFET resulting in ZVS (Zero Voltage Switching). However, the reverse recovery of the body diode will cause switching losses when the other switch turned on. When MOSFETs Q1 or Q3 starts switching as a main boost converter switch, they must dissipate both turn ON and turn OFF losses.

The switching energies for SiC MOSFETs are dependent on the gate resistance and the drain current as shown in Figure 13. The switching energy variation on junction temperature is minimum. For MOSFET Q3, the ON/OFF current in positive half cycle is varying as shown in Figure 11. In the negative half cycle, the switching losses indicates the diode recovery losses:

$$P_{SW-Q3} = \frac{1}{2\pi} \left(\int_0^{\pi} F_s (e_{ON}(\theta) + e_{OFF}(\theta)) d\theta + \int_{\pi}^{2\pi} \frac{1}{2} F_s Q_{rr} U_{dd} d\theta \right)$$

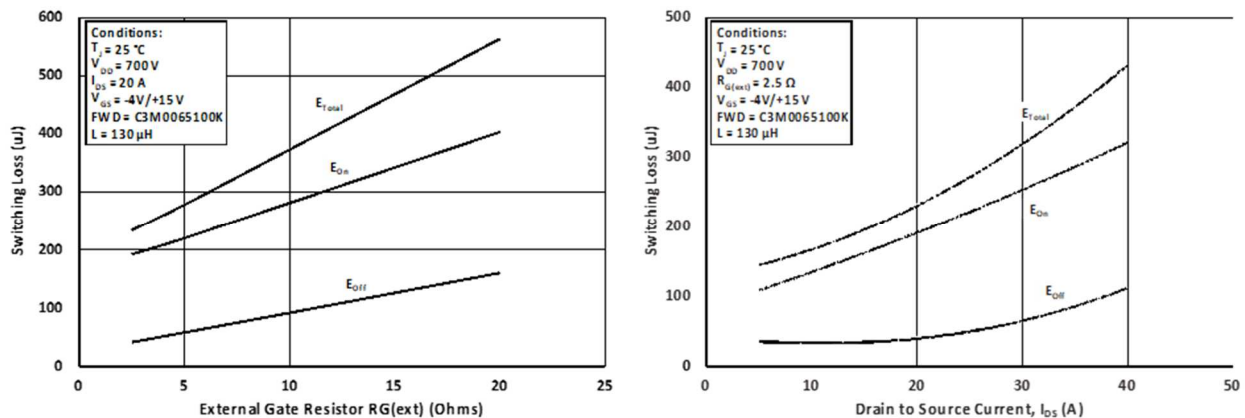


Figure 12: Wolfspeed's C3M0065100K, switching energy vs drain current (right) and switching energy vs gate resistance at 700 V (Left)

The turn ON and turn OFF losses are the functions of instantaneous drain current as shown in Figure 13. The switching loss profile for MOSFET Q1 over one AC cycle is shown in Figure 14. The average switching loss over one AC cycle is computed to be 14.56 W per switch pair.

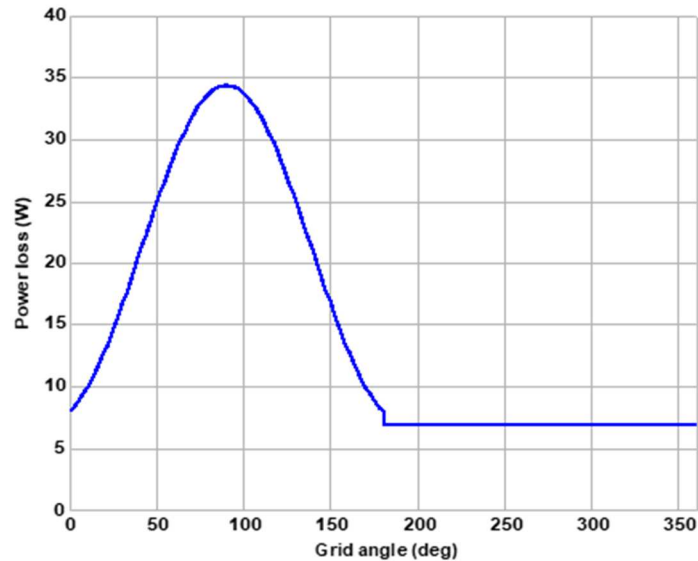


Figure 13: Switching loss for Q1 over one AC cycle

The total losses in the AC-DC stage are:

$$P_{ac-dc\ loss} = (4 \times P_{CD-mosfet}) + (2 \times P_{SW-Q3}) + P_{inductor}$$

$$P_{ac-dc\ loss} = 126.6\ W$$

4.1.2 DC-DC Power Stage

For the DC-DC converter stage, the input voltage is taken from the output of the AC-DC stage. The range of this input voltage is from 390 VDC to 680 VDC with an additional superimposed ripple of 26V. The ripple frequency is approximately equal to the double of the line frequency. The output of the DC-DC power stage is connected to the battery that has an availability of wide voltage range (250 VDC-450 VDC). Galvanic isolation should be required between AC and the battery side. The common topology for isolated DC-DC converter is the phase shifted full bridge topology with a constant switching frequency. Some issues with this topology include ZVS in the primary switches occur for a small range of load; higher leakage external inductance is required to achieve ZVS for larger loads which results in duty cycle loss; for higher battery voltage applications, the turn OFF voltage spike in the secondary switches is higher which further increase the overall losses or designer need to utilize snubbers or active clamp circuits. The use of constant frequency full bridge converter is not recommended for high voltage applications as they have high losses and high EMI issues. Dual active bridge (DAB) options were also explored for DC/DC stage but were not found very suitable. Simulation studies showed that a CLLC converter with its bi-directional property was most suited for this application. Resonant converters are a better choice to achieve low EMI in both high input voltage and high output voltage cases as well.

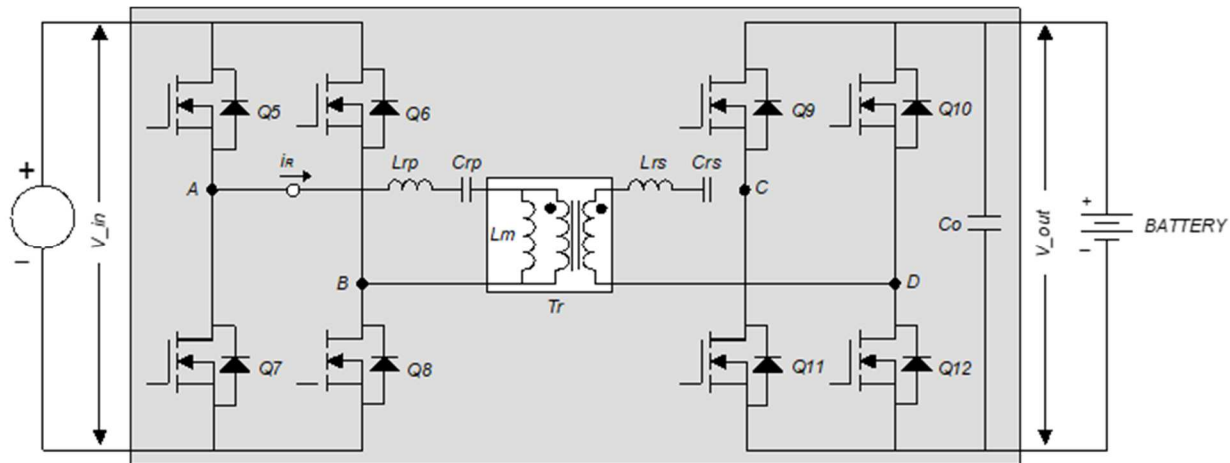


Figure 14: Bi-directional CLLC resonant converter power stage

The DC-DC converter stage is a bidirectional resonant converter or a CLLC converter as shown in Figure 15. This converter is similar to the conventional LLC converter with an additional LC pair on the secondary side. For a wide output voltage range, LLC resonant converter is suitable since ZVS occurs at turn ON for all the switches, leakage inductance is a part of resonance action and resonance frequency can be kept higher to reduce size of the converter.

An LLC resonance converter typically operates at its most efficiency when it operates at resonance frequency. At resonance frequency, turn OFF current is equal to the magnetizing current, and the circulating energy is smaller. Magnetizing inductance loss can be reduced because frequency vs gain characteristic is not required. Some of the efficiency is of course compromised because the PFC inductor is not optimized and leads to higher losses at higher DC link voltage. Still, compared to variable resonance frequency operation, CLLC converter leads to higher overall efficiency. Thus DC-DC stage has been designed to operate at resonance frequency of operation which means that the DC link voltage varies in response to the battery voltage and current.

Referring to Figure 16, L_{rp} , L_{rs} (combined with the leakage inductance) and L_m along with C_{rp} and C_{rs} form a part of resonance network. In battery charging mode, MOSFETs Q5 to Q8 form a full bridge work as quasi square wave generator whereas the body diodes of Q9 to Q12 act as rectifiers and vice versa in the inverter mode. The magnetizing inductance L_m is a part of transformer T_r , which provides galvanic isolation between battery and the grid. The power stage specifications of the DC-DC stage have been shown in Table 5.

Table 5: Specifications of DC-DC Stage

| Parameters | Values | Notes |
|------------------------------|---------------|------------|
| DC Bus Voltage Range | 390 V – 680 V | AC-DC Mode |
| | 480 V-680 V | DC-AC Mode |
| Battery Voltage Range | 250 V – 450 V | AC-DC Mode |
| | 320-450 V | DC-DC Mode |

| | | |
|-----------------------------|----------|---|
| Output Power | 6.6 kW | AC-DC Mode: For battery voltage range of 250 V to 450 V and grid voltage of 200 V |
| | 3.3 kW | DC-AC Mode |
| Isolation Voltage | > 2.5 kV | In both modes for any operating condition |
| Resonance Frequency | 200 kHz | |
| Converter Efficiency | > 98% | |

Converter Analysis and Operation:

The equivalent model for the resonant converter in charging mode is shown in the top portion of Figure 16. The primary side bridge output v_{AB} is a square wave with peak magnitude as of input voltage and switching frequency of F_s . The circuit is in resonance in most of the cases and the current i_p will be sinusoidal. Thus, the voltage v_{AB} can also be assumed to be sinusoidal with fundamental voltage responsible for power transfer. The load resistance can be shifted to the rectifier input and all the components when referred to transformer primary yield a first harmonic approximation (FHA) circuit as shown in lower half of Figure 16.

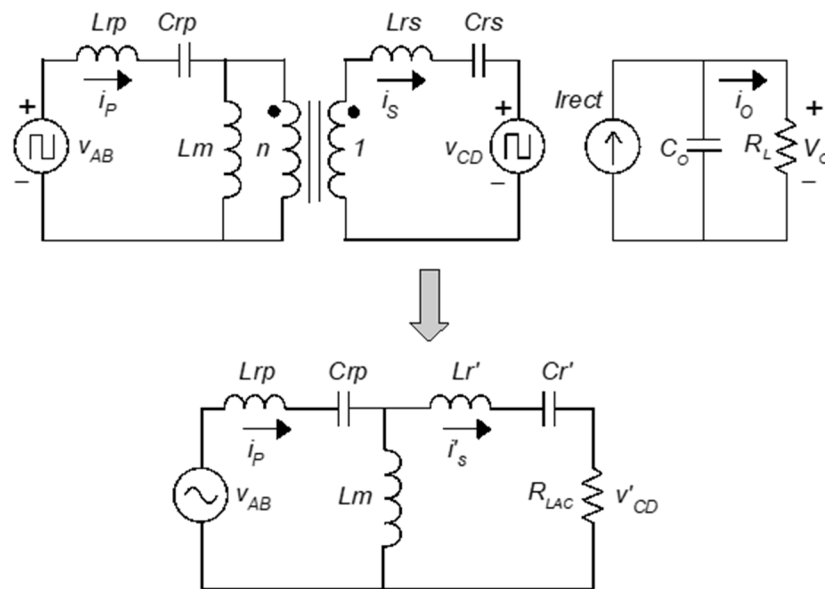


Figure 15: Equivalent circuit (top) and FHA model of resonant converter (bottom)

The approximated sinusoidal voltage of the FHA model is:

$$v_{AB} = \frac{4 V_{in}}{\pi} \sin(2\pi F_s t)$$

The resonant elements and load referred to primary are:

$$L'_r = n^2 L_{rs}; \quad C'_r = \frac{C_{rs}}{n^2}$$

$$R_{LAC} = n^2 \frac{8}{\pi^2} R_L$$

The load side parameters are:

$$I_O = \frac{2n}{\pi} \sqrt{2} I'_S$$

$$V_O = I_O R_L$$

From the FHA model, the converter transfer function to evaluate gain is derived as:

$$\frac{v_{CD}(s)}{v_{AB}(s)} = \frac{Z_m R_{LAC}}{Z_1 Z_2 + Z_1 (R_{LAC} + Z_m) + Z_m (R_{LAC} + Z_2)}$$

Where

$$Z_m = sL_m$$

$$Z_1 = sL_{rp} + \frac{1}{sC_{rp}}$$

$$Z_2 = sL_{r'} + \frac{1}{sC_{r'}}$$

The voltage gain curve for different frequencies at unity transformer ratio are shown in Figure 17. The gain of the converter is unity at primary side series resonant frequency and that is the desired operating point under normal operating condition. For switching frequency higher than resonance frequency, the gain is less than unity and vice-versa.

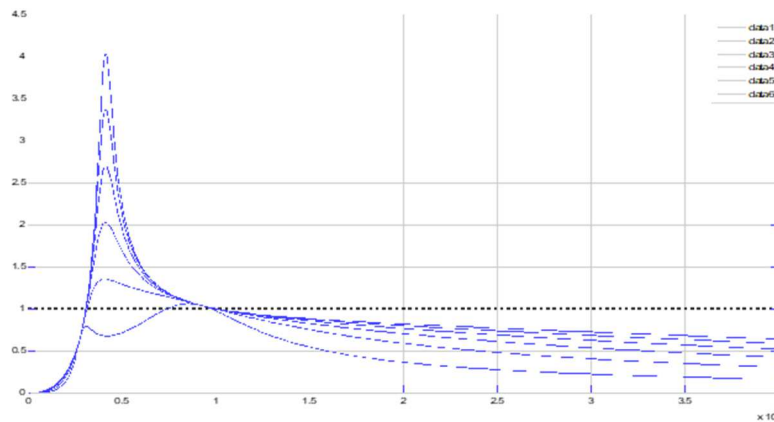


Figure 16: Voltage gain versus operating frequency for different loads

Converter Operation:

This converter operates at the resonance frequency which is decided by resonance elements of primary and secondary side. The gain for this converter is thus always unity, although the converter can operate below or above resonance frequency if required, including during starting when the converter starts at 300 kHz and slowly comes to 200 kHz to avoid inrush current in output capacitors. The primary side MOSFETs turn ON at zero voltage and turn OFF at small current which is equal to the magnetizing current of the transformer at resonance frequency. Secondary MOSFETs turn ON and turn OFF at zero voltage because the body diode of the corresponding MOSFET turns ON before a gate signal is given to the MOSFET.

Low reverse recovery body diode characteristics of SiC diodes are thus utilized here. In case of Si MOSFET, synchronous operation of body diodes may not be possible at this frequency because of their large recovery time. It is to be noted that a very small voltage across body diode is available for reverse recovery and in phase shifted full bridge topology, failures have been reported due to this while using Si MOSFET. The major converter waveforms are shown in Figure 18 with six operating modes for a standard LLC converter. Mode 3 is not present in this converter as it works at resonance frequency.

1. **Mode 1** corresponds to the dead-time duration where no power is transferred to the secondary side of the converter. Primary side current charges drain source capacitance of MOSFETs Q6 and Q7. The current also discharges that of MOSFETs Q5 and Q8 following which it conducts through antiparallel diodes of MOSFETs Q5 and Q8.
2. **Mode 2** corresponds to the instant when MOSFETs Q5 and Q8 are turned ON at zero voltage since body diodes are already conducting. The primary current changes its direction to positive and power is transferred to the secondary. Magnetizing current builds up slowly but L_m doesn't participate in resonance. Mode 2 ends at resonance operation (i.e., when primary current equals the magnetizing current). Also, power transfer to secondary stops at the end of mode 2.
3. **Mode 3** starts when instantaneous primary current meets the magnetizing current. Secondary current is zero and primary current is same as magnetizing current. Magnetizing inductance and primary side resonance elements form a resonant tank till MOSFET Q5 turned OFF.
4. **Mode 4** is again the dead-time duration (and therefore similar to Mode 1) but the internal capacitors of MOSFETs Q5 and Q8 are charged and the internal capacitors of MOSFETs Q6 and Q7 are discharged.
5. **Mode 5** is similar to Mode 2 where MOSFETs Q6 and Q7 are turned ON at zero voltage and power is transferred to secondary diodes of MOSFETs Q9 and Q12.
6. **Mode 6** corresponds to end of resonance in primary and power transfer to secondary. Also, it corresponds to beginning of resonance involving the magnetizing current as in mode 3.

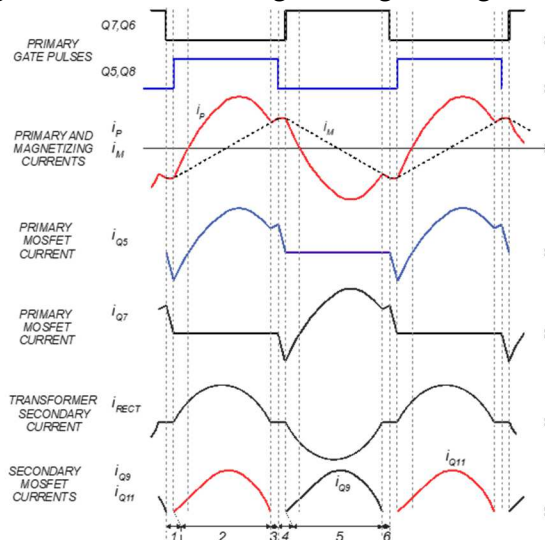


Figure 17: CLLC converter waveforms in charging mode

7. The converter works higher than the resonance frequency during the start and gain is less than unity under that condition so that it can slowly charge the output capacitors.

DC-DC Converter Design:

Design of the resonant network can be an iterative process because the choice of components affects performance parameters like efficiency, regulation, operating frequency range, power loss, and individual component stress. Designing the converter means selecting resonance components and transformer magnetizing inductance apart from turns ratio and dead time. Listed below are certain factors (and certain basic resonant parameters) that a user should consider.

Transformer Turns Ratio:

Considering a minimum DC link voltage of 390V and operation at resonant frequency (gain = 1) with a minimum output voltage of 250 V, the turns ratio with assumption of ideal switches will be:

$$n = \frac{390 \times 1}{250} = 1.56 \text{ (ratio of 1.5 is selected)}$$

Resonant frequency for both primary and secondary:

$$F_r = 200 \text{ kHz}$$

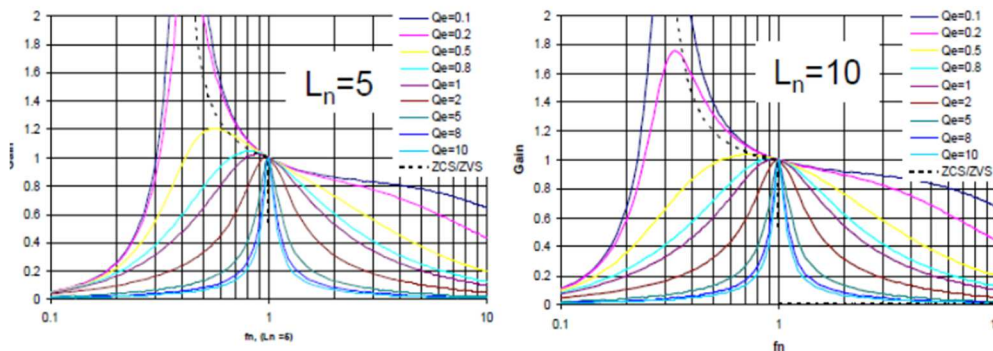


Figure 18: Gain vs frequency characteristics of LLC resonant converter

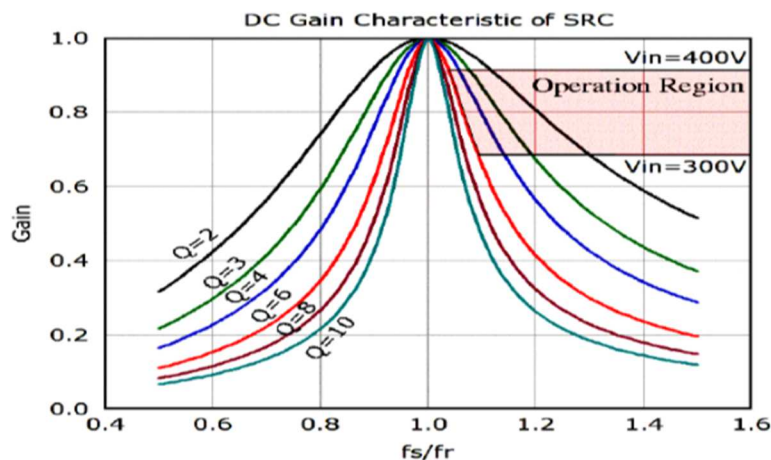


Figure 19: Gain vs frequency characteristics of series resonant converter

Ratio of magnetizing inductance to resonance inductance L_n : The converter voltage gain and operating frequency range depends on L_n . If L_n is small, the operating frequency range is small, and vice-versa. The value of L_n thus can be selected without considering operating frequency. A very high value of L_n would cause the converter to degenerate into a series resonance converter. Figure 19 and 20 shows the characteristics of an LLC

resonance converter and series resonance converter. The difference is that gain of series resonance converter drops sharply above and below resonance frequency.

A value of $L_n(100\mu H) = \frac{L_m}{L_r} = 8$ has been selected here, but a ratio of 10 or even 12 should work equally well. Higher value of L_n shall require a smaller air gap in the transformer which leads to a reduction in flux fringing in the air gap. Higher the value of L_m also means smaller magnetizing current and less conduction losses in transformer.

Design of Resonance Inductor and Capacitor Values:

Let us define $L_{eq} = L_{rp} + L'_r$

& $C_{eq} = C_{rp} + C_r'$

$$Q_p = \frac{L_{eq}}{C_{eq}} \text{-----Value of Q as seen from the primary side}$$

$$Q_p = \sqrt{\frac{L_{eq}}{C_{eq} R_{LAC}}} \text{ where } Q_p \text{ is the value as seen from the primary side.}$$

A starting point for the design of resonance tank can be given now as:

$$Q_p = .5$$

$$L_{rp} = L'_r$$

$$C_{rp} = C_r'$$

$$L_m = L_n * L_{rp}$$

$$F_r = 200 \text{ kHz}$$

Following the above criteria, table below shows the components values obtained:

Table 6: Specifications of DC-DC Stage

| | L_{rp} | L_{rs} | C_{rp} | C_{rp} | L_m |
|---------------------------------|----------|----------|-------------|----------------|-------|
| Values | 11 uH | 4.88 uH | 56 nF | 126 nF | 88 uH |
| Full load voltage stress | | | 280 V (RMS) | 185.12 V (RMS) | |

Where the value of voltage stress across the resonance capacitors have been obtained by the below equation:

$$\text{Peak input current on primary side} = I_{pri} = \frac{6600 * \pi}{390 * .95 * 2} = 27.98 \text{ A}$$

$$\text{Peak input current on secondary side} = I_{sec} = \frac{6600 * \pi}{250 * 2} = 41.46 \text{ A}$$

Here an efficiency figure of 95% has been assumed for the input current and 100% efficiency has been considered for the secondary side current. 6600 W is the rated power and 390 VDC and 250 VDC are the minimum input and output voltages of CLLC converter.

Peak voltage stress on resonance capacitors on primary and secondary side are given by:

$$\text{Peak voltage stress on primary resonance capacitor} = V_{pri} = \frac{I_{pri}}{2 * \pi * F_r * C_{rp}} = 397 \text{ V}$$

$$\text{Peak voltage stress on secondary resonance capacitor} = V_{sec} = \frac{I_{sec}}{2 * \pi * F_r * C_{rs}} = 261.8 \text{ V}$$

Below table shows the actual values which have been used for this prototype:

Table 7: Actual Values of CLLC Resonant Components Used for Prototype

| | L_{rp} | L_{rs} | C_{rp} | C_{rs} | L_m |
|---------------------------------|----------|----------|-------------|-------------|--------|
| Values | 12 uH | 8 uH | 56 nF | 84 nF | 100 uH |
| Full load voltage stress | | | 280 V (RMS) | 277 V (RMS) | |

Selection of Capacitors:

Film capacitors are used for primary and secondary resonance capacitors. Voltage and current rating of these film capacitors must be verified. Requirements of Voltage and Current rating must be satisfied as given in Table 7. Voltage rating of film capacitors reduces significantly with the increment in frequency as shown in Figure 21.

As shown in Figure 21, 6.8nF cap can be used up to 250 V and 2.2nF can be used up to 375 V. For purposes of the measurements below, we used a 4.7nF capacitor.

Power dissipation in resonance capacitors: at 400 V input and 250 V output:

Measured value of ESR on LCR meter=35mohm

$$\text{Power dissipation in each primary resonance capacitor} = I_{pri}^2 * R = 19.8^2 * \frac{0.035}{12} = 1.14 \text{ W}$$

$$\text{Power dissipation in each secondary resonance capacitor} = I_{sec}^2 * R = 27.8^2 * \frac{0.035}{18} = 1.67 \text{ W}$$

$$\text{Power dissipation in each primary resonance capacitor} = .095 \text{ W}$$

$$\text{Power dissipation in each secondary resonance capacitor} = .083 \text{ W}$$

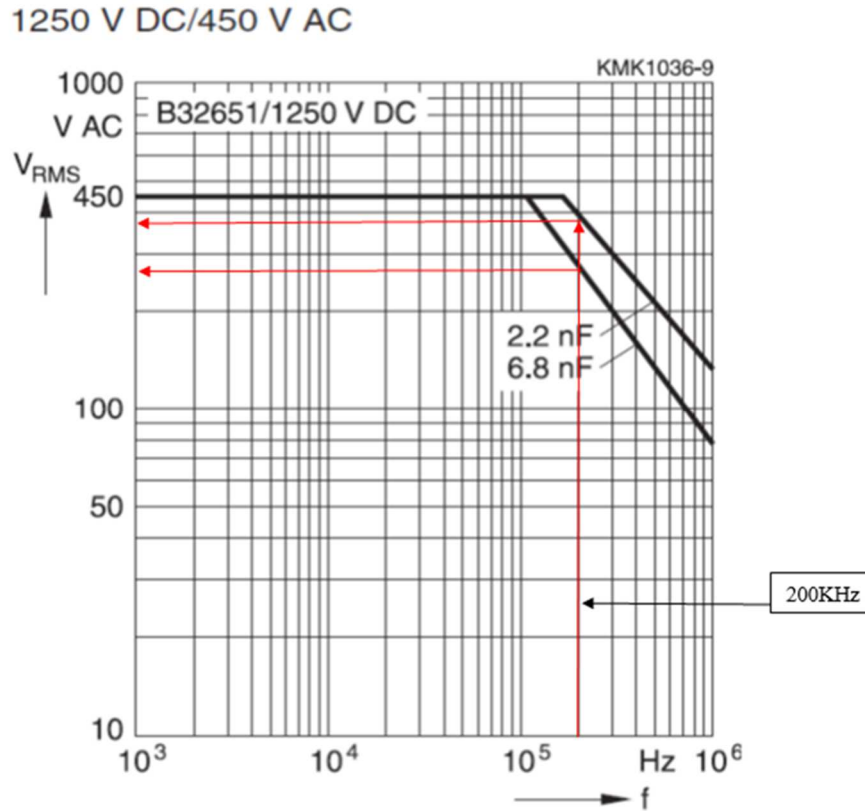


Figure 20: Frequency vs AC voltage rating of resonant capacitor

Following table indicates the details of the CLLC resonance inductor:

Table 8: CLLC Resonant Inductor Details

| | Value | Core | Turns | Rdc | Res loss | Cor loss |
|----------|------------|------------|-------|----------|----------|----------|
| L_{rp} | 12 μ H | EE42/21/15 | 18 | 9.8 mohm | | |
| L_{rs} | 8 μ H | EE42/21/15 | 12 | 4.6 mohm | | |

Design Flow Chart of CLLC Bi-Directional Resonance Converter:

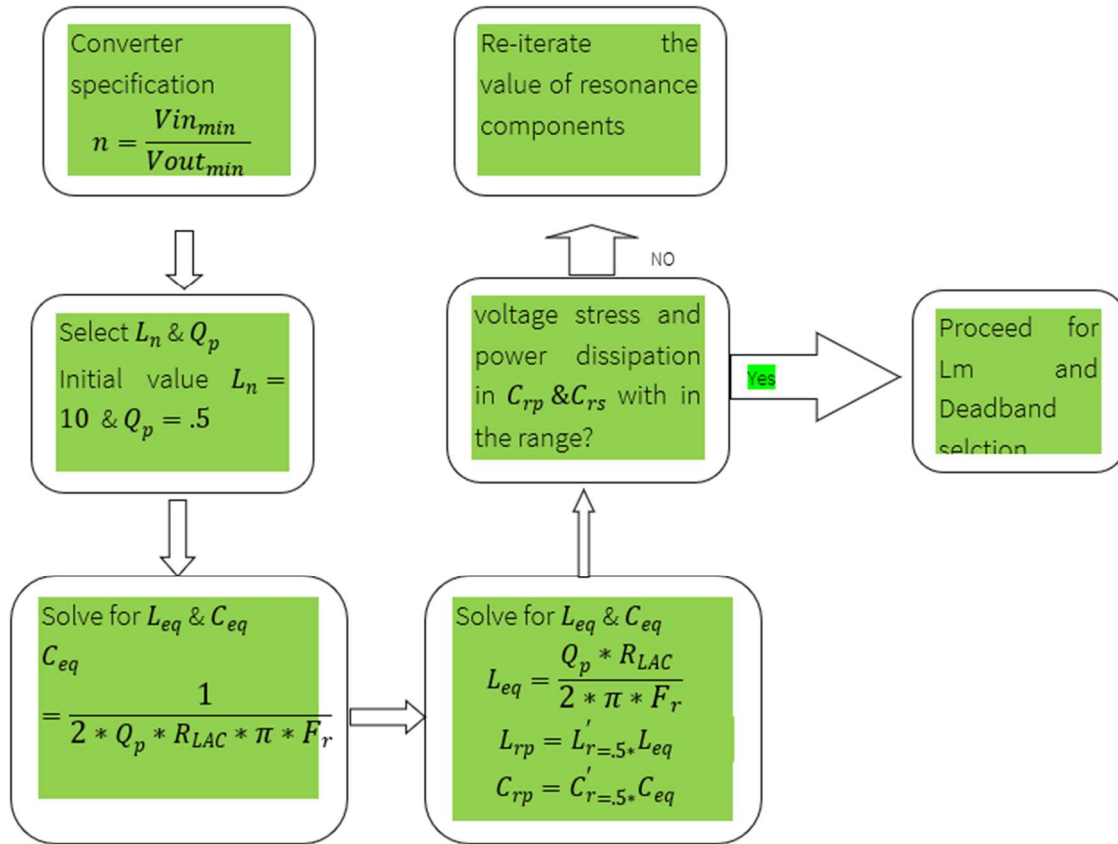


Figure 21: Design flow chart of CLLC bi-directional resonance converter

A Check on the Value of Magnetizing Inductance:

A fixed frequency DC/DC converter provides flexibility in choosing magnetizing inductance L_m as compared to a variable frequency inverter but the value still has to be designed to ensure that ZVS of the primary switch happens during the dead time. The methodology described below can be used to check ZVS of primary switches.

$$.5 * (L_r * I_m^2 + L_m * I_m^2) \geq .5 * 4 * C_{oss} * V_{dc}^2$$

As $L_m \gg L_r$ this condition can be reduced to:

$$.5 * (L_m * I_m^2) \geq .5 * 4 * C_{oss} * V_{dc}^2$$

Where C_{oss} is the energy related output capacitance of the MOSFET:

I_m (magnetizing current) can be given as:

$$I_m = \frac{V_{dc} * T}{L_m * 4}$$

Putting value of I_m in equation 1:

$$L_m = \frac{T^2}{(64 * C_{oss})}$$

Putting the actual value for this design $T=5\mu\text{sec}$ and $C_{oss}=80\text{pf}$, the value of $L_m=4882\ \mu\text{H}$.

This is the maximum value of magnetizing inductance above which energy in magnetizing inductance is less than the C_{oss} energy. In fact, the value of magnetizing energy must be more than 10 times the capacitive energy so that magnetizing current remains constant during the dead time which may put a limit of $L_m=488\ \mu\text{H}$ for this application.

Another constraint arises as a result of dead time. ZVS of the primary switch must happen during the dead time provided. If the magnetizing current I_m remains constant during dead time (T_d) (which is likely because the energy in L_m is much larger than capacitive energy), it is likely that I_m charges and discharges C_{oss} linearly.

$$I_m = \frac{4 * C_{oss} * V_{dc}}{T_d}$$

By putting the value of I_m in L_m equation:

$$L_m = \frac{(T_d * T)}{(16 * C_{oss})}$$

Using a dead time of 200nsec and value of other parameters mentioned in the above equation, the value of $L_m=781\ \mu\text{H}$. Again, L_m value must be lower than this value so that ZVS is obtained within the dead time (preferably with more than a 100% margin so that other parasitic capacitances and variation in C_{oss} of the MOSFETs are taken into consideration). A value of $100\ \mu\text{H}$ has been used for purposes of this design to achieve ZVS within deadtime.

The frequency Vs gain characteristics at 10% of load ,50% load and 100% load are given in Figures 23 and 24. These gain curves have been obtained by simulation and using values which have been used in actual prototype. There is not much difference between $100\ \mu\text{H}$ and $200\ \mu\text{H}$ curves except at very light load. This converter is supposed to work at resonance frequency with unity gain so it makes sense to have a higher magnetizing inductance and consequently lower magnetizing current which increases the efficiency due to lower overall current in the transformer.

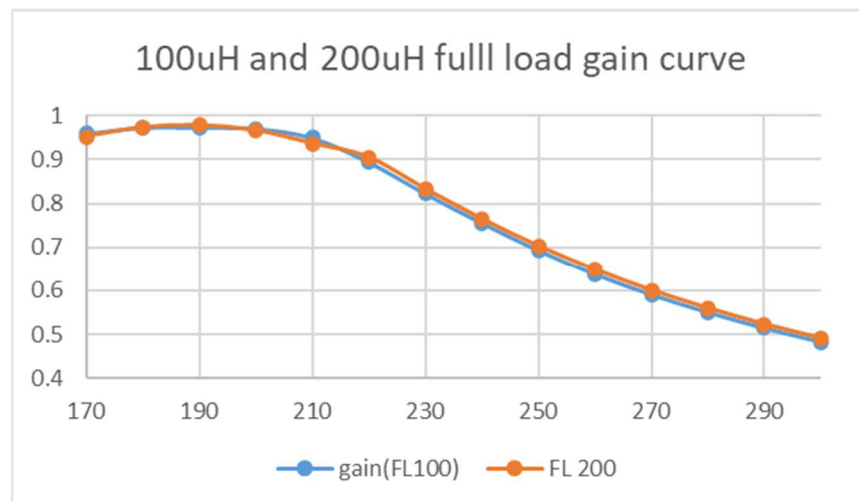


Figure 22: Gain vs frequency of CLLC for 100 uH and 200 uH L_m @ full load

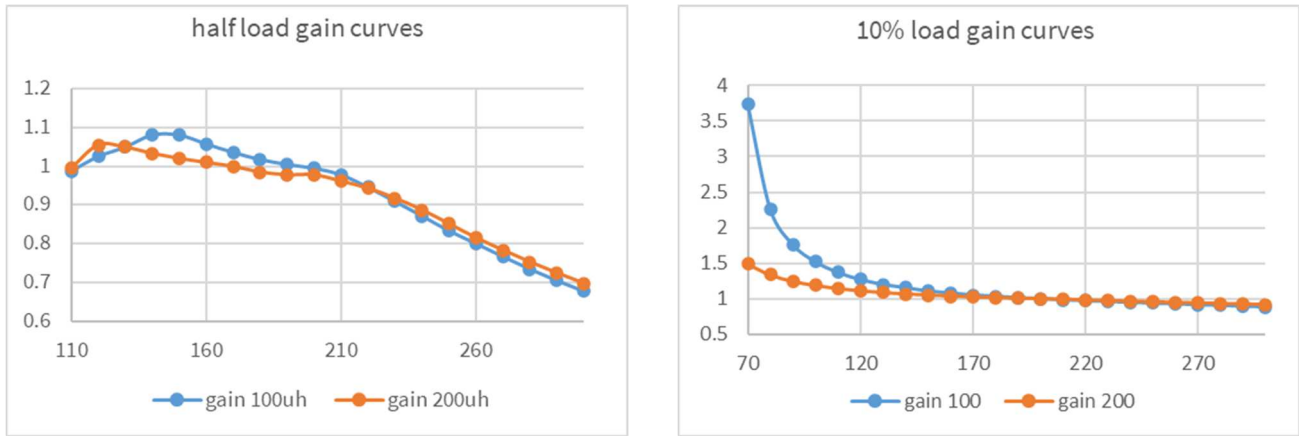


Figure 23: Gain vs frequency of CLLC for 100 uH and 200 uH Lm @ half load and 10% load

Selection of Dead Time for Primary CLLC MOSFETs:

Complementary (top & bottom) MOSFETs of CLLC converter are gated after a dead time of Td as shown in Figure 25.

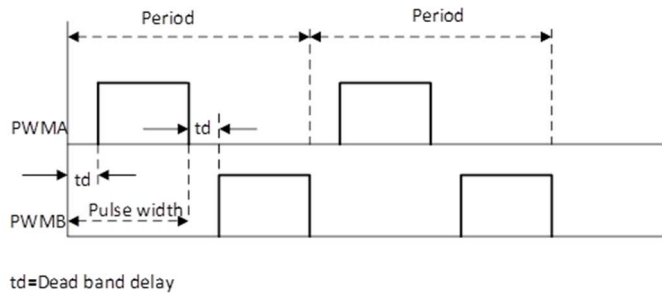


Figure 24: CLLC gate waveform showing deadtime

The design of this dead time is important for the converter operation. Apart from ensuring that the complementary MOSFETs do not get shorted, another very important function of dead time is to provide ZVS of CLLC MOSFETs. Too little or too high a dead time affects the converter operation and efficiency as shown in Figure 26.

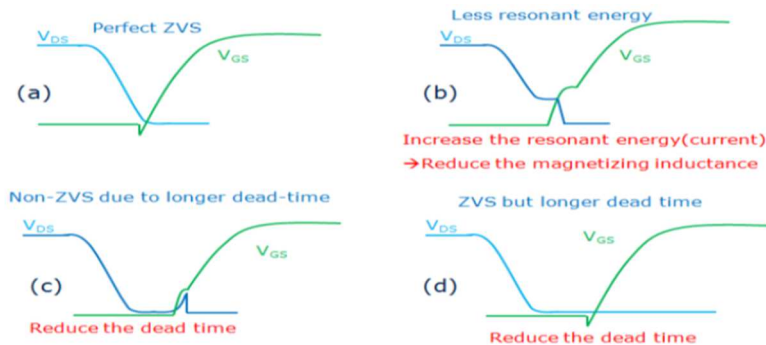


Figure 25: CLLC deadtime and ZVS relation

Equation for dead time for full bridge CLLC converter is given by:

$$T_d = 4 * C_{oss}(cir) * \frac{V_{dc}}{I_{mag}}$$

where C_{oss} (cir) is the MOSFET output capacitance (circuit related).

If we assume $C_{oss}=80\text{pf}$; for 1000 V, 65mohm part:

$$T_d=4*80e-12*400/5=25.6\text{nsec for 400 VDC bus}$$

$$T_d=4*80e-12*680/8.5=25\text{nsec for 680 VDC bus}$$

Following dead times can be tabulated for magnetizing inductances of 100 μH and 200 μH :

Table 9: Dead Time Required for 100 μH and 200 μH Lm

| | 100 μH | 200 μH |
|-------------|-------------------|-------------------|
| 400 VDC bus | 25.6 nsec | 51.2 nsec |
| 680 VDC bus | 25 nsec | 50 nsec |

It appears that T_d is independent of DC bus voltage magnitude because I_{mag} also changes with the DC bus voltage. Dead time given in the present design is 200 nsec so either we land with condition (c) or condition (d) as shown in Figure 26. If resonance frequency of the converter is high, condition (c) is more likely due to short resonance current period. Condition (c) results in non-ZVS condition of the converter, while condition (d) only results in some loss of duty cycle.

Computation to Avoid Condition (c):

A user should attempt to avoid condition (c) (as shown in Figure 26) because of the extra reverse recovery losses in MOSFET body diode, loss of duty cycle, disruption in normal resonance cycle, and non-ZVS condition during switch ON that arise from condition (c). Set forth below is the maximum value of dead time that should be allowed in order to avoid condition (c).

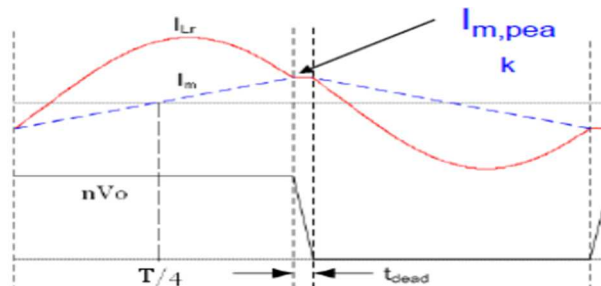


Figure 26: CLLC dead time and ZVS condition

If the dead time is extended beyond the value shown in Figure 27, I_{mag} decreases linearly and normal resonance cycle occurs through the body diode of the MOSFETs. If pulses are switched ON before the primary current has gone to zero then the normal resonance continues through the MOSFET. If not, the total primary current comes to zero, buildup of magnetizing current stops at zero and body diode starts recovering, which builds up the voltage in the MOSFET and leads to non-ZVS condition.

Equation for current beyond when voltage across the MOSFET has gone to zero can be written as:

$$I_{mag} * (1 - t/(.25 * T)) = I_{peak} * \text{Sin}(wt)$$

Now I_{peak} for a 6.6 kW converter at 400 VDC bus is given by 26 A and for 680 VDC bus is given by 15.2 A.

The primary current reaches zero when the magnetizing current= $I_{peak} \sin(\omega t)$

The above equation can be used to compute a value of time which can be allowed beyond computed dead time given in Table 9. Since the equation is non-linear, it can be used numerically and values for 400 VDC are given in Table 10.

Table 10: Computed Dead Time for 400 VDC Bus Condition

| 400V DC Bus Condition (Time) | I_{mag} (Amp) | $I_{peak} \sin(\omega t)$ (Amp) |
|------------------------------|-----------------|---------------------------------|
| 50 nsec | 4.8 | 1.6 |
| 100 nsec | 4.6 | 3.25 |
| 150 nsec | 4.4 | 4.87 |
| 200 nsec | 4.2 | 6.46 |

As reflected in Table 10, at around 150 nsec, resonance current is equal to magnetizing current which extends the dead time above ((150 nsec+25 nsec)=200 nsec)) and leads to non-ZVS condition. Table 11 reflects similar computations for 680 V condition.

Table 11: Computed Dead Time for 680 VDC Bus Condition

| 680V DC Bus (Time) | I_{mag} | $I_{peak} \sin(\omega t)$ |
|--------------------|-----------|---------------------------|
| 50 nsec | 8.16 | .95 |
| 100 nsec | 8.14 | 1.9 |
| 150 nsec | 7.48 | 1.64 |
| 200 nsec | 7.14 | 3.78 |
| 300 nsec | 6.46 | 5.59 |
| 350 nsec | 6.12 | 6.47 |

For 680 V operation, this condition arrives at around 300 nsec which can be tolerated up to (300+25) = 325 nsec (maximum delay).



400 V Operation



680 V Operation

Figure 27: Comparison of ZVS for 400 V (left) and 680 V (right) operation

The oscilloscope waveforms (as shown in Figure 28) show the validity of the concept. On the left side of Figure 28, from 400 v operation and 300 nsec dead time, it clearly shows the effect of non-ZVS condition (green waveform dip), while on the right side of Figure 28, from 680 V operation and 300 nsec dead time, there is no non-ZVS condition. This dip vanished when the dead time was brought down to 200 nsec. These calculations illustrate that this phenomenon does not occur at light load because I_{image} takes around $T/4$ time to go to zero.

Selection of Dead Time Between Primary CLLC MOSFETs and Secondary CLLC MOSFETs:

Another important criterion is to select the dead time between the turn ON of the primary CLLC MOSFETs and secondary synchronous MOSFETs. ZVS of synchronous MOSFETs happens due to the resonance load current.

The dead time required shall be defined by the equation:

$$T_{\text{dead}} = \frac{4 * C_{\text{oss}} * v_{\text{out}}}{I_{\text{m}} * \sin(\omega t)}$$

where I_{m} is the load current amplitude in secondary.

Integrating the above equation, we get

$$T_{\text{dead}} = \frac{\cos^{-1}(1 - C_{\text{oss}} * V_{\text{out}})}{I_{\text{m}}}$$

This equation can be solved for the dead time which is load current dependent. It is clear that the lower load requires higher dead time and vice versa. Failure to observe this condition may result in non ZVS operation of the synchronous MOSFETs.

DC-DC Transformer Design:

Input voltage = 480 V rated at 320 V battery output

Output voltage = 320 V

Maximum output power = 6600 W

Maximum output current = 22 A

DC DC normal efficiency = 98%

$$\text{Turns ratio} = n = \frac{VPFC_{nom}}{V_{o_{nom}} + 0.5} = 1.5$$

$$I_{o_{nom}} = \frac{P_o}{V_{o_{nom}}} = 20.625 \text{ A}$$

Transformer Window Coefficient $Kw_t = 0.35$

Set $Bmax_t = 0.12T$ single quadreant

Primary current density $Jmax_{tp} = 5A/mm^2$

Frequency of DC DC = $freq_{dcdc} = 200 \text{ kHz}$

$$\text{Minimum required AeAw of the transformer} = \frac{Lm * I_{pk_{nom}} * I_{rms_{nom}}}{Bmax * Kw_t * Jmax_{tp}} = 1.901 * 10^{-7} m^4$$

For PQ50 50

$$Ae = 328 \text{ mm}^2$$

$$\text{Number of secondary turns} = Nts = \frac{V_{o_{nom}} + 0.4}{4 * Bmax * Ae_{pq5050} * freq_{dcdc}} = 10.213$$

$$\text{Max number of secondary turns} = Nts_{max} = \frac{V_{o_{max}} + 0.4}{4 * Bmax * Ae_{pq5050} * freq_{dcdc}} = 14.342$$

Actual secondary turns = 12

Actual Primary turns = $1.5 * 12 = 18$

$$\text{Air gap required} = lg_{tf} = \frac{u_0 * N^2 * Ae_{pq5050}}{Lm} = 1.423 * 10^{-3} \text{ m}$$

Based on the skin depth, AWG38 of litz wire 350 numbers in parallel are used in primary and

Total DC resistance of the transformer primary = 13.7mohm

Total DC resistance of the transformer secondary = 5.46mohm

4.1.3 Control Structure of the Converter

There are two completely separate converters running in cascade: a) a Totem-pole PFC converter and b) a fixed frequency CLLC converter (as shown in Figure 29). Both are bi-directional and both run independently. The PFC converter has a 2 loop structure (as shown in Figure 34). The outer voltage loop controls the DC link voltage and generates a reference for inner current loop. The inner current loop maintains a sinusoidal current which is in phase with the input grid voltage. CLLC converter always runs at fixed frequency (resonance) and does not have any kind of closed loop control.

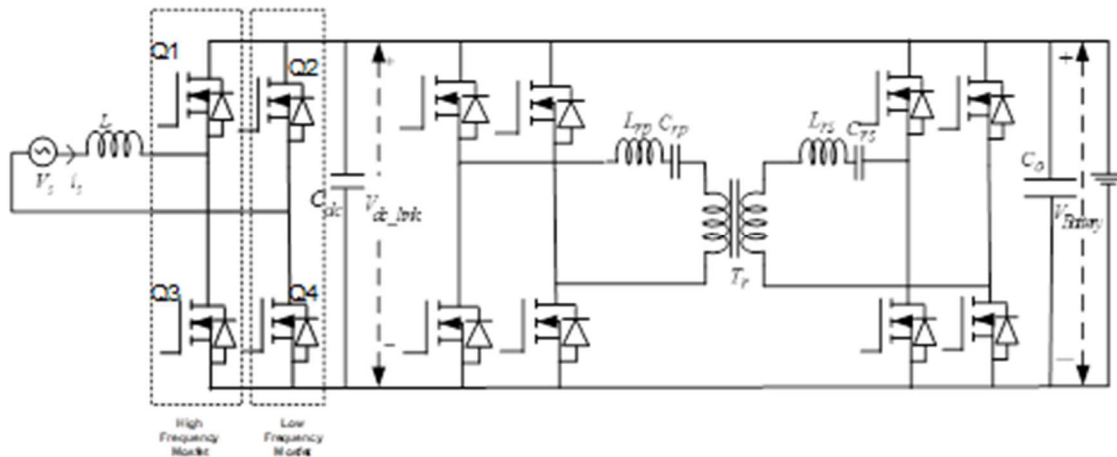


Figure 28: System schematic diagram

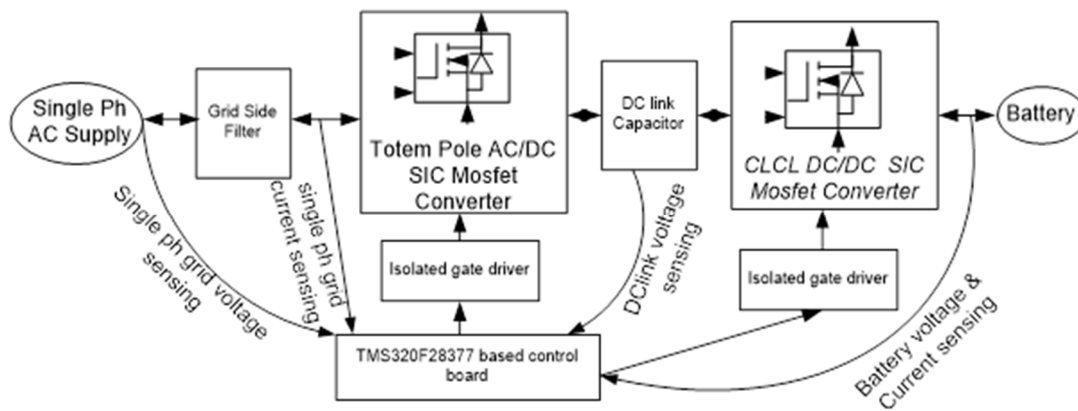


Figure 29: Signal interconnection diagram

Figure 30 shows the control block diagram of the converter as implemented. Control blocks have been implemented on a Texas Instruments® (P/N: TMS320F28377) Delfino® floating point processor. Please refer to the schematic of the DSP board (as shown in Appendix) for detailed hardware circuit description. Coding has been done in CCS platform.

Referring to the control block diagram in Figure 34, V_{DC_ref} is set based on output voltage and V_{DC_fb} is the DC link voltage. PI (Proportional Integral) voltage controller is implemented based on PI compensator whose frequency bandwidth is set to a low value. Current reference thus generated is added with output current which acts as feed forward for fast dynamic response. Resulting signal is multiplied with sinusoidal signal obtained from PLL (Phase Locked Loop) to set the current reference for the current loop. This reference signal is in phase with input grid voltage and tracks it at every point in time.

Selection of PLL for the Converter:

PLL is required to track the phase and frequency of the signal in a grid connected system. A robust design of PLL should be able to track the grid voltage and frequency despite considerable noise in the system and should be fast enough to detect a phase or frequency change. Commonly adopted PLL configurations for single phase systems are inverse park PLL, second order generalized integrator (SOGI) PLL and enhanced PLL (EPLL).

It has been widely reported in literature that EPLL is the least sensitive PLL to the disturbances like DC bias, harmonics and phase jump, so, EPLL was adopted for this converter. Figure 31 shows the block diagram of EPLL.

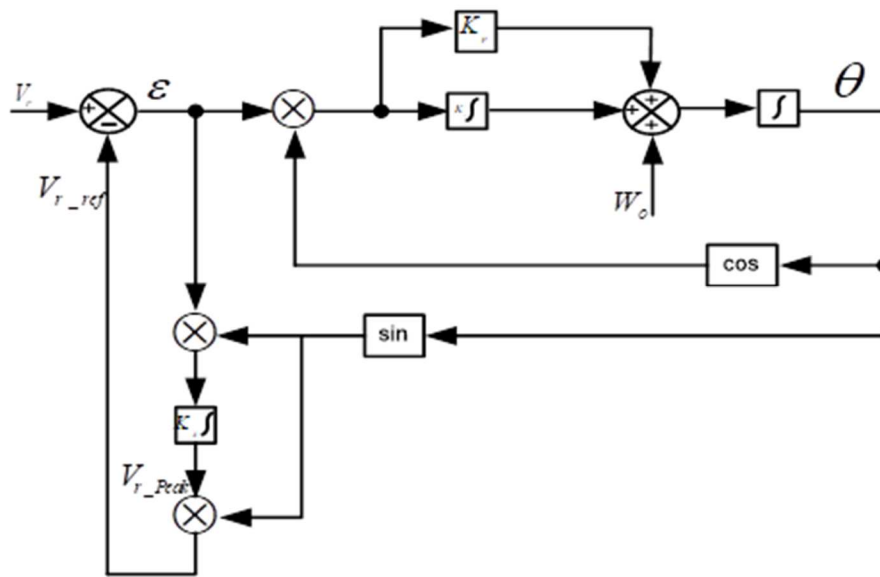


Figure 30: EPLL block diagram

There are 2 types of controllers which act on the current error obtained after the subtraction block. First is typically used as a PI compensator and second is a string of resonance controllers. PI compensators are typically used for DC signals. The error signal here is sinusoidal and the integral part in PI compensator leads to a phase difference between the error signal and its response because unlike a DC signal it cannot settle to a steady state value. Figure 32 shows the response of various compensators to the sinusoidal signal. It can be seen that the integral response is delayed by 90 degrees and the proportional response exactly mimics the input signal. PI response thus would be an addition of the response of P and I signals.

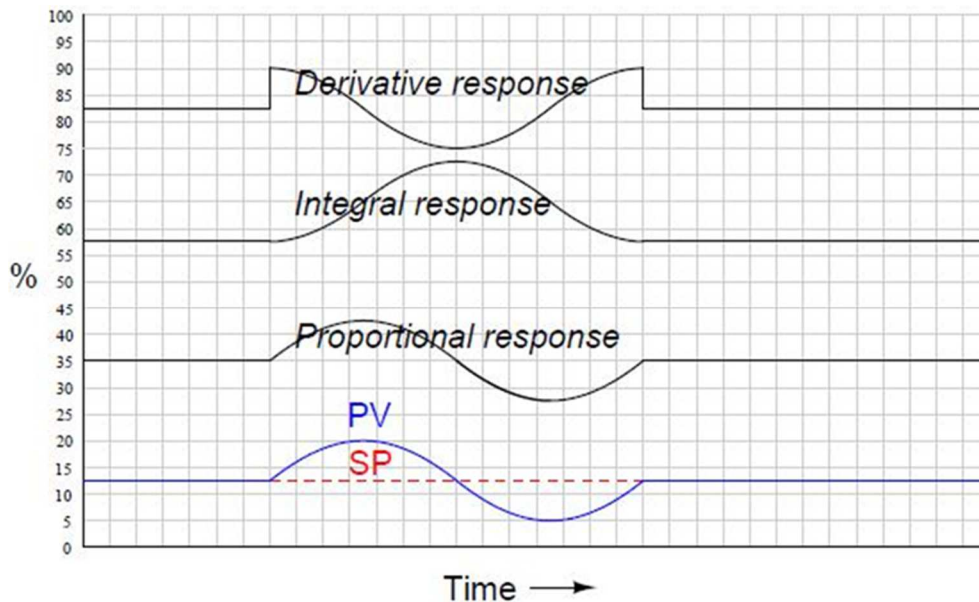


Figure 31: Response of various compensators to the sinusoidal signal

Delayed response of the controller is undesirable and would lead to phase error in tracking as well as overshoot and undershoot under transient conditions. One way to solve this problem is to have a larger P part and smaller I part but P part larger than a certain value leads to oscillations. If we are using DSP, in that case P & I can be tuned for different values of load and best values of P * I can be tabulated in the processor. The problem of phase lag can be more severe if the error signal consists of signals which are the harmonics of fundamental and very difficult to be compensated without considerable phase lag.

A better approach could be to use resonance controller for time varying signals. If it is assumed that the error signal consists of a DC part and various harmonics of sinusoidal signals, then DC part can be compensated with normal PI compensator and AC portion can be compensated with resonance controllers. Since resonance compensators are tuned to a particular frequency, not all harmonics can be compensated and those which are dominant should be compensated. In this application, it can be safely assumed that the error signal does not have a DC component and it consists of fundamental of line frequency and its harmonics. In that case, the fundamental can be compensated with PI controllers and harmonics can be compensated with resonance controllers. It is possible to compensate fundamental with the resonance controllers as well.

Table 12: Controllers and Their Transfer Functions

| Controller | Transfer Function |
|--------------|---|
| PI | $K_p + \frac{K_i}{s}$ |
| Ideal PR | $K_p + K_i \left(\frac{s}{s^2 + \omega_0^2} \right)$ |
| Practical PR | $K_p + K_i \left(\frac{2\omega_c s}{s^2 + 2\omega_c s + \omega_0^2} \right)$ |

Response of the PR controller is shown in Figure 33.

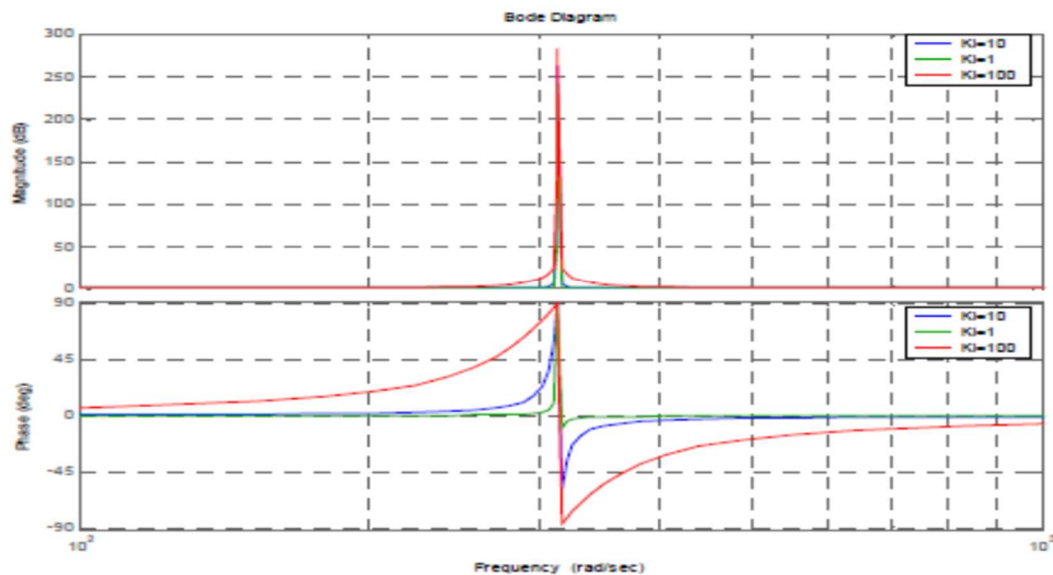


Figure 32: Response of resonance controller tuned to a particular frequency

Figure 33 shows that if the response of resonance controller is tuned to a particular frequency, it has infinite gain for the selected frequency and no gain for the other frequency components. In this application, PI compensator has been used for the fundamental frequency and resonance controllers have been used for the 3rd, 5th, 7th, and 11th harmonics.

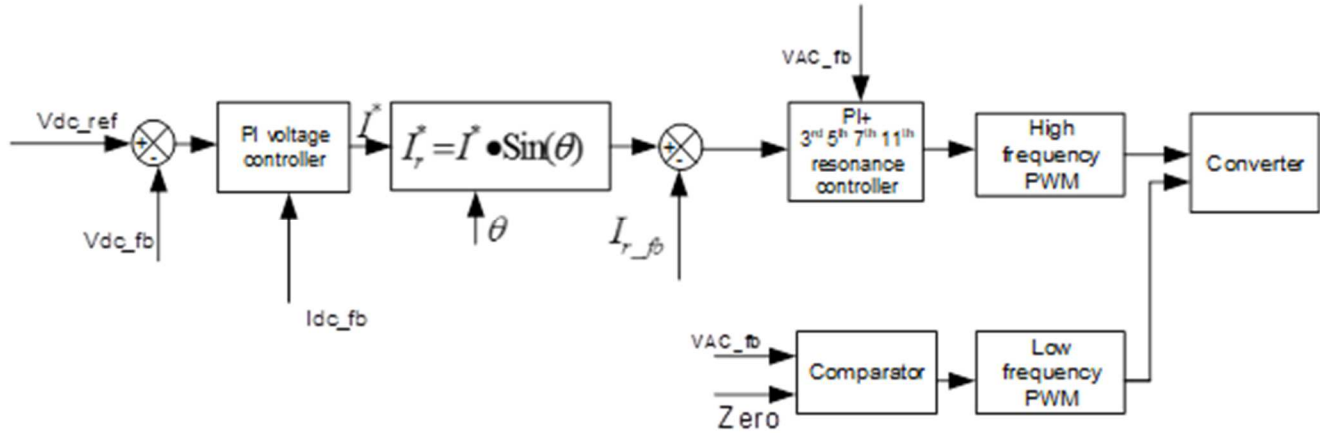


Figure 33: System control block diagram

4.1.4 Gate Drive Circuitry

The gate drive circuitry is based on isolated gate driver ICs (Integrated Circuits) with up to 1200 V isolation on the high voltage side and 3.75 kV isolation on the battery side. A dual rail supply is used to prevent unintentional turn ON of MOSFETs. The requirement of gate drive power with a gate drive voltage swing of 15 V and -2.5 V is:

$$P_{gate(ac-dc)} = V_g Q_g F_s = (15 + 2.5) \times 35n \times 67k = 0.04W$$

$$P_{gate(dc-dc)} = V_g Q_g F_s = (15 + 2.5) \times 35n \times 200k = 0.122W$$

The isolated dual polarity gate driver supplies for each driver IC is generated from an isolated DC-DC converter module (P/N: QA15115 from MORNSON) powered up by external 15 V source as in Figure 35. The power supply module generates dual supply of +15 V and -2.5 V with each output capable of handling 100 mA current. The module also provides isolation of up to 3.5 kV.

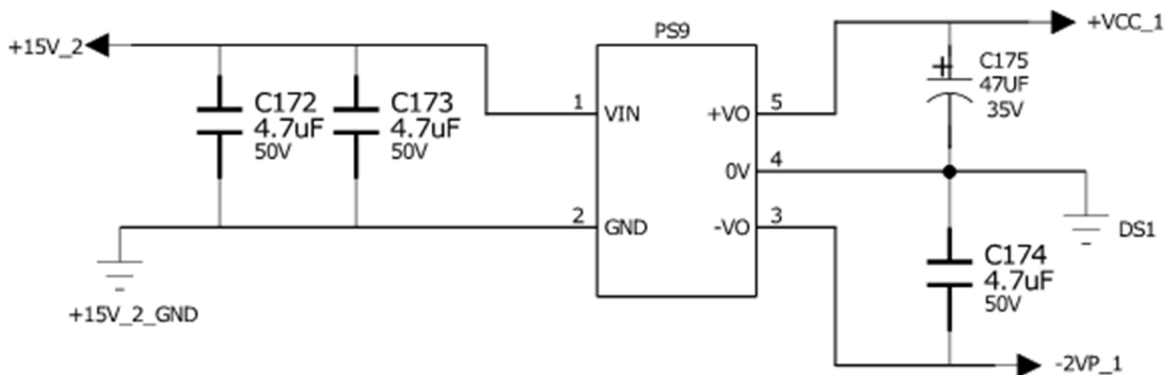


Figure 34: Gate driver supply using QA15115R2

Note: While designing the isolated driver, designers must evaluate the Input and output parasitic capacitances.

Gate Drive Circuitry for High Voltage Side MOSFETs:

The high voltage side MOSFETs are driven using an Infineon Technologies AG gate driver (P/N: 1EDI30I12MHXUMA1) as shown in Figure 36. The driver features 3A peak source and sink current capability, up to 1200 V isolation and active miller clamp for gate which along with the negative supply provides an additional protection against parasitic turn ON of the MOSFET. The input is driven from 3 V to 15 V range signals and supports direct CMOS level signals.

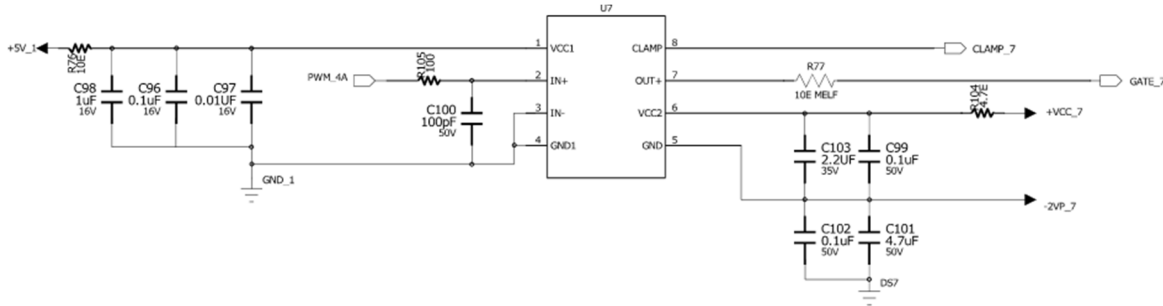


Figure 35: Gate drive circuitry with IEDI30I12MHXUMA1

The non-inverting PWM input to the driver comes from the controller through a 5V output level buffer. A small filter network (R105 and C100) is placed close to input pins. The buffered input and 5V bias supply is routed from the control card. RC filtering of the control and driver side supply provides another level of supply noise immunity. The driver output is connected to the gate pin through the gate resistance and the clamp pin is directly connected to the gate pin close to the MOSFET.

Other functional features with the gate driver IC are:

1. Operating bias voltage of up to 17 V on input side and 18 V on output side. Under-voltage protection at 2.85 V and 12 V on input and output sides respectively below which the output is held low.
2. Low internal voltage drop in driver intended to ensure lower driver dissipation
3. Clamping of the gate voltage to supply voltage when the gate voltage rises in the event of short circuit because of feedback through Miller capacitance
4. Active Miller clamp protection (including when the MOSFET is in OFF state) can turn ON in a half bridge configuration. The dv/dt of the MOSFET while turning ON causes a current to take a path through the gate pin. The clamp pin sinks this current across a low impedance path by monitoring the gate voltage

Note: Designers must take care of the propagation delay while designing the driver.

Gate Drive Circuitry for Battery Side MOSFETs:

The battery side MOSFETs are driven from an isolated gate driver (P/N: Si8261BCC-C-IS from Silicon Laboratories, Inc.) as shown in Figure 37. The driver is capable of supporting gate current of up to 4 A with input to output isolation of about 3.75 kV. The output of the driver follows the input current through the LED. The current through the input LED of driver should be greater than 6 mA for output to rise. To support this current, a non-inverting buffer IC (P/N: MCP1402 from Microchip Technology) is used.

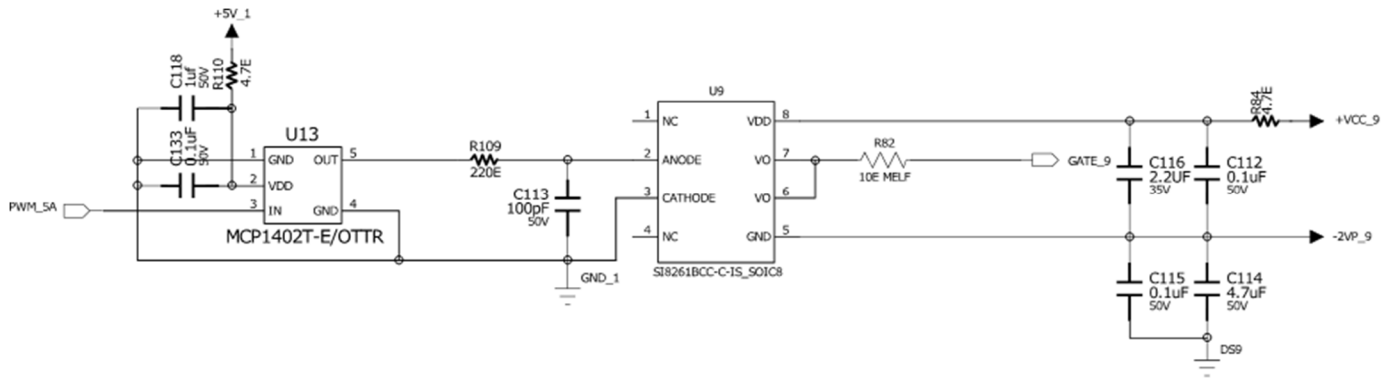


Figure 36: Gate drive circuit using Si8261BCC-C-IS

The input of the buffer is TTL and CMOS logic level compatible and is driven by a level shift IC in control card. The output is non-inverting and has peak voltage magnitude of 5 V. The input current to the driver IC is limited by using a current limiting resistor such that:

$$I_F = \frac{5 - V_F}{R_F} > (I_{Fon} = 6 \text{ mA})$$

The driver input current is limited to 10 mA. With the maximum LED forward drop voltage of 2.8 V, the current limiting resistor selected is 220Ω.

On the driver output side, the isolated supply is generated through isolated DC-DC converter modules (as shown in Figure 35). The driver IC has a UVLO threshold of 7.9 V and 0.5 V hysteresis below which the output is pulled low irrespective of input current. A similar feature is implemented for input LED current also (as shown in Figure 37).

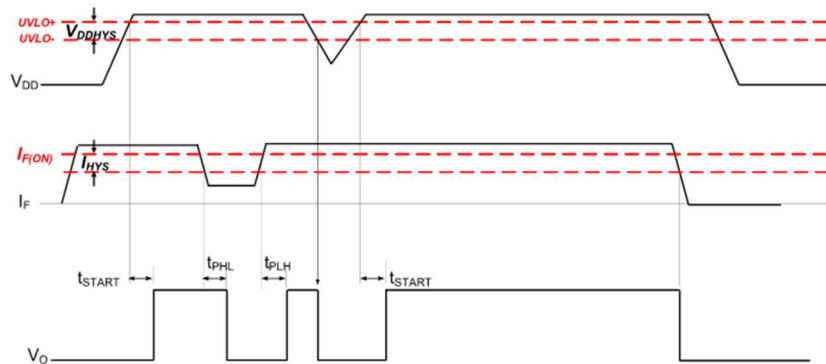


Figure 37: Input and output supply protections for Si8261BCC

The internal resistances of the driver will dissipate some power depending on the current drawn by the gate, and the power dissipated in input diode and the IC internal power consumption is:

$$P_{driver} = (V_{DD}I_{DD}) + (V_F I_{Favg}) + \left(\frac{1}{2} Q_G V_G F_{SW} \left(\frac{R_{OH}}{R_{OH} + R_G} + \frac{R_{OL}}{R_{OL} + R_G} \right) \right)$$

The driver current requirement I_{DD} and the ON and OFF resistances R_{OH} and R_{OL} are obtained from driver datasheet. The average input current depends on peak input current and duty cycle of gate pulse. A part of the

gate drive power is dissipated in resistances of transistors of driver output stage R_{OH} and R_{OL} . The maximum power dissipated in the driver is:

$$P_{driver} = (17.5 \times 2.5 \text{ m}) + (2.8 \times 10 \text{ m} \times 0.5) + \left(\frac{1}{2} 35n \times 17.5 \times 200k \left(\frac{5.1}{5.1 + 10} + \frac{2}{2 + 10} \right) \right) = P_{driver} = 0.088 \text{ W}$$

The maximum possible power dissipation in the driver is 1 W to prevent the junction temperature reaching the maximum permissible limit of 140°C, when operating at ambient temperature of 25°C. With the calculated power dissipation, the maximum temperature in the driver is 35°C.

Gate Resistor Calculation and Selection:

The gate resistors are intended to ensure that the peak gate currents during turn ON and OFF are within the maximum capacity of the driver and the minimum internal resistance of the MOSFET gate and the driver IC. Furthermore, the resistance can be increased or decreased. A 10Ω gate resistance is used for all the MOSFETs. A 1Ω resistor close to the MOSFET gate and source pins together limits the peak gate current to 1.46 A when the gate voltage makes a transition from -2.5 V to 15 V during turn ON or vice-versa. For the AC-DC stage where two MOSFETs are paralleled, a single gate resistor from driver followed by two separate resistors close to each MOSFET gate are used.

The pulsed current will remain during the MOSFET rise and fall time and the resistor should withstand repetitive pulsed power of:

$$P_{pulsed-gate} = \left(\frac{15 + 2.5}{10} \right)^2 \times 10 = 25.52 \text{ W}$$

The continuous pulsed current handling capability for resistors of standard package with respect to pulse width is shown in Figure 39. The package that can safely handle the pulsed power is the 1206 package.

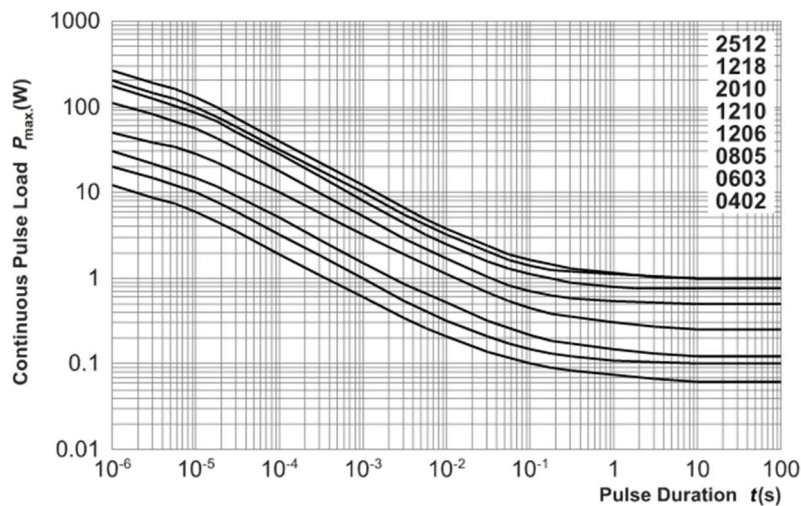


Figure 38: Pulsed power ratings for thick film chip resistors

4.1.5 Design and Layout Considerations for High Frequency Switching

SiC MOSFETs and diodes enable the switching frequency to reach 100 kHz or more without significant loss in efficiency as compared to Si devices. The indirect benefits of high switching frequencies are reduction in filter size, cooling requirements and overall system cost. However, with high switching frequency and at high power levels, the EMI filters need to be designed more accurately.

Kelvin Connection for Gate:

With a 3 pin MOSFET connection with a common source pin, the rate of decay of drain current during turn OFF causes a voltage drop across the parasitic inductance of source pin and trace. The induced voltage in opposition with the gate voltage causes a reduction in gate current and slows down the switching transition period. The MOSFET cannot reach its full switching transition capability and causes increase in the switching energies. Also, when devices are paralleled, the difference in stray inductances can cause imbalance in dynamic current sharing.

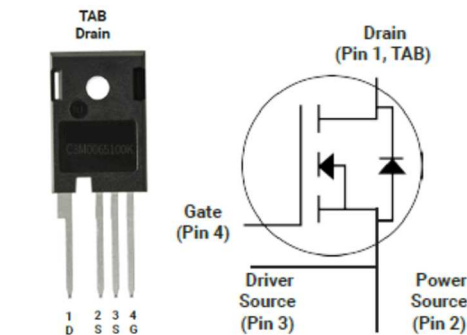


Figure 39: C3M0065100K in a TO-247-4 package

Wolfspeed’s C3M 1000 V, 65 mΩ, C3M0065100K MOSFET come in a 4pin package with a separate pin for gate driver source connections as shown in Figure 40. The Kelvin source pin of TO-247-4 package along with the isolation in gate driver circuitry results in very low inductance in driver source pin. The negative feedback effect due to the inductance minimization, enabling faster switching and lower switching losses. The switching loss data for Wolfspeed’s 3 pin (P/N: C3M0065090D) and 4 pin (P/N: C3M0065100K) package MOSFETs of same rating is shown in Figure 41, which illustrates a significant reduction in switching loss at higher currents.

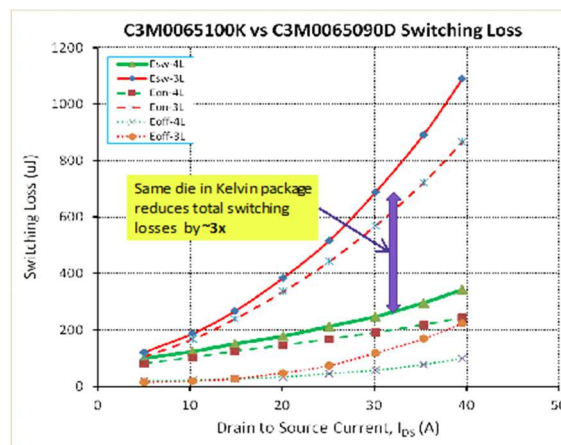


Figure 40: Switching energies of Wolfspeed’s SiC MOSFETs in a TO-247-3 and TO-247-4 packages

Layout Considerations on the Gate Side:

Since the devices are in parallel position to achieve higher efficiency, the gate connections are designed to be symmetrical to aid in dynamic current sharing. The static current sharing is inherently achieved by the positive temperature coefficient characteristics of the ON state resistance and equal gate voltage to both MOSFETs. It is also important to reduce the switching loop in gate circuitry to minimize ringing in gate voltages, considering the low threshold voltage of the MOSFETs.

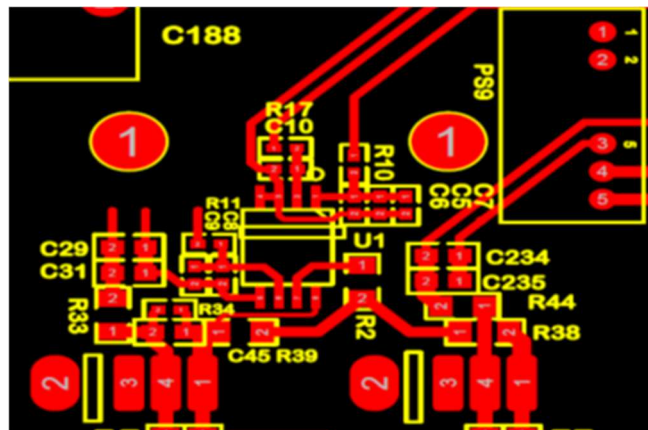


Figure 41: Gate connections to paralleled SiC MOSFETs

A section of gate side layout for Q1 and Q2 is shown in Figure 42. The gate driver is placed as close as possible to the MOSFETs. The gate driver and signals associated with the gate are placed on the top layer of PCB with the power traces running in the subsequent layers. The paralleled devices have a common gate resistor R2 following which the trace lengths to gates are equal for both. The decoupling capacitors on the -2.5 V are placed close to the resistor from source pin to minimize loop inductance and provide tight coupling between source and -2.5 V node.

The parasitic gate drain capacitance in the board is kept to a minimum so that it is below the MOSFET internal gate drain (miller) capacitance. At higher dv/dt situations, coupling of voltage rise in drain can affect the gate traces and cause spurious gate voltage transitions. The decrease in parasitic gate drain capacitance is also achieved by keeping sufficient distance between gate and drain tracks or by keeping them in different layers and avoiding any overlap between the two tracks. The effect can also be minimized by using higher gate resistance (which in turn causes rise in switching losses) or using negative gate voltage to turn OFF the MOSFET or using gate drivers with active miller clamp.

Reducing Loop Inductance in Power Section & Symmetric Positioning of Devices:

The stray inductances in power side loops cause high ringing in the switching nodes. The result is additional voltage stress on the devices and rise in losses when the loops have high dv/dt . The loop size reduction is achieved by closely placing the components of AC-DC stage (as shown in Figure 43).

The top and bottom MOSFETs of the full bridge network are placed as close as possible. The positions are such that a straight trace connects top MOSFET source and bottom MOSFET drain pins. A ceramic capacitor for decoupling is connected directly between the top MOSFET drain and bottom MOSFET source pin to absorb the energy in stray inductance during switching. A RC snubber is also placed close to the devices to reduce

oscillations caused by switching. The snubber network is placed close to both paralleled legs with high frequency switching.

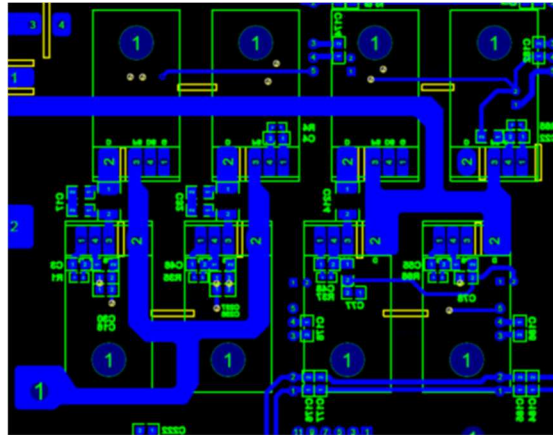


Figure 42: Power traces (bottom) and snubber capacitors for AC-DC stage

To minimize high frequency ripple voltage, film capacitors with capacitance greater than the capacitance of snubber capacitors are placed adjacent to each full bridge network. An electrolytic capacitor bank to reduce ripple voltage amplitude at double the line frequency is connected at a distance. The electrolytic capacitor bank can also be made as a separate board. The symmetrical layout of traces with respect to each parallel MOSFET need to be checked properly, since the layout is the most important parameter in equal sharing of current under all conditions.

Minimizing EMI Due to Inductor:

In a hard-switching application at higher frequencies, the parasitic capacitance of the inductor between windings or layers of inductor and the stray inductance in power switching loop leads to ringing in drain voltage. The capacitance between adjacent windings will not lead to significant parasitic inductance due to low voltage between them. But the dv/dt across capacitor between adjacent layers will be high enough.

A single layer winding is an ideal solution for minimizing parasitic capacitance of inductor. Sufficient insulation between inter layers of windings can also reduce this parasitic capacitance. To minimize the radiated noise from core, twisting the windings can be done within the core to generate a radiated flux cancellation mechanism (as shown in Figure 44).

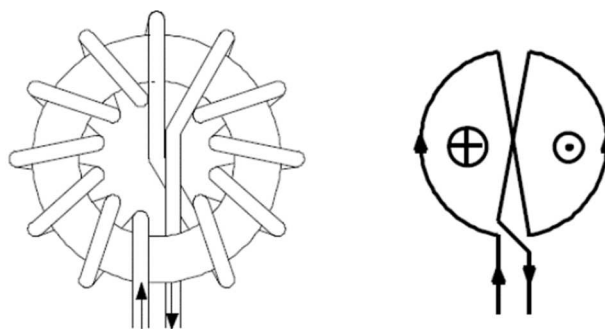


Figure 43: Winding structure to reduce radiated emission from inductor

4.2 Controller Board

Note: A larger copy of any diagram in this Section 4.2 may be obtained upon request by contacting Wolfspeed at forum.wolfspeed.com.

The block diagram of the controller card is shown in Figure 45. The controller board houses the Texas Instruments® TMS320F28377 dual core Delfino® microcontroller. The TMS320F28377 is a powerful 32-bit floating-point microcontroller unit designed for advanced closed-loop control applications and digital power conversion. The 32-bit C28x floating-point CPU provides 200 MHz of signal processing performance. The controller supports up to 1MB of onboard flash memory with error correction code (ECC) and up to 164 KB of SRAM. Two 128-bit secure zones are also available on the CPU for code protection. The ancillary components of this controller include ADCs with comparator, DACs, PWMs, eCAPs, and eQEPs.

The controller signals are galvanically isolated from the power stage. The board to board connectors are placed such that the signals from controller board to gate drivers/sensors are as short as possible. The voltages and currents to be measured are routed to the controller board through cables and terminal blocks. The supply for the controller and the on-board sensors is generated through the on-board regulators powered from external 7V supply. For the gate drivers, separate external power supply of 15V is used which is routed to the power board along with the PWM signals.

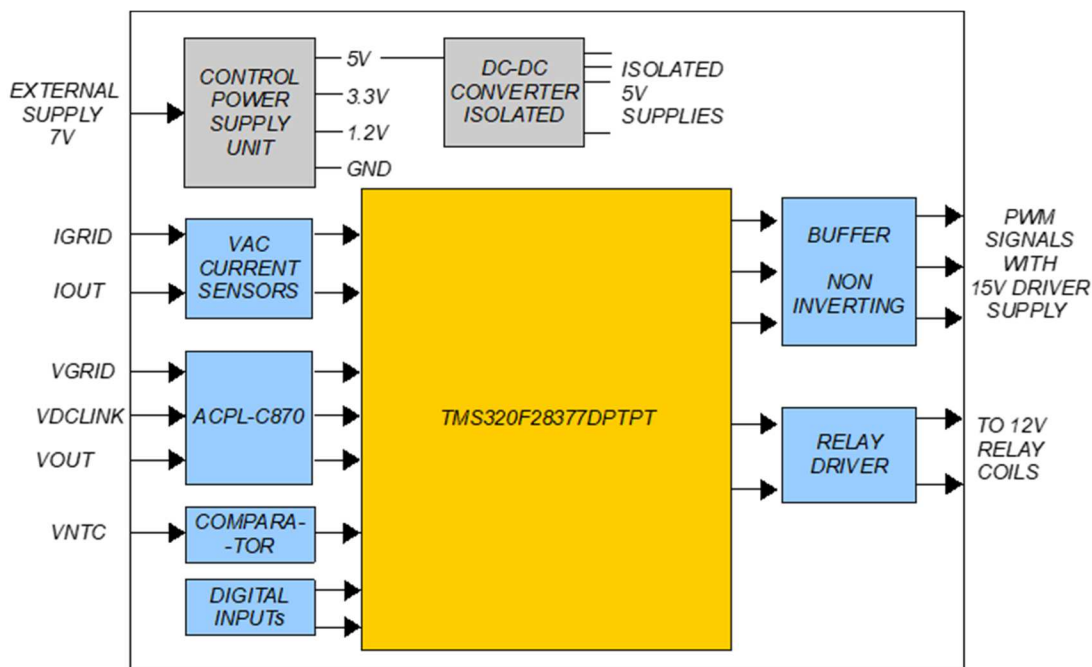


Figure 44: Controller board block diagram

4.2.1 Power Supply Requirements

Major components of the controller board that consume most of the power are: the microcontroller, the buffer ICs, analog isolation amplifiers and the VAC current sensors. An estimate of power consumption is given in Table 13.

Table 13: Controller Board Power Consumption Estimates

| Voltage | Current | Power | Notes |
|---------|---------|---------|--|
| 3.3 V | 0.105 A | 0.35 W | Maximum current on VDDIO, VDDA and VDD3VFL |
| 1.2 V | 0.36 A | 0.432 W | Maximum current on VDD at 200 MHz |
| 5 V | 0.08 A | 0.4 W | Buffer ICs for 12PWM signals |
| | 0.08 A | 0.4 W | VAC sensor consumption |
| | 0.026 A | 0.13 W | ACPL-C780 |
| | 0.1 A | 0.5 W | Additional safety margin (100 mA) |

For the microcontroller power supplies of 3.3 V and 1.2 V, a dual output low dropout regulator is used as shown in Figure 46.

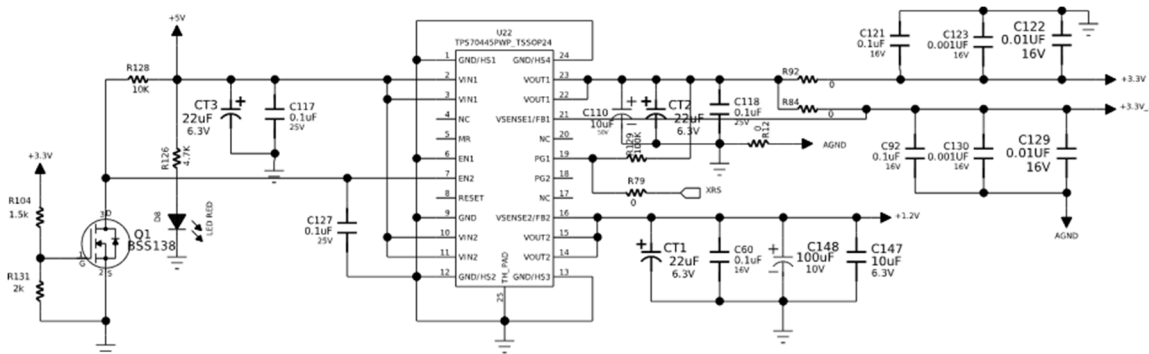


Figure 45: Generating controller power supply using TPS70445

A linear regulator is used for generating 5 V from an external 7 V regulated supply. The controller supplies of 3.3 V and 1.2 V are generated from this 5 V input through TPS70445 (as the input to the regulator needs to be just 250mV, more than the output). The 3.3 V and 1.2 V outputs can be loaded up to 1 A and 2 A respectively. The supply voltage supervisors (SVS) on the regulator are used to monitor the voltages and drive the RESET pin of controller to low in case the voltage values fall outside the specified range. Brief descriptions of the pins used are below.

- 1. Input:** The input to both regulators is regulated at 5 V. The internal bias voltages are generated from VIN1 pin. For input below 2.4 V, the UVLO function disables the regulator. Decoupling capacitors of 22uF and 0.1uF are placed close to the regulator IC.
- 2. Enable pins:** The regulators are enabled when the corresponding enable pins are held low. The 3.3 V regulator is always enabled by EN1 pin tied to the ground. When 3.3 V output builds up, MOSFET Q1 is turned ON and EN2 gets tied to ground. The EN2 pin is pulled up to 5 V when the 3.3 V supply is not available. Thus, 1.2 V generation is automatically disabled in case 3.3 V output gets shut down.
- 3. Sense pins:** To keep output stable, the sense pins are connected to the regulator outputs.
- 4. Power good:** The power good pins are open drain pins and are driven low when the respective output voltage drops below 95% of the rated value. A power good pin of 3.3 V output is routed to the RESET pin of the microcontroller to reset in case of supply fail.

Power Dissipation in TPS704405:

The power dissipation in the regulators is impacted mostly by the difference in input and output voltages. The combined power loss due to both regulators is:

$$P_{reg} = (V_{IN} - V_{OUT1})I_{OUT1} + (V_{IN} - V_{OUT2})I_{OUT2}$$

$$P_{reg} = (5 - 3.3)0.105 + (5 - 1.2)0.36 = 1.55W$$

The power loss has to be dissipated to the ambient in form of heat to prevent the device thermal shutdown caused by the junction temperature rising to 150°C.

The PWP package of regulator has a thermal pad that is connected to the ground pin and hence the ground plane. The capacity can be increased if air flow is also provided to the pad. The thermal impedance for different copper area along with different airflow is shown in Figure 47. For an ambient temperature at 50°C, to limit the junction temperature to 125°C, the effective thermal resistance should be:

$$R_{thJA} = \frac{125 - 50}{P_{reg}} = \frac{48.4^{\circ}C}{W}$$

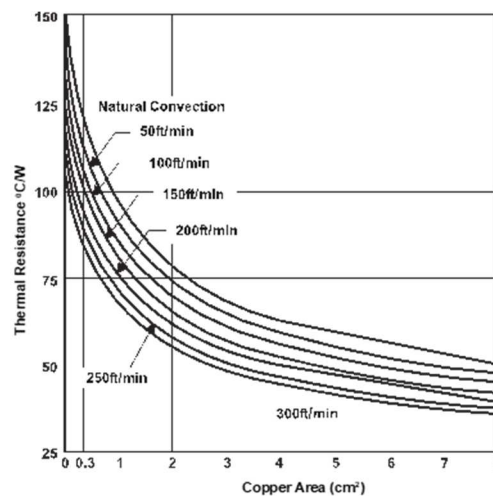


Figure 46: TPS70445 thermal resistance versus dissipation area

From the plot in Figure 47, the copper heatsink area required to maintain junction temperature within 125°C will be approximately 8cm² with natural convection.

Other Supplies:

1. Reference voltage to ADC pins: The reference voltage to the controller ADC pins is 3.3 V. To achieve tight regulation in reference voltage and prevent any noise interference, a low drift low power precision voltage reference IC REF3230 is used (as shown in Figure 48).

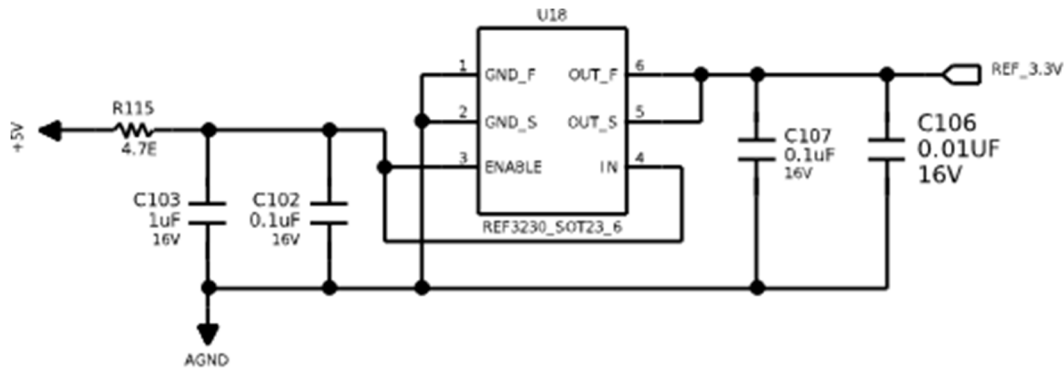


Figure 47: Generating ADC reference voltage using REF3230

The reference is stable with any capacitive load and can operate at inputs as low as 5mV above the output voltage and drive loads up to 10mA. The output voltage has a variation of +/-7mV with a drift of maximum 20ppm/^oC.

2. **Reference voltage for current and voltage measurements:** For the VAC current sensors, an external voltage reference is provided which corresponds to the zero-current output voltage of the sensor. The voltage reference IC from Intersil (P/N: ISL21010CFH315Z) generates 1.5 V reference with accuracy of +/- 0.2%. Similarly, for the grid voltage feedback, a reference of 1 V is generated by using voltage drop across 100Ω resistor, which is further used to set up current reference of 10 mA by using a programmable current source from Linear Technology Corp. (P/N: LT3092).
3. **Isolated supplies to isolation amplifiers:** For all the bias voltages of the analog isolation amplifiers, an isolated DC-DC converter module from MORNSUN (P/N: B0505XT) is used (as shown in Figure 35). The power supply has a 5 V input and 5 V output isolated by 1.5 kV. The device can support up to 200 mA output and has a protection against short circuit.

4.2.2 Analog Feedbacks

All analog feedback circuitry contained within this charger is a part of the controller board. The grid voltage, DC bus voltage and the output voltage are brought to the board through 2 pin headers. The current sensors for grid and the output current are in the controller board with a current sensing path routed to the controller board via power cables.

Voltage Feedbacks:

The voltage feedbacks are isolated through an optically isolated voltage sensor ACPL-C780 as shown in Figure 49. The IC has input voltage range of 2 V and 1GΩ input impedance, unity gain differential outputs with isolation of 5 kV from the inputs. The input is scaled down to 2 V range using resistive potential divider. The isolator outputs are followed by a differential amplifier stage (as shown in Figure 49) for the DC bus voltage feedback.

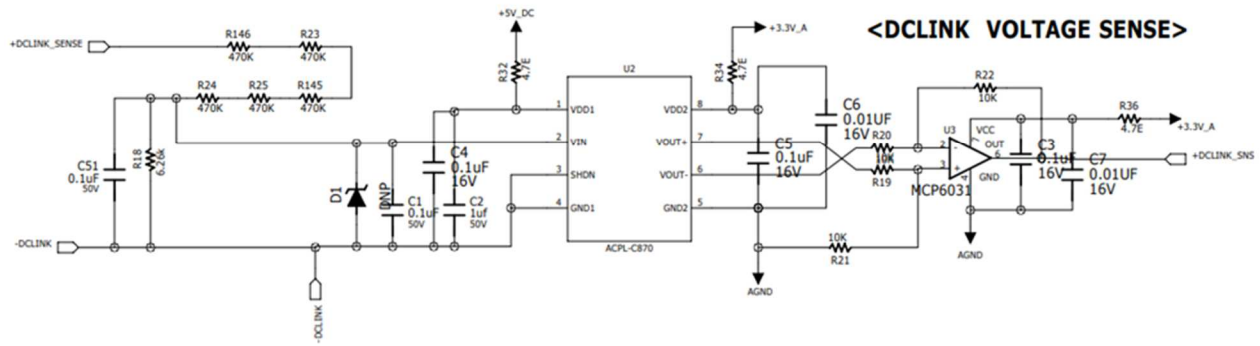


Figure 48: DC bus voltage feedback using ACPL-C870

The shutdown of amplifier is disabled by connecting the SHDN pin to ground. The primary and secondary side supplies are decoupled by a set of ceramic capacitors close to the pins. The secondary and differential amplifier is biased with 3.3 V with rail-to-rail op-amp. Thus, the controller pins never cross 3.3 V.

The isolation amplifier has unity gain, and the differential amplifier is also designed for unity gain. The attenuation of feedback network is decided by the resistive divider network alone.

$$A_{dclink} = \frac{6.26k}{6.26k + 2350K} = 2.6567 \times 10^{-3}$$

The nominal input voltage for ACPL-C780 (as shown in Figure 48) is 2 V and full-scale input is 2.46 V. For protection of the input pins, a 2.2 V Zener is placed across input pins. The maximum DC bus voltage that can be sensed linearly is:

$$V_{dclink-SNS} = \frac{2.2}{A_{dclink}} = 828V$$

The DC bus voltage feedback is linear up to 2.2 V for the DC bus feedback of 882 V. Beyond this 882V value, the feedback saturates and remains at 2.2 V.

Similarly, for the output DC voltage feedback, the linear sensing range is:

$$V_{out-SNS} = \frac{2.2}{A_{vout}} = 532V$$

For the grid voltage sensing, the feedback has to be level shifted to accommodate both positive and negative half of the grid voltages. A 1 V stable and accurate reference is generated using LT3092 (as shown in Figure 50) and added to the grid voltage attenuation network. The constant current output generated by LT3092 is:

$$I_{out-LT3092} = \frac{10\mu R_{set}}{R_{out}} = \frac{10\mu \times 47k}{470||100||100} = 10.4mA$$

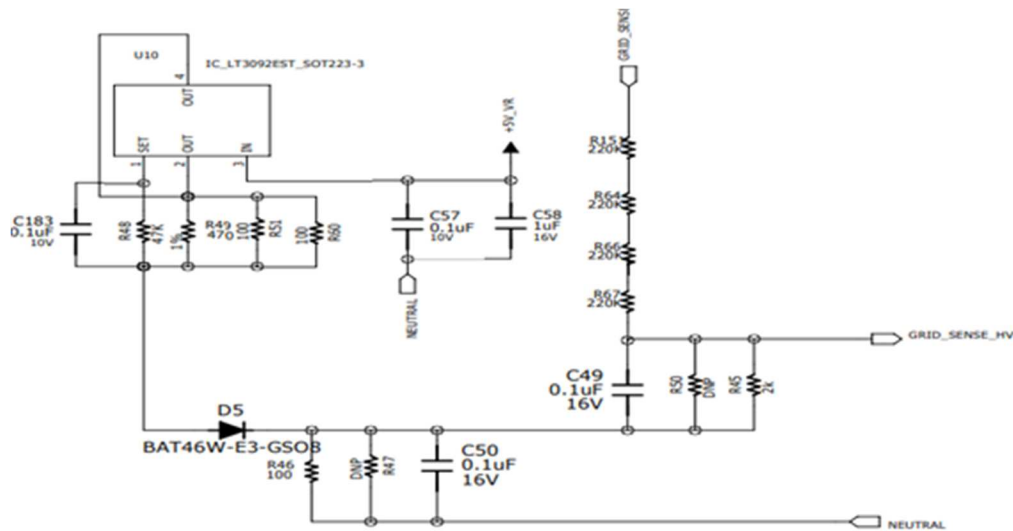


Figure 49: Generating a 1 V reference voltage for grid voltage feedback

The constant current source is connected across a standard resistance of 100Ω to generate 1.0V reference (it can be adjusted accurately using a parallel tuning resistor). The differential amplifier gain on isolation amplifier secondary is also kept at unity. With the superposition principle, the output voltage of the divider network is:

$$V_{ac-div} = 0.9977 + (V_{grid} \times 22.675 \times 10^{-4})$$

The feedback voltage for grid voltage of 0V is 0.9975 V. The positive peak is clamped to 2.2 V and the negative voltage to 0 V. The voltage feedbacks are terminated to the ADC pins through a RC low pass filter stage placed close to the microcontroller.

Current Feedbacks:

The type of currents measured in the system are grid current, output current and the bridge current of the DC-DC converter. The grid and output current feedbacks, used for closed loop control, system monitoring and protection, are derived from a VACUUMSCHMELZE GmbH & Co. KG current sensor module (P/N: T60404-N4646-X161). For the bridge current, a high frequency current sense transformer from Pulse Electronics (P/N: PE-67100NL) is used.

The grid current measurement using VAC sensor is shown in Figure 51. The sensing range of sensor is 50 A (RMS) nominal and 172 A peak. The sensor has an internal reference of 2.5 V±2.5 mV for zero current output which is independent of bias voltage of 5 V at VC pin. The sensor sensitivity is 12.5 mV/A, however as 2 turns have been used inside the sensor, sensitivity changes to 25 mv/A. External reference voltage in range of 0 to 4 V can be applied to VREF pin.

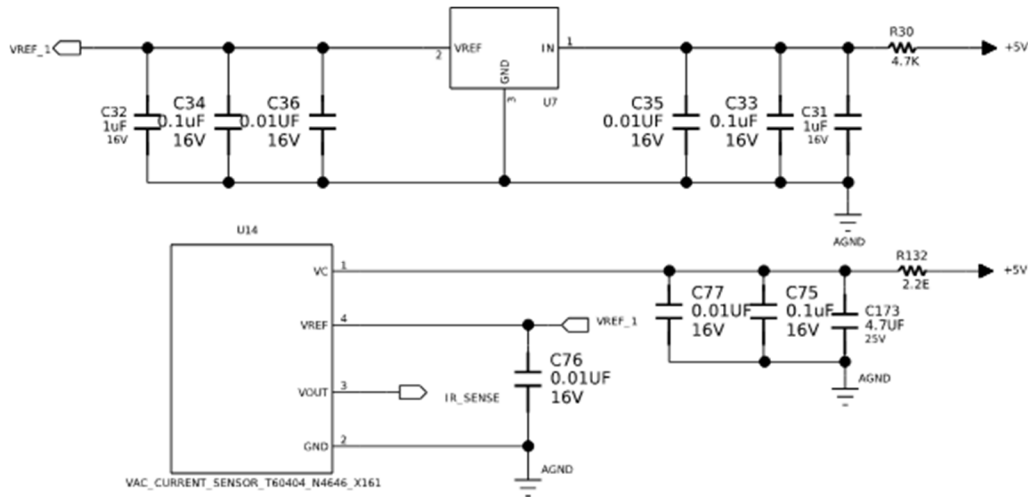


Figure 50: Grid current measurement using VAC sensor

An external reference of 1.5 V is generated through a voltage reference generator from Intersil (P/N: ISL2101D) and given to the current sensor. The new feedback voltage for 0 A current is 1.5 V. The negative peak current that can be sensed is:

$$I_{ac-SNS-pk} = \frac{1.5}{0.025} = 60A$$

The value of PFC peak current as computed earlier is:

$$I_{SWpk} = I_{Lmax} + \frac{\Delta I_L}{2} = \frac{6600}{200} \sqrt{2} + \frac{15}{2} = 54.17A.$$

This implies that any negative peak more than 60 A shall be computed as 60 A, however, the positive peak can go up to 66 A for which the output voltage will be 3.3 V. Software protection should work well below this value. Though the system currents cannot go to such high levels, the current has to be well within 66A for the ADC pin to be within 3.3 V level. The current transformer feedback from bridge of DC-DC converter is used for the protection and the system trip, in case the current crosses a preset threshold level. The scaled down current is rectified before reaching the 10Ω burden resistance. The overcurrent protection is implemented using the internal comparators of the analog pin. The feedback voltage is 3.3 V for peak input current of 33 A.

4.2.3 Controller Pin Assignments

The microcontroller peripherals used in the charger system are ePWMs, ADCs and GPIOs.

PWM Pins:

The controller supports 12 ePWM modules or 24 ePWM pins with 8 submodules, that can provide HRPWM (high resolution PWM outputs). The PWM outputs can be made available at the GPIOs. The output from comparator submodule can be to the PWM trip inputs through X-BAR. In the charger, the PWM used are listed in Table 14. All PWM pins used are of high resolution type and are controlled by fault inputs scanned at GPIOs and the outputs from internal analog comparator submodules through X-BAR.

Table 14: PWM Pins of the Microcontroller

| Pin No. | Pin Name | Pin Used As | Remarks |
|---------|----------|-------------|--|
| 160 | GPIO0 | EPWM_1A | Ac-dc converter stage leg 1 top PWM signal Active high output |
| 161 | GPIO1 | EPWM_1B | Ac-dc converter stage leg 1 bottom PWM signal Active high output |
| 162 | GPIO2 | EPWM_2A | Ac-dc converter stage leg 2 top PWM signal Active high output |
| 163 | GPIO3 | EPWM_2B | Ac-dc converter stage leg 2 bottom PWM signal Active high output |
| 164 | GPIO4 | EPWM_3A | Dc-dc converter primary leg 1 top PWM signal Active high output |
| 165 | GPIO5 | EPWM_3B | Dc-dc converter primary leg 1 bottom PWM signal Active high output |
| 166 | GPIO6 | EPWM_4A | Dc-dc converter primary leg 2 top PWM signal Active high output |
| 167 | GPIO7 | EPWM_4B | Dc-dc converter primary leg 2 bottom PWM signal Active high output |
| 18 | GPIO8 | EPWM_5A | Dc-dc converter secondary leg 1 top PWM signal Active high output |
| 19 | GPIO9 | EPWM_5B | Dc-dc converter secondary leg 1 bottom PWM signal Active high output |
| 1 | GPIO10 | EPWM_6A | Dc-dc converter secondary leg 2 top PWM signal Active high output |
| 2 | GPIO11 | EPWM_6B | Dc-dc converter secondary leg 2 bottom PWM signal Active high output |

ADC Pins:

The controller ADC module is a successive approximation style ADC. There are 4 ADC modules with a resolution that can be selectable between 12 bits (290ns conversion) and 16 bits (915ns conversion). The ADC supports single ended and differential signals. The single ended signals are referred to VREFLO pins. The ADC triggering, and conversion sequencing is accomplished through configurable start-of-conversions (SOCs). Multiple SOCs can be configured for the same trigger, channel, and/or acquisition window as desired.

The ADC signals used in charger are listed in Table 15. All the signals are single ended with VREFHI signals connected to 3.3V and the VREFLO pins connected to VSS. All the signals have a RC filter network prior to connection to the microcontroller. The pin impedance, which is dependent on ADC clock (5 MHz to 50 MHz) decides the filter resistance. The pin has parasitic input capacitance of maximum 12.9pF and 117pF (for ADCINB0 due to VDAC functionality) and the filter capacitance should be at least 100 times higher.

Table 15: ADC Pins of the Microcontroller

| Pin No. | Pin Name | Pin Used As | Remarks |
|---------|----------|-------------|--|
| 31 | ADCINC2 | ADCINC2 | DCLINK_SNS: Dc bus voltage feedback |
| 38 | ADCINA5 | ADCINA5 | GRID_SNS : Grid voltage feedback |
| 40 | ADCINA3 | ADCINA3 | VOUT_SNS: Output voltage feedback |
| 44 | ADCIN14 | ADCIN14 | CT_SENSNE: Dc-dc bridge current feedback |
| 39 | ADCINA4 | ADCINA4 | IOUT_SENSE: Output current feedback |
| 49 | ADCINB3 | ADCINB3 | IR_SENSE: Grid current feedback |
| 47 | ADCINB1 | ADCINB1 | ADC reference voltage monitoring |
| 46 | ADCINB0 | ADCINB0 | NTC over-temperature feedback monitoring |

GPIO Pins:

The GPIOs of the controller have up to 12 independent peripheral signals multiplexed per pin along with the CPU controlled input output capability. There are 6 ports and up to 168 GPIO pins. In the charger, GPIOs are used for control of relays, indication LEDs and receive user selectable digital inputs (as listed in Table 16).

Table 16: GPIO Pins of the Microcontroller

| Pin No. | Pin Name | Pin Used As | Remarks |
|---------|----------|-------------|--|
| 24 | GPIO24 | GPIO24 | For control of grid side relay to bypass charging resistor. Active high output |
| 23 | GPIO23 | GPIO23 | For control of output side relay (Not mounted) Active high output |
| 142 | GPIO76 | GPIO76 | Indication / debug LED 1 Active high output |
| 143 | GPIO77 | GPIO77 | Indication / debug LED 2 Active high output |
| 144 | GPIO78 | GPIO78 | Indication / debug LED 3 Active high output |
| 145 | GPIO79 | GPIO79 | Indication / debug LED 4 Active high output |
| 131 | GPIO43 | GPIO43 | Control switch: for ON/OFF control Active high / low output (settable) |
| 134 | GPIO70 | GPIO70 | Control switch: for charging/ inverter mode selection, Active high / low output (settable) |

5. Performance Data

The completely assembled system (as shown in Figure 52) of Wolfspeed's CRD-06600FF10N, 6.6 kW Bi-directional EV On-board Charger is tested at the load conditions that are listed in Table 2. The individual

converters are independently tested for functionality and performance. The cascaded system is also tested for full load range and the results are presented in this section.

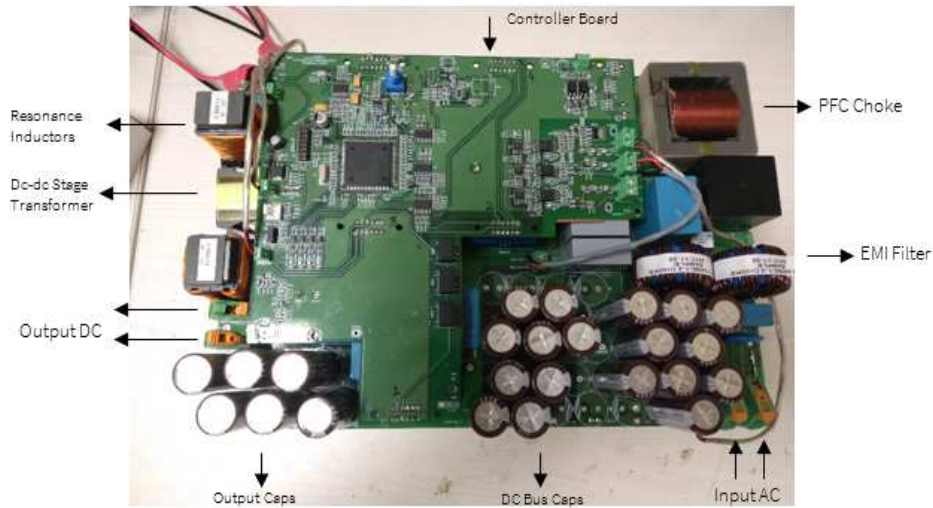


Figure 51: Wolfspeed's CRD-06600FF10N, 6.6 kW Bi-directional EV On-board charger (fully assembled)

AC-DC Stage:

The AC-DC stage has nominal output voltage of 390 V but can go up to 680V for operating DC-DC stage at resonant frequency. One of the legs has switching frequency of 67 kHz. The gate voltage (yellow) and drain to source voltage (green) are shown in Figure 53 for the DC link voltage of 680 V and the gate resistance of 10 Ω . There is no ringing or oscillations observed in the gate voltage. The waveforms of the MOSFETs used for synchronous rectification and the zero-voltage switching can be seen at turn ON and turn OFF.



Figure 52: High frequency MOSFET's gate voltage (yellow) and drain to source voltage (green) during turn ON and turn OFF

The top and bottom MOSFETs are switched with complementary gate pulses with adequate dead-time. The top and bottom MOSFET voltages (Yellow and Green) of high frequency switching leg at 680 V output along with the inductor current (pink) are shown in Figure 54. There is no peak overshoot or high level of ringing in the drain source voltage during turn OFF.

The grid voltage (Blue) and inductor current (pink) for 1.4 kW and 6 kW power are shown in Figure 55. At 1.4 kW load, the current drawn from grid was 6.25 A and the current THD was 10.736%. In both cases, the inductor

current waveform closely follows the grid voltage. At 6 kW load, the grid current was 26.73 A with a THD of 6.37%. In both cases, the output voltage was set to 680 V.



Figure 53: Top and bottom MOSFET voltages (yellow and green) along with the inductor current (pink)

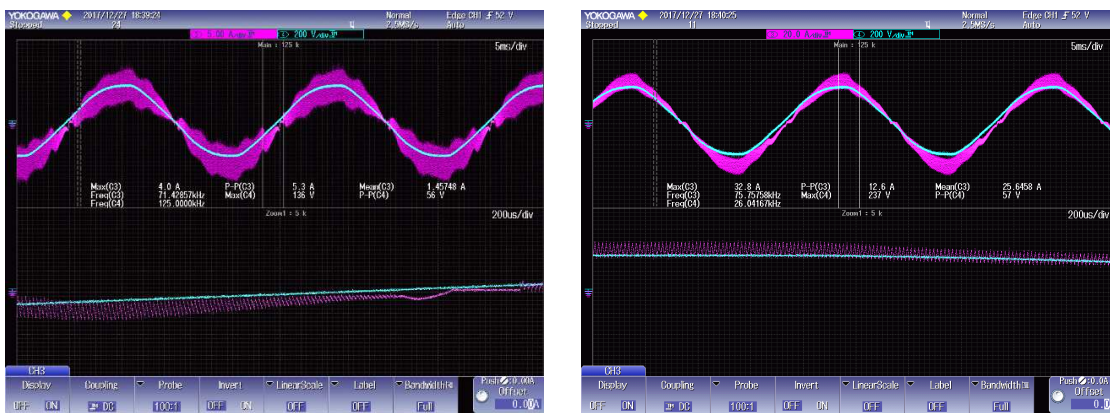


Figure 54: Grid voltage (blue) and inductor current (pink) at 1.4 kW and 6 kW

The measured efficiency of the AC-DC stage including the input EMI filter for 390 V and 680 V output over the entire load range are shown in Figure 56. In both cases, the peak efficiency is maintained close to 98%.

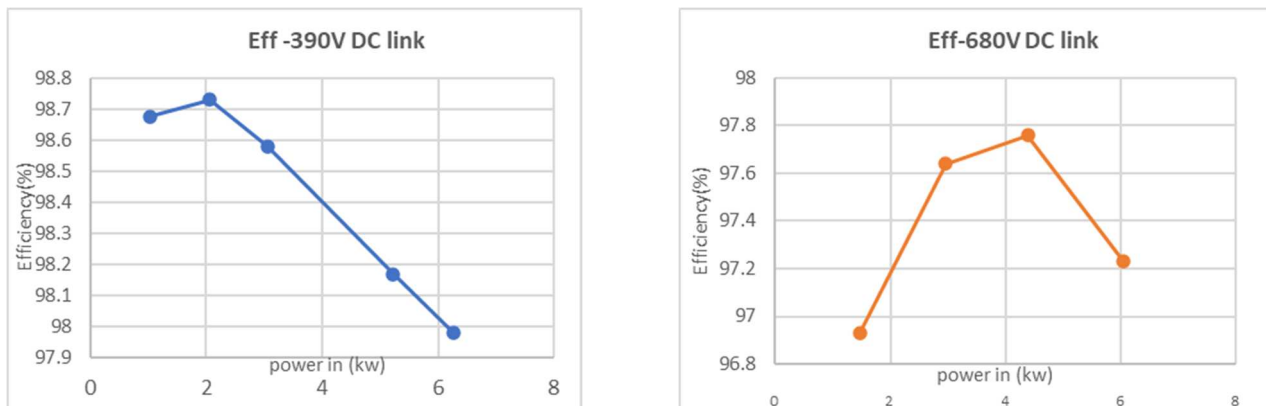


Figure 55: AC-DC converter measured efficiency at 390 V and 680 VDC link voltages

DC-DC Stage:

The DC-DC converter is tested with resistive load and for output voltage regulation. The input voltage is varied to make the converter operate close to resonance frequency and attain the required gain. The primary current (Pink) and the primary MOSFET gate (Green) and drain source (Yellow) voltages at no load are shown in

Figure 57. The three waveforms at full load for 280 V (limited to 4.5 kW) output and 450 V output (at 6.2 kW) are shown in Figure 58.



Figure 56: Primary current (pink), MOSFET gate (green) voltage and drain to source (yellow) voltage at no load

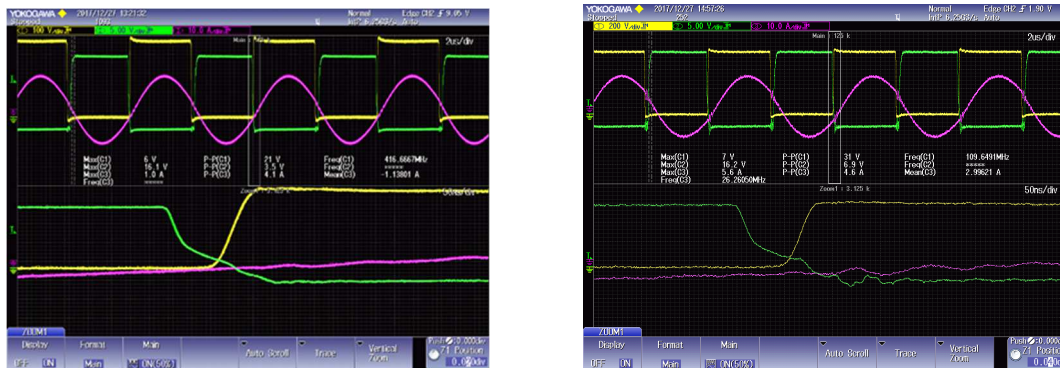


Figure 57: Primary current (pink), MOSFET gate (green) voltage and drain to source voltage (yellow) at 260 V and 450 V output

The measured DC-DC converter efficiency with resistive load at 260 V and 450 V outputs over entire load range is shown in Figure 59.

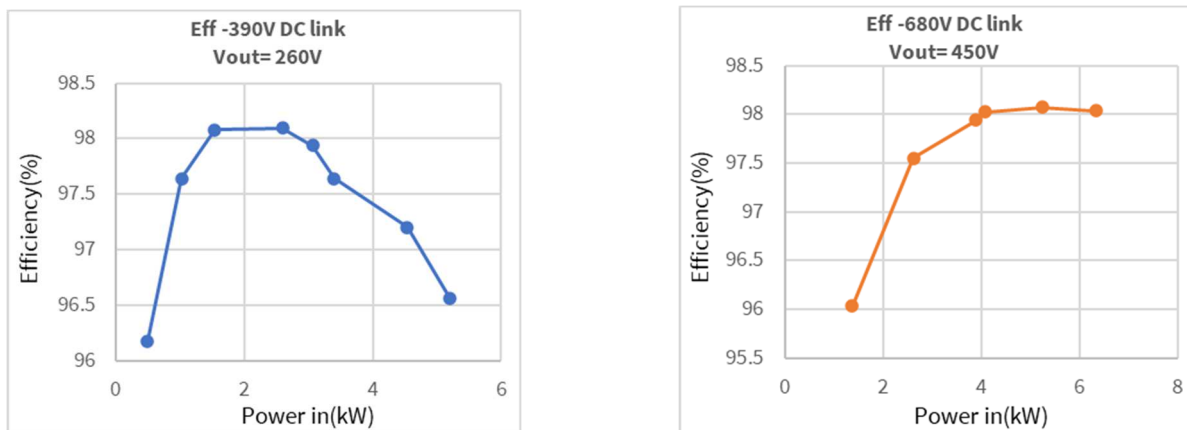


Figure 58: DC-DC converter efficiency at 260 V and 450 V output voltages

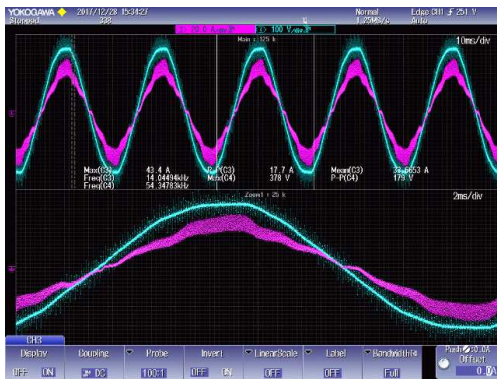
Cascaded System:

The total system is powered up with 230 V grid input. The DC output reference is set to 260 V and loaded to 4.3 kW. The input voltage and current waveforms and the power analyzer readings for input and output are shown in Figure 60. The waveforms and power analyzer readings for 450V and 6.6 kW output are shown in Figure 61.



| 8 change items | Element 1 | Element 2 | Element 3 | Element 4 |
|----------------|-----------|-----------|-----------|-----------|
| Urms [V] | 230.56 | 0.1586 | 399.70 | 262.06 |
| Irms [A] | 19.631 | 0.0000 | 0.0045 | 16.485 |
| P [W] | -4.5144 k | 0.0001 | -0.08 | 4.3201 k |
| η [%] | -95.696 | | | |
| Uthd [%] | 2.244 | 204.151 | --OF-- | --OF-- |
| Ithd [%] | 5.092 | 394.786 | --OF-- | --OF-- |
| U-ripple [%] | ----- | | | |
| λ [] | -0.9974 | Error | -0.0423 | 1.0000 |

Figure 59: Grid voltage (blue) and current (pink) waveforms and power analyzer readings for 260 V output



| 8 change items | Element 1 | Element 2 | Element 3 | Element 4 |
|----------------|-----------|-----------|-----------|-----------|
| Urms [V] | 231.89 | 0.2771 | 0.6760 k | 448.61 |
| Irms [A] | 29.407 | 0.0000 | 0.0105 | 14.403 |
| P [W] | -6.772 k | 0.0003 | -0.0001 k | 6.461 k |
| η [%] | -95.411 | | | |
| Uthd [%] | 2.981 | 257.189 | --OF-- | --OF-- |
| Ithd [%] | 9.179 | 365.921 | 858.696 | --OF-- |
| U-ripple [%] | ----- | | | |
| λ [] | -0.9931 | Error | -0.0129 | 1.0000 |

Figure 60: Grid voltage (blue) and current (pink) waveforms and power analyzer readings for 450 V output

The efficiency for 260 V and 450 V outputs at various loading conditions is shown in Figure 62.

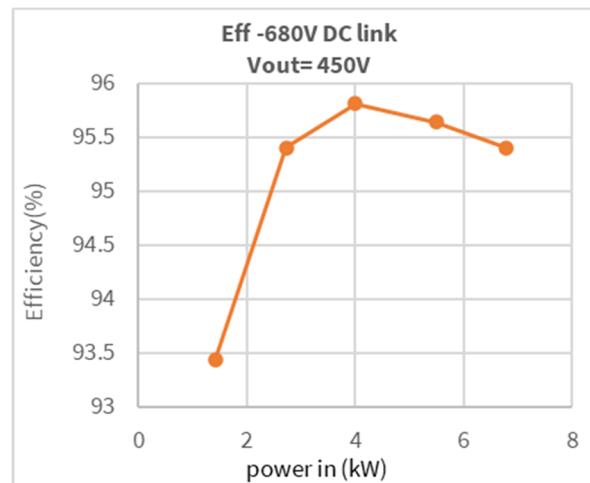
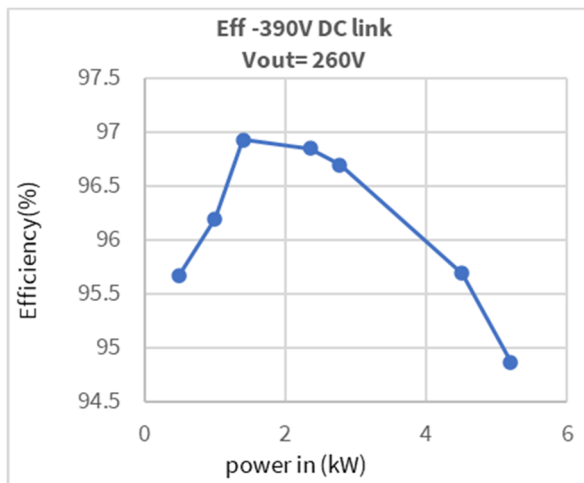
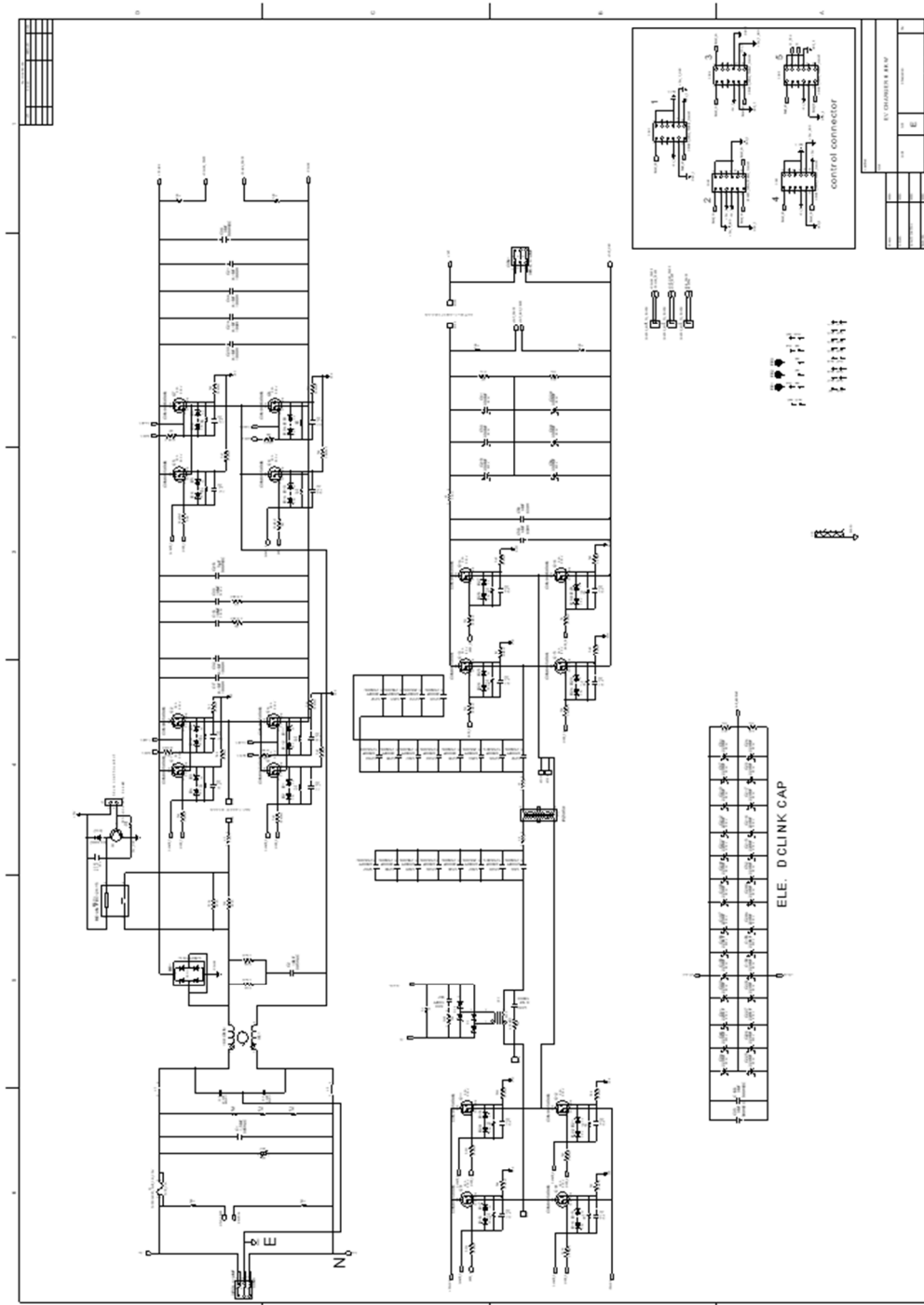


Figure 61: Charging mode efficiency at two 260 V and 450 V output voltages

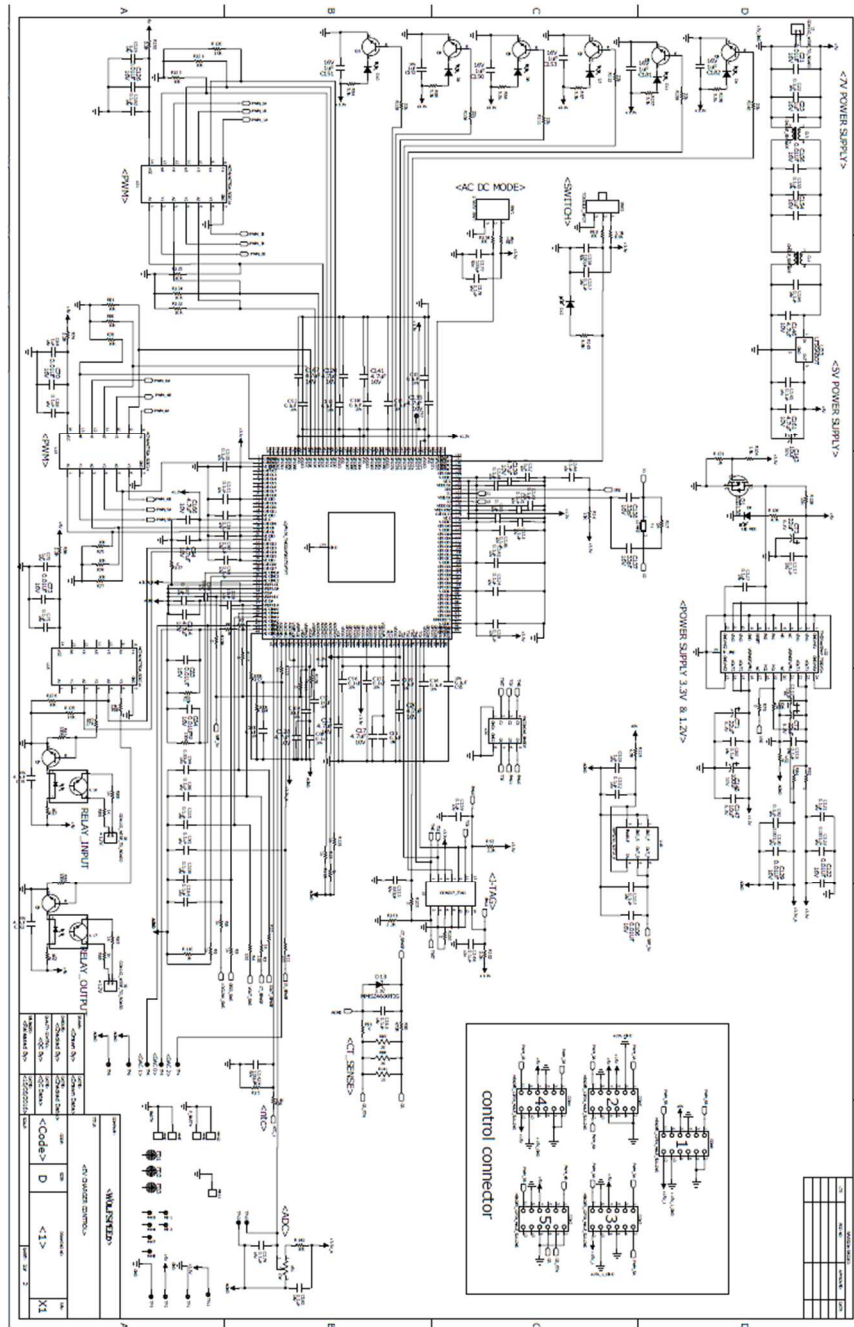
6. Appendix

Note: A larger copy of any schematic in this Section 6 may be obtained upon request by contacting Wolfspeed at forum.wolfspeed.com.

Power Board Schematics:



Control Board Schematic:



Bill of Materials:

Power Board:

| Sr No | Qty | Reference | Description | Manufacturer | Manufacturer P/N | Package |
|-------|-----|--|--|--------------|------------------------|---------|
| 1 | 1 | BD1 | BRIDGERECT SINGLE PHASE 1000 V 25 A TH | COMCHIP | GBU2510- G_DNP | TH |
| 2 | 8 | C6 C12 C65 C73 C81 C89 C97 C105 | CAP CER 0.01UF 10% 16 V X7R 0603 | TDK CORP. | C1608X7RIC103 K | CAP0603 |
| 3 | 8 | C5 C11 C64 C72 C80 C88 C96 C104 | CAP 0.1 uF 10% 16 V X7R 0603 | KEMET | C0603X104K4R ACTU | CAP0603 |
| 4 | 16 | C8 C14 C67 C75 C83 C91 C99 C107 C112 C117 C119-120 C126 C128 C133 C139 | CAP CER 0.1 uF 10% 50 V X7R 0603 | KEMET | C0603C104K5R ACTU | CAP0603 |
| 5 | 8 | C7 C13 C66 C74 C82 C90 C98 C106 | CAP CER 1.0 uF 10% 16 V X5R 0603 | KEMET | C0603C105K4P ACTU | CAP0603 |
| 6 | 4 | C118 C125 C127 C134 | CAP CER 1 uf 10% 50 V X7R 0603 | PANASONIC | CL10A105KB8N NNC | CAP0603 |
| 7 | 12 | C9 C63 C71 C79 C87 C95 C103 C111 C116 C124 C132 C143 | CAP0603 2.2 UF 35 V X5R | MURATA | GRM188R6YA22 5KA12D | CAP0603 |
| 8 | 12 | C30-31 C86 C94 C102 C110 C115 C123 C131 C142 C226 C228 | CAP CER 0.1 uF 10% 50 V X7R 0805 | TDK | C0805C104K5R AC7410 | CAP0805 |
| 9 | 1 | C62 | CAP0805 100PF 50 V | TDK | YFF21AC1H101 MT0Y0N | CAP0805 |
| 10 | 16 | C3-4 C19-20 C22 C37-38 C42-43 C45-50 C55 | CAP CER 1nF 10% 50 V X7R 0805 | MURATA | C0805C102K5R ACTU | CAP0805 |
| 11 | 4 | C69-70 C77-78 | CAP CER 1uF 10% 50 V X7R 0805 | MURATA | | CAP0805 |

| Sr No | Qty | Reference | Description | Manufacturer | Manufacturer P/N | Package |
|-------|-----|---|---|--------------------|-------------------------|---|
| 12 | 4 | C16 C29 C225 C227 | CAP CER 2.2uF 10% 50 V X7R 0805 | MURATA | GRM32ER71H22 5KA88L | CAP0805 |
| 13 | 47 | C25-27 C34 C40 C85 C93 C101 C109 C114 C122 C130 C141 C144- 146 C148-150 C152-154 C156- 158 C160-162 C164-166 C168- 170 C172-174 C176-178 C180- 182 C184-186 C191 | CAP CER 4.7uF 10% 50 V X7R 0805 | MURATA | GRM32ER71H47 5KA88L | CAP0805 |
| 14 | 2 | C18 C33 | CAP CER 10000PF 10% 1000 V X7R 1206 | MURATA | GRM31CR73A10 3 kW03L | CAP1206 |
| 15 | 4 | C17 C32 C51-52 | CAP CER 1812 0.01 UF 1000 V COG/NPO | KEMET | C1812C103JDG ACAUTO | CAP1812 |
| 16 | 1 | C189 | CAP CER 1812 0.1 UF 1000 V X7R | KEMET | C1812C104KDR AC7800 | CAP1812 |
| 17 | 2 | C21 C44 | CAP CER 1812 DNP | KEMET | DNP | CAP1812 |
| 18 | 20 | C23-24 C135- 138 C193 C195 C204 C210-219 C224 | CAP ELECT 220 uF 400 V DC RADIAL | RUBYCON | 400BXW220MEF R18X50 | DIA-18MM, LEAD SPACE- 7.5MM, H-50 |
| 19 | 1 | C54 | CAP ELECT 390 uF 500 VDC RADIAL | united chemicon | VLXS501VSN391 MA50S | DIA-35MM, LEAD-10MM, H-52.5MM |
| 20 | 1 | C1 | FILM CAPACITOR 1.5 UF 305 VAC | EPCOS | B32923C3155M | CAPFILM_26.5 X12MM P- 22.5MM H- 22mm |
| 21 | 1 | C2 | FILM CAPACITOR 10 UF 20% 305 VAC RADIAL | EPCOS | B32926H3106M | CAPFILM_42M MX28MM P- 37.5MM H- 42.5mm |

| Sr No | Qty | Reference | Description | Manufacturer | Manufacturer P/N | Package |
|-------|-----|--|--|---------------------|------------------------|--|
| 22 | 3 | C35-36 C188 | CAPFILM 3UF 900 VDC 5% RADIAL | VISHAY BC COMP. | MKP184853009 4K2 | CAPFILM_ 15MMX32MMX 25MM, P- 27.5MM |
| 23 | 30 | C39 C53 C56 C60-61 C190 C192 C194 C196- 203 C205-209 C220-223 C229- 233 | CAPFILM 4700pPF 10% 1.25 KVDC RADIAL | EPCOS | B32651A7472K0 00 | CAPFILM 13MMX5MM P=10MM, H- 11MM |
| 24 | 2 | C58-59 | FILM CAPACITOR 4UF 630V | VISHAY | B32794D2405K | CAPFILM_11/3 15MM |
| 25 | 2 | YC1-2 | CAP CERMIC 4700PF 440 VAC RADIAL | KEMET | C947U472MZVD BA7317 | DIA 11MM P- 7.50MM |
| 26 | 13 | C28 C41 C147 C151 C155 C159 C163 C167 C171 C175 C179 C183 C187 | CAP 47 UF 35 V ELECT PW RADIAL | PANASONIC | ECA-1VM470I | 5/2.5MM TH |
| 27 | 1 | C57 | CAP FILM 5 UF 900 VDC 5% RADIAL | KEMET | C4AE0BU4500A 11J | CAP_FILM_19X 31.5MMx29.2M M P-27.5MM |
| 28 | 4 | J1-4 | CONN.TERM BLOCK 2POS. 5MM PCB | PHOENIX CONTACT | 1935161 | TH_5MM |
| 29 | 1 | CON5 | CONN TER BLOCK 3POS. 7.5MM 41AMP 30DEG | PHOENIX CONTACT | 1792232 | 3POS. 7.5MM |
| 30 | 1 | CT1 | xfrmr current sense 37a 20mh t/h | PULSE | PE-67300NL | TH |
| 31 | 13 | PS1-13 | DC/DC Converter for SiC Driver low voltage | MORNSON | QA15115R2 | SIP PACK |
| 32 | 12 | C10 C15 C68 C76 C84 C92 C100 C108 C113 C121 C129 C140 | CAP CER 100pF 10% 50 V X7R 0603 | VISHAY/VITRAM ON | VJ0603Y101KXA CW1BC | CAP0603 |

| Sr No | Qty | Reference | Description | Manufacturer | Manufacturer P/N | Package |
|-------|-----|--|---|----------------------|-----------------------|---------------------------|
| 33 | 16 | D2 D4 D6 D10 D12 D14 D16 D18 D20 D22 D24 D26 D28 D30 D32 D34 | DIODE BZX-384- C16,115 ZENER 16 V | NXP Semiconductor | BZX384-C16,115 | SOD-323 |
| 34 | 16 | D1 D3 D5 D9 D11 D13 D15 D17 D19 D21 D23 D25 D27 D29 D31 D33 | DIODE BZX-384- C3V0,115 ZENER 3V | NXP SEMI | BZX-384- C3V0,115 | SOD-323 |
| 35 | 1 | D8 | DIODE STANDARD 1000 V 1A MELF | DIODES INC. | DL4007-13- | MELF |
| 36 | 2 | D7 D35 | DIODE SCHOT BAT754S 30V SOT23 | NEXPERIA USA | BAT754S,215 | SOT23 |
| 37 | 1 | D36 | DIODE ZENER 1W 2.1 V SMB | ON Semiconductor | | SMB |
| 38 | 1 | XL1 | EMI 2 LINE COOMON MODE CHOKE TH 160 OHM@100MHZ 75A | LAIRD | CM5441Z101B- 10 | TH |
| 39 | 1 | F2 | FUSE 15A LEADED CARTRIDGE | LITTLE FUSE | 0217015.MXEP | TH |
| 40 | 1 | F1 | FUSE HOLDER CLIP 30A 315V | LITTLE FUSE | 0122 0093 | FUSE CLIP |
| 41 | 5 | CON2-4 CON6-7 | HEADER 12POS 2.54 pitch DUAL T-HOLE | SULLINS CONN. | EBC06DRXH | CON2X6 |
| 42 | 1 | HS1 | HEAT SINK 6.6 kW | | Customized | |
| 43 | 8 | U1-8 | IC Single Channel IGBT Gate Driver 1200 V PG-DSO-8 | INFINEON TECH. | 1EDI30I12MHXU MA1 | PG-DSO-8 |
| 44 | 4 | U13-16 | IC MOSFET DRIVER 500MA SOT-23-5 | MICROCHIP | MCP1402T- E/OTTR | SOT-23-5 |
| 45 | 1 | L3 | INDUCTOR 150 UH 40 AMP | COIL WINDING | EK55246-341M- 40AH | 58MMX58MM, H-35MM |
| 46 | 1 | L4 | INDUCTOR FIXED 12 UH 19 A 4.3 MOHM | | Customized | SMD_35X28.6 MM, H-47MM |

| Sr No | Qty | Reference | Description | Manufacturer | Manufacturer P/N | Package |
|-------|-----|------------------------------------|--|-------------------------|--------------------|--|
| 47 | 1 | L6 | INDUCTOR_FIXED_180NH_65A_0.15M OHM_SMD | WURTH ELE. | 7443082018A | SMD_10X8MM, H-MM |
| 48 | 1 | L5 | INDUCTOR FIXED 7.6 UH 20 A 3.5 MOHM | | Customized | 35MMX28.6MM , H-43MM |
| 49 | 2 | L1-2 | INDUCTOR TORRIOD POWER 20 UH 40 A TH | MICROMETALS | OP-134090-2 | 36MM DIA, W-21MM |
| 50 | 1 | Q17 | TRANS MMBT2222A GP NPN SOT23 | FAIRCHILD | MMBT2222A | SOT23 |
| 51 | 16 | Q1-16 | MOSFET, N-Channel 1000 V, 65 mΩ TO-247-4 | WOLFSPEED SEMICONDUCTOR | C3M0065100K | TO-247 |
| 52 | 1 | VRV1 | MOV VERISTOR510 V 10KA DISK 20MM | EPCOS | B72220S2321K101 | TH HOLE 20mm dia, 27mm high 10mm pitch |
| 53 | 2 | CON1 CON8 | PCB TERMINAL BLOCK SINGLE POS | PHOENIX CONTACT | PLA5/1-7 5-1792216 | SINGLE POS. |
| 54 | 2 | RV1-2 | PTC RESET FUSE 440 V 86MA RADIAL | APCOS | B59751C0120A070 | TH_13MMX7.5 MM, H-18MM RAD |
| 55 | 1 | RLY1 | RELAY GEN PURPOSE 12 V 40 A SPST | TE CONN. | T9VV1K15-12S | RELAY12V_TH_40A |
| 56 | 8 | R17 R21 R62 R96 R99 R102 R105 R108 | RES 100 Ohm 1% 1/10 W 0603 | Vishay/Dale | CRCW0603100R FKEA | RES0603 |
| 57 | 8 | R3 R10 R23 R63 R70 R73 R76 R79 | RES 10.0 OHM 0.1% 1/10W 0603 | Vishay/Dale | TNPW060310R0 BEEA | RES_0603 |
| 58 | 8 | R1 R9 R32 R35 R37 R47 R50 R66 | RES 10k 1% 1/10 W 0603 | PANASONIC | ERJ-3GEYJ103V | RES0603 |
| 59 | 8 | R36 R20 R4 R48-49 R34 R65 R16 | RES 10k 1% 1/10 W 0603 | PANASONIC | ERJ-3GEYJ103V | RES0603 |

| Sr No | Qty | Reference | Description | Manufacturer | Manufacturer P/N | Package |
|-------|-----|--|--|--------------|-------------------------|--------------------|
| 60 | 4 | R91 R93 R103 R109 | RES0603 220E 1% 1/10W | PANASONIC | ERJ-3GEYJ221V | RES0603 |
| 61 | 16 | R11 R19 R61 R84 R87 R90 R95 R98 R101 R104 R106- 107 R110-113 | RES 4.7E 1% 1/10 W 0603 | YAGEO | RC0603JR- 074R7L | RES0603 |
| 62 | 1 | R78 | RES0805 100E 5% SMD | PANASONIC | ERJ-6GEYJ101V | RES0805 |
| 63 | 1 | R69 | RES0805 100E 5% SMD | PANASONIC | ERJ-6GEYJ103V | RES0805 |
| 64 | 6 | R22 R25-29 | RES 0.0 OHM 1/10W 5% 1206 | PANASONIC | ERJ-8GEY0R00V | RES1206 |
| 65 | 1 | R7 | RES1206 1K 1% 1/4W | PANASONIC | ERJ-8GEYJ102V | RES1206 |
| 66 | 6 | R12 R14-15 R57 R59 R114 | RES 1.0M 1% 1/4W 1206 | VISHAY/DALE | CRCW12061M00 FKEA | RES1206 |
| 67 | 12 | R2 R5 R24 R64 R71 R74 R77 R80 R82 R85 R88 R92 | SURFACE MOUNT RESISTOR 10E MELF | YAGEO | MMA02040C100 8FB300 | 3.5X1.4MM |
| 68 | 31 | R8 R13 R18 R30 R33 R39-46 R51- 54 R58 R60 R67- 68 R81 R83 R86 R89 R94 R97 R100 R115-117 | RES SMD 1 OHM 1% 1/4W MELF | VISHAY | MMA02040C100 8FB300 | 3.5X1.4MM 1206 |
| 69 | 1 | R38 | RES SMD 1 OHM 1% 1/4W MELF | VISHAY | MMA02040C100 8FB300 | 3.5X1.4MM 1206 |
| 70 | 3 | R6 R31 R75 | RES SMD 4.7 OHM 1% 1/4W MELF | VISHAY | MCFRFTDV4R70 | 3.5X1.4MM_12 06 |
| 71 | 2 | R72 R118 | RES 1.00 Ohm 5% 2W AXIAL | TE CONN. | ROX2SJ1R0 | RES_AXIAL_2 W |
| 72 | 2 | R55-56 | RES 270K Ohm 5% 3W | YAGEO CORP. | FMP300JR-73- 270K-ND | RES_270K_3W |
| 73 | 4 | U9-12 | DGTL ISOLATED GATE DRIVER 3.75KV SOIC8 | SILICON LABS | Si8261BCC-C-IS | SOIC8 |

| Sr No | Qty | Reference | Description | Manufacturer | Manufacturer P/N | Package |
|-------|-----|-----------|-----------------------|--------------|------------------|-----------|
| 74 | 1 | T1 | TRANSFORMER PQ5050 | | Customized | 50MMX50MM |

Controller Board:

| Sr. No | Qty | Reference | Description | Manufacturer | Manufacturer P/N | Package |
|--------|-----|--|---|--------------------|----------------------|---------|
| 1 | 3 | U2 U4 U8 | Precision Optically Isolated Voltage Sensor | AVAGO TECH | ACPL-C870 | SO-8 |
| 2 | 1 | Q1 | MOSFET N-CH BSS138 220MA SOT23 | FAIRCHILD SEMI. | BSS138 | SOT23 |
| 3 | 2 | C123 C130 | CAP CER 0.001UF 10% 16V X7R 0603 | KEMET | C0603C102R4RACT | CAP0603 |
| 4 | 26 | C6-7 C21 C26-27 C29-30 C35-36 C42-43 C65-66 C70 C73 C76-77 C83-84 C106 C122 C126 C129 C156 C175-176 | CAP CER 0.01 UF 10% 16 V X7R 0603 | TDK CORP. | C1608X7RIC103K | CAP0603 |
| 5 | 42 | C11-12 C14-16 C18-19 C44 C53 C57 C59 C62 C64 C67 C78-79 C85 C87-88 C93 C95- 98 C100 C105 C111-113 C116 C119 C124 C131- 134 C136 C140 C144 C149 C159 C183 | CAP 0.1 uF 10% 10 V X7R 0603 | KEMET | C0603C104K8RACT U | CAP0603 |
| 6 | 31 | C3-5 C10 C22 C24-25 C28 C33- 34 C39-41 C49- 50 C60 C68 C71 C75 C92 C102 C107 C121 C145 C155 C157 C160 | CAP 0.1 uF 10% 16 V X7R 0603 | KEMET | C0603X104K4RACT U | CAP0603 |

| Sr. No | Qty | Reference | Description | Manufacturer | Manufacturer P/N | Package |
|--------|-----|--|-------------------------------------|---------------------|-----------------------------|---------|
| | | C172 C174 C178 C184 | | | | |
| 7 | 4 | C101 C179-180 C91 | CAP 0.1 uF 10% 16 V X7R 0603 | KEMET | C0603X104K4RACT U | CAP0603 |
| 8 | 5 | C86 C99 C108 C163-164 | CAP 0.1 uF 10% 16 V X7R 0603 | KEMET | C0603X104K4RACT U | CAP0603 |
| 9 | 3 | C117-118 C127 | CAP 0.1 uF 10% 25 V X7R 0603 | KEMET | C0603X104K3RACT U | CAP0603 |
| 10 | 5 | C1 C8 C37 C51- 52 | CAP CER 0.1 uF 10% 50 V X7R 0603 | KEMET | C0603C104K5RACT U | CAP0603 |
| 11 | 3 | C158 C177 C142 | CAP CER 100pF 10% 50 V X7R 0603 | VISHAY/VITRAM ON | 77- VJ0603Y101KXACB C | CAP0603 |
| 12 | 4 | C89-90 C104 C109 | CAP CER 10 uF 10% 10 V X5R 0603 | MURATA | GRM188R61A106K E69D | CAP0603 |
| 13 | 19 | C23 C150-151 C153-154 C181- 182 C31-32 C58 C61 C63 C69 C72 C103 C125 C152 C165 C171 | CAP CER 1.0 uF 10% 16 V X5R 0603 | KEMET | C0603C105K4PACT U | CAP0603 |
| 14 | 7 | C2 C9 C38 C185- 188 | CAP CER 1uF 10% 50 V X7R 0603 | PANASONIC | CL10B105K8NNNC | CAP0603 |
| 15 | 1 | C115 | CAP CER 330pF 10% 50 V 0603 | TDK | C1608JB1H331KT0 00N | CAP0603 |
| 16 | 2 | C137-138 | CAP CER 33pF 10% 16 V NPO 0603 | AVX CORP | 0603YC330JAT2A | CAP0603 |
| 17 | 14 | C13 C17 C20 C94 C114 C120 C128 C135 C139 C141 C146 C161 C166- 167 | CAP CER 4.7 uF 10% 10 V X5R 0603 | TDK | C1608X5R1A475K | CAP0603 |
| 18 | 2 | C74 C162 | CAP CER 4.7 uF 10% 35 V X5R 0603 | MURATA | GRM188R6YA475K E15D | CAP0603 |
| 19 | 2 | C48 C173 | CAP CER 4.7 uF 10% 25 V 0805 | MURATA | GRM21BR61E475K A12L | CAP0805 |
| 20 | 12 | C45-47 C54-56 C80-82 C168-170 | CAP CER 4.7 uF 10% 50 V X7R 0805 | MURATA | GRM32ER71H475K A88L | CAP0805 |

| Sr. No | Qty | Reference | Description | Manufacturer | Manufacturer P/N | Package |
|--------|-----|-----------------------------|--|-----------------------|--------------------|-----------------------------|
| 21 | 1 | C147 | CAP CER 10 uF 10% 6.3 V X5R 1206 | SAMSUNG | CL31A106KQHNNNE | CAP1206 |
| 22 | 1 | C148 | CAP ELECT 100 uF 20% 10 V FK SMD | UNITED CHEMI-CON | EMVA100ADA101MF55G | CAPELEC_ALUM_6.3MM DIA |
| 23 | 1 | C110 | CAP ELECT 10 uF 20% 50 V FK SMD | PANASONIC | EEV-FK1H100UR | CAPELEC_ALUM_5X5.8MM_FK_SMD |
| 24 | 1 | C143 | CAP ELECT 10 uF 20% 50V TH RADIAL | PANASONIC | ECEA1HKS100 | TH |
| 25 | 3 | CT1-3 | CAP 22 uF TANT 6.3 V 10% case size-c/6032-28 SMD | KEMET | T495C226 | CAPTANT_T491C |
| 26 | 4 | CL1-4 | COMMON MODE FILTER SMD | BOURNS | SRF0905-500Y | SMD |
| 27 | 1 | CON1 | TER BLOCK 2POS. 2.54 MM PCB | ON SHORE TECH | OSTVN02A150 | TH 2.54MM |
| 28 | 8 | J1-4 J6-9 | CONN.TERM BLOCK 2POS. 5MM PCB | PHONIX CONTACT | 1935161 | TH_5MM |
| 29 | 1 | J5 | J-TAG CONNECTER 14-PIN | TE CONN. | 1-1634688-4 | 14-PIN J-TAG |
| 30 | 1 | Y1 | CRYSTAL 10MHZ 18PF 60 OHM | CTS FREQUENCY CONTROL | ATS100B-E | TH HOLE |
| 31 | 5 | R31 R56 R74 R130 R132 | RES 2.2 Ohm 1% 1/10 W 0603 | YAGEO | RC0603JR-072R2L | RES0603 |
| 32 | 10 | R5-9 R13 R110 R113 R118-119 | RES 1k 1% 1/10 W 0603 | Vishay/Dale | CRCW06031K00FK EA | RES0603 |
| 33 | 1 | R82 | RES 7.5k 1% 1/10 W 0603 | Vishay/Dale | ERJ-3EKF1202V | RES0603 |
| 34 | 3 | R12 R91 R127 | RES 0.0 OHM 5% 1/10 W 0603 | VISHAY/DALE | CRCW06030000Z0E B\ | RES0603 |
| 35 | 1 | D5 | DIODE MBAT46 W-V 100 V 150MA SOD123 | VISHAY SEMI. | BAT46W-E3-GSO8 | SOD123 |
| 36 | 1 | D13 | DIODE ZENER 2.2 V 500MW SOD-123 | ON Semiconductor | MMSZ4680TIG | SOD-123 |

| Sr. No | Qty | Reference | Description | Manufacturer | Manufacturer P/N | Package |
|--------|-----|-------------|---|--------------------------------|------------------|----------|
| 37 | 3 | D1-3 | DIODE ZENER DNP SOD-123 | | DNP | SOD-123 |
| 38 | 5 | CON2-6 | CON 12POS 2.54 pitch DUAL T-HOLE | SULLINS CONN. | EBC06MMMD | CON2X6 |
| 39 | 2 | U7 U19 | IC PRECISION REF 1.5VREF SOT23 | INTERSIL | ISL21010CFH315Z | SOT23-3 |
| 40 | 1 | U10 | IC CURRENT SENSOR | LINEAR TECH. | LT3092EST#PBF | SOT223-3 |
| 41 | 1 | U11 | IC DIGITAL ISO 3CH TRI-STATE 16SOIC | SI8430 | SI8430AB-D-IS1 | SOIC16 |
| 42 | 8 | D4 D6-12 | LED RED 0805 SMD | ROHM | SML-211UTT-86 | LED0805 |
| 43 | 1 | U23 | IC LF50ABDT REG 1.5 A 5VOLT DPAK | STMicroelectro nics | LF50ABDT | DPAK |
| 44 | 1 | U12 | IC LM258 Dual OpAmp SOIC8 | ST MICRO | LM258DT | SOIC8 |
| 45 | 1 | U1 | microcontroller TMS320F28377D | TEXAS INSTRUMENT | TMS320F28377DPT | LQFP-176 |
| 46 | 3 | U13 U15 U21 | IC BUFFER NONINVERTING SOIC14 | FAIRCHILD SEMICONDUCT OR | MC74VHCT50A | SOIC14 |
| 47 | 3 | U3 U5 U9 | IC MCP6031 single OpAmp SOIC8 | Microchip | MCP6031-E/SN | SOIC8 |
| 48 | 8 | Q2-9 | TRANS MMBT2222A GP NPN SOT23 | FAIRCHILD | MMBT2222A | SOT23 |
| 49 | 2 | U16-17 | OPTICAL SWITCH, TRANSISTOR OUTPUT 4SMD | SHARP MICRO ELECTRIC | PC817XNNIP0F | 4SMD |
| 50 | 1 | U20 | TVS DIODE 5.5VWM 8 VC 8MSOP | ST MICRO | PACDN046MR | 8MSOP |
| 51 | 1 | VR1 | POT 1K OHM ¼ W PLASTI LINEAR | BOURNS | 3310Y-001-102L | TH |
| 52 | 4 | PS1-4 | 0.25W, FIXED INPUT, ISOLATED & UNREGULATED SINGLE OUTPUT | MORNSON | B0505XT-1WR2 | SMD |
| 53 | 1 | U18 | IC REF3230 SERIES VOLTAGE REFERANCE | TEXAS | REF3230AIDBVT | SOT23-6 |

| Sr. No | Qty | Reference | Description | Manufacturer | Manufacturer P/N | Package |
|--------|-----|--|------------------------------------|-------------------|----------------------|----------|
| 54 | 9 | R79 R84 R92 R100 R103 R108- 109 R116-117 | RES 0.0 OHM 1/10 W 5% 0603 | VISHAY/DALE | CRCW06030000Z0E A | RES0603 |
| 55 | 1 | R104 | RES 1.5k 1% 1/10 W 0603 | Vishay/Dale | CRCW06031K50FK EA | RES0603 |
| 56 | 7 | R1-2 R59 R61 R107 R114 R129 | RES, 100K, 1%. 1/10 W, 0603, TF | Vishay/Dale | CRCW0603100KFK EA | RES0603 |
| 57 | 3 | R3 R10 R142 | RES 100 Ohm 1% 1/10 W 0603 | Vishay/Dale | CRCW0603100RFK EA | RES0603 |
| 58 | 7 | R11 R46 R51 R60 R98 R134 R4 | RES 100 Ohm 1% 1/10 W 0603 | Vishay/Dale | CRCW0603100RFK EA | RES0603 |
| 59 | 2 | R52-53 | RES 10.0 OHM 0.1% 1/10W 0603 | Vishay/Dale | TNPW060310R0BE EA | RES_0603 |
| 60 | 29 | R14-15 R19-22 R26-29 R38-41 R75-78 R80-81 R120-125 R128 R135-136 | RES, 10K, 1%. 1/10 W, 0603, TF | Vishay/Dale | CRCW060310K0FK EA | RES0603 |
| 61 | 5 | R63 R65 R73 R88-89 | RES, 1K, 1%. 1/10 W, 0603, TF | Vishay/Dale | CRCW06031K00FK EA | RES0603 |
| 62 | 1 | R17 | RES 1M 1% 1/10 W 0603 | VISHAY/DALE | CRCW06031M00FK EA | RES0603 |
| 63 | 3 | R93 R101-102 | RES, 2.2K, 1%. 1/10 W, 0603, TF | Vishay/Dale | CRCW060310K0FK EA | RES0603 |
| 64 | 6 | R105-106 R111- 112 R138 R140 | RES 22K 1% 1/10 W 0603 | PANASONIC- ECG | ERJ-3EKF2202V | RES0603 |
| 65 | 2 | R57-58 | RES, 27K, 1%. 1/10 W, 0603 | VISHAY | CRCW060327K0FK EA | RES0603 |
| 66 | 1 | R45 | RES 2K 1% 1/10 W 0603 | VISHAY/DALE | ERJ-3EKF1202V | RES0603 |
| 67 | 1 | R131 | RES 2K 1% 1/10 W 0603 | VISHAY/DALE | ERJ-3EKF1202V | RES0603 |
| 68 | 8 | R83 R94-97 R99 R137 R139 | RES 3.3K 1% 1/10 W 0603 | VISHAY/DALE | CRCW06033K30FK EA | RES0603 |
| 69 | 10 | R32-36 R42-44 R68 R115 | RES 4.7E 1% 1/10 W 0603 | YAGEO | RC0603JR-074R7L | RES0603 |
| 70 | 5 | R30 R55 R72 R126 R133 | RES 4.7 K 1% 1/10 W 0603 | VISHAY/DALE | MC00063W060314 K7 | RES0603 |
| 71 | 1 | R54 | RES 470K 1% 1/10 W 0603 | PANASONIC | ERJ-3EKF4703V | RES0603 |

| Sr. No | Qty | Reference | Description | Manufacturer | Manufacturer P/N | Package |
|--------|-----|------------------------|---------------------------------|------------------|-------------------|-------------|
| 72 | 1 | R49 | RES 470 OHM 1% 1/10 W 0603 | Vishay/Dale | CRCW0603470RFK EA | RES0603 |
| 73 | 1 | R90 | RES 470 OHM 1% 1/10 W 0603 | Vishay/Dale | CRCW0603470RFK EA | RES0603 |
| 74 | 1 | R48 | RES 47K 1% 1/10 W 0603 | VISHAY/DALE | CRCW060347K0FK EA | RES0603 |
| 75 | 1 | R16 | RES, 5.1K, 1%, 1/10 W, 0603 | PANASONIC | ERJ-3EKF5101V | RES0603 |
| 76 | 1 | R18 | RES 6.26K 1% 1/10 W 0603 | PANASONIC | ERJ-3EKF60261V | RES0603 |
| 77 | 1 | R143 | RES0603 6.8K 5% 1/10W | PANASONIC | ERJ-3GEYJ682V | RES0603 |
| 78 | 1 | R37 | RES 7.8K 1% 1/10W 0603 | VISHAY/DALE | CRCW06037K8FKE A | RES0603 |
| 79 | 1 | R50 | DNP | | DNP | RES0603 |
| 80 | 1 | R47 | RES DNP 1% 1/10W 0603 | Vishay/Dale | DNP | RES0603 |
| 81 | 4 | R147-150 | RES2512 10 OHM 5% 1 W | PANASONIC | ERJ-1TYJ100U | RES1206 |
| 82 | 2 | R62 R87 | RES1206 1K 1% ¼ W | PANASONIC | P1.0KECT | RES1206 |
| 83 | 4 | R64 R66-67 R151 | RES 220K 1% 1/4W 1206 | VISHAY/DALE | CRCW12061M00FK EA | RES1206 |
| 84 | 9 | R23-25 R69-71 R144-146 | RES1206 470K 1%1/4 W | PANASONIC | ERJ-8ENF4703V | RES1206 |
| 85 | 1 | R141 | RES 15 Ohms 1% ¼ W 1210 | PANASONIC | ERJ-14YJ150V | RES1210 |
| 86 | 2 | R85-86 | RES 20 Ohms 1% ¼ W 1210 | PANASONIC | ERJ-14YJ200V | RES1210 |
| 87 | 1 | SW1 | SWITCH SLIDE SPDT 300 MA 6 V | E-SWITCH | EG1270 | TH_2.54M M |
| 88 | 1 | SW2 | SWITCH TOGGLE SPDT 0.4 VA | NKK SERIES | B12AB | SWT_TH SPDT |
| 89 | 1 | U22 | IC REG LDO 3.3 V/1.2 V 24HTSSOP | TEXAS INSTRUMENT | TPS70445PWP | TSSOP24 |
| 90 | 2 | U6 U14 | VAC CURRENT SENSOR | VAC | T60404-N4646-X161 | TH_4PIN |

7. References

- [1] Robert L Steilgerwald, "A Comparison of Half-Bridge Resonant Converter Topologies", IEEE Transactions on Power Electronics, Vol.3, No.2, April 1988.
- [2] G. Glanzer, T. Sivaraman, J. I. Buffalo, M. Kohl, and H. Berger, "Cost-efficient integration of electric vehicles with the power grid by means of smart charging strategies and integrated on-board chargers," in *Environment and Electrical Engineering (EEEIC), 2011 10th International Conference on*, 2011, pp. 1-4.
- [3] C. C. Chan and K. T. Chau, "An overview of power electronics in electric vehicles," *Industrial Electronics, IEEE Transactions on*, vol. 44, pp. 3-13, 1997.
- [4] J. Tianyang, Z. Junming, W. Xinke, S. Kuang, and W. Yousheng, "A Bidirectional LLC Resonant Converter with Automatic Forward and Backward Mode Transition," *Power Electronics, IEEE Transactions on*, vol. 30, pp. 757-770, 2015.
- [5] Z. U. Zahid, Z. Dalala, and L. Jih-Sheng, "Design and control of bidirectional resonant converter for Vehicle-to-Grid (V2G) applications," in *Industrial Electronics Society, IECON 2014 - 40th Annual Conference of the IEEE*, 2014, pp. 1370-1376.
- [6] J. H. Jung, H. S. Kim, M. H. Ryu, and J. W. Baek, "Design Methodology of Bidirectional CLLC Resonant Converter for High-Frequency Isolation of DC Distribution Systems," *Power Electronics, IEEE Transactions on*, vol. 28, pp. 1741-1755, 2013.
- [7] B. Yang, "Topology investigation for front end DC/DC power conversion for distributed power system," Virginia Polytechnic Institute and State University, 2003.
- [8] W. Kramer, S. Chakraborty, B. Kroposki, A. Hoke, G. Martin, and T. Markel, "Grid Interconnection and Performance Testing Procedures for Vehicle-To-Grid (V2G) Power Electronics," National Renewable Energy Laboratory (NREL), Golden, CO. 2012.

8. Revision History

| Date | Revision | Changes |
|--------------|----------|---------------------------------|
| July 2018 | B | First issue |
| January 2024 | 2 | Branding and formatting updates |

9. Important Notes

Purposes and Use

Wolfspeed, Inc. (on behalf of itself and its affiliates, "Wolfspeed") reserves the right in its sole discretion to make corrections, enhancements, improvements, or other changes to the board or to discontinue the board.

THE BOARD DESCRIBED IS AN ENGINEERING TOOL INTENDED SOLELY FOR LABORATORY USE BY HIGHLY QUALIFIED AND EXPERIENCED ELECTRICAL ENGINEERS TO EVALUATE THE PERFORMANCE OF WOLFSPEED POWER SWITCHING DEVICES. THE BOARD SHOULD NOT BE USED AS ALL OR PART OF A FINISHED PRODUCT. THIS BOARD IS NOT SUITABLE FOR SALE TO OR USE BY CONSUMERS AND CAN BE HIGHLY DANGEROUS IF NOT USED PROPERLY. THIS BOARD IS NOT DESIGNED OR INTENDED TO BE INCORPORATED INTO ANY OTHER PRODUCT FOR RESALE. THE USER SHOULD CAREFULLY REVIEW THE DOCUMENT TO WHICH THESE NOTIFICATIONS ARE ATTACHED AND OTHER WRITTEN USER DOCUMENTATION THAT MAY BE PROVIDED BY

WOLFSPEED (TOGETHER, THE “DOCUMENTATION”) PRIOR TO USE. USE OF THIS BOARD IS AT THE USER’S SOLE RISK.

Operation of Board

It is important to operate the board within Wolfspeed’s recommended specifications and environmental considerations as described in the Documentation. Exceeding specified ratings (such as input and output voltage, current, power, or environmental ranges) may cause property damage. If you have questions about these ratings, please contact Wolfspeed at forum.wolfspeed.com prior to connecting interface electronics (including input power and intended loads). Any loads applied outside of a specified output range may result in adverse consequences, including unintended or inaccurate evaluations or possible permanent damage to the board or its interfaced electronics. Please consult the Documentation prior to connecting any load to the board. If you have any questions about load specifications for the board, please contact Wolfspeed at forum.wolfspeed.com for assistance.

Users should ensure that appropriate safety procedures are followed when working with the board as serious injury, including death by electrocution or serious injury by electrical shock or electrical burns can occur if you do not follow proper safety precautions. It is not necessary in proper operation for the user to touch the board while it is energized. When devices are being attached to the board for testing, the board must be disconnected from the electrical source and any bulk capacitors must be fully discharged. When the board is connected to an electrical source and for a short time thereafter until board components are fully discharged, some board components will be electrically charged and/or have temperatures greater than 50° Celsius. These components may include bulk capacitors, connectors, linear regulators, switching transistors, heatsinks, resistors and SiC diodes that can be identified using board schematic. Users should contact Wolfspeed at forum.wolfspeed.com for assistance if a board schematic is not included in the Documentation or if users have questions about a board’s components. When operating the board, users should be aware that these components will be hot and could electrocute or electrically shock the user. As with all electronic evaluation tools, only qualified personnel knowledgeable in handling electronic performance evaluation, measurement, and diagnostic tools should use the board.

User Responsibility for Safe Handling and Compliance with Laws

Users should read the Documentation and, specifically, the various hazard descriptions and warnings contained in the Documentation, prior to handling the board. The Documentation contains important safety information about voltages and temperatures.

Users assume all responsibility and liability for the proper and safe handling of the board. Users are responsible for complying with all safety laws, rules, and regulations related to the use of the board. Users are responsible for (1) establishing protections and safeguards to ensure that a user’s use of the board will not result in any property damage, injury, or death, even if the board should fail to perform as described, intended, or expected, and (2) ensuring the safety of any activities to be conducted by the user or the user’s employees, affiliates, contractors, representatives, agents, or designees in the use of the board. User questions regarding the safe usage of the board should be directed to Wolfspeed at forum.wolfspeed.com.

In addition, users are responsible for:

- Compliance with all international, national, state, and local laws, rules, and regulations that apply to the handling or use of the board by a user or the user’s employees, affiliates, contractors, representatives, agents, or designees.
- Taking necessary measures, at the user’s expense, to correct radio interference if operation of the board causes interference with radio communications. The board may generate, use, and/or radiate radio frequency energy, but it has not been tested for compliance within the limits of computing devices pursuant to Federal Communications Commission or Industry Canada rules, which are designed to provide protection against radio frequency interference.
- Compliance with applicable regulatory or safety compliance or certification standards that may normally be associated with other products, such as those established by EU Directive 2011/65/EU of the European Parliament and of the Council on 8 June 2011 about the Restriction of Use of Hazardous Substances (or the RoHS 2 Directive) and EU Directive 2002/96/EC on Waste Electrical and Electronic Equipment (or WEEE). The board is not a finished product and therefore may not meet such standards. Users are also responsible for properly disposing of a board’s components and materials.

No Warranty

THE BOARD IS PROVIDED “AS IS” WITHOUT WARRANTY OF ANY KIND, INCLUDING BUT NOT LIMITED TO ANY WARRANTY OF NON-INFRINGEMENT, MERCHANTABILITY, OR FITNESS FOR A PARTICULAR PURPOSE, WHETHER EXPRESS OR IMPLIED. THERE IS NO REPRESENTATION THAT OPERATION OF THIS BOARD WILL BE UNINTERRUPTED OR ERROR FREE.

Limitation of Liability

IN NO EVENT SHALL WOLFSPEED BE LIABLE FOR ANY DAMAGES OF ANY KIND ARISING FROM USE OF THE BOARD. WOLFSPEED’S AGGREGATE LIABILITY IN DAMAGES OR OTHERWISE SHALL IN NO EVENT EXCEED THE AMOUNT, IF ANY, RECEIVED BY WOLFSPEED IN EXCHANGE FOR THE BOARD. IN NO EVENT SHALL WOLFSPEED BE LIABLE FOR INCIDENTAL, CONSEQUENTIAL, OR SPECIAL LOSS OR DAMAGES OF ANY KIND, HOWEVER CAUSED, OR ANY PUNITIVE, EXEMPLARY, OR OTHER DAMAGES. NO ACTION, REGARDLESS OF FORM, ARISING OUT OF OR IN ANY WAY CONNECTED WITH ANY BOARD FURNISHED BY WOLFSPEED MAY BE BROUGHT AGAINST WOLFSPEED MORE THAN ONE (1) YEAR AFTER THE CAUSE OF ACTION ACCRUED.

Indemnification

The board is not a standard consumer or commercial product. As a result, any indemnification obligations imposed upon Wolfspeed by contract with respect to product safety, product liability, or intellectual property infringement do not apply to the board.